

Radiocarbon analysis of dissolved organic carbon from ice cores

Inaugural dissertation
of the Faculty of Science,
University of Bern

presented by

Ling Fang

from China

Supervisor of the doctoral thesis:

Prof. Dr. Margit Schwikowski

Department of Chemistry and Biochemistry, University Bern

Laboratory for Environmental Chemistry, Paul Scherrer Institute

Radiocarbon analysis of dissolved organic carbon from ice cores

Inaugural dissertation
of the Faculty of Science,
University of Bern

presented by

Ling Fang

from China

Supervisor of the doctoral thesis:

Prof. Dr. Margit Schwikowski

Department of Chemistry and Biochemistry, University Bern
Laboratory for Environmental Chemistry, Paul Scherrer Institute

Accepted by the Faculty of Science.

Bern, 2. June 2020

The Dean

Prof. Dr. Zoltan Balogh

The past has no existence except as it is recorded in the present.

John Archibald Wheeler, "Beyond the Black Hole"

Contents

Summary	10
1 Introduction	16
1.1 Climate change	16
1.2 The effect of atmospheric aerosols on climate	17
1.3 Glacier archives	20
1.4 ¹⁴ C dating of ice cores	22
1.5 Objectives	26
Bibliography	29
2 Methodology.....	34
2.1 Separation of the particulate organic and elemental carbon fraction	34
2.2 DOC extraction for ¹⁴ C analysis	35
2.3 Radiocarbon analysis.....	37
2.3.1 General concept	38
2.3.2 ¹⁴ C measurement.....	38
2.3.3 ¹⁴ C applications.....	41
Bibliography	44
3. Extraction of dissolved organic carbon from glacier ice for radiocarbon analysis	48
Abstract.....	49
3.1 Introduction	50
3.2 Experimental.....	51
3.2.1 Extraction Setup.....	52
3.2.2 Sample Preparation and Decontamination.....	56
3.2.3 DOC extraction	57
3.3 Characterization.....	59
3.3.1 Oxidation Efficiency	59
3.3.2 Standards and Blank	60
3.3.3 Natural Ice Samples	64

3.4 Conclusions	65
Bibliography	66
4. Radiocarbon dating of alpine ice cores with the dissolved organic carbon (DOC) fraction	70
Abstract.....	71
4.1 Introduction	72
4.2 Sample preparation and ¹⁴ C analysis	74
4.3 Results	77
4.3.1 DOC and WIOC concentration.....	77
4.3.2 ¹⁴ C results.....	81
4.4 Discussion.....	83
4.4.1 Potential contribution of carbonates to WIOC dating.....	83
4.4.2 Age scales	86
4.5 Conclusion	90
Bibliography	92
5. ¹⁴C age constraints in the Mt. Hunter, Alaska ice core: implications for Central Alaska Holocene ice extent and climate	96
Abstract.....	97
5.1 Introduction	98
5.2 Methods	100
5.2.1 Annual layer counting (ALC) in the Mt. Hunter ice core.....	100
5.2.2 Mt. Hunter ice core ¹⁴ C analysis	102
5.3 Results	103
5.3.1 Mt. Hunter ice core ¹⁴ C data	103
5.3.2 Age scale modeling.....	108
5.4 Discussion.....	110
5.4.1 Implications for North Pacific/Arctic ice core chronologies	110
5.4.2 Holocene ice extent and hydroclimate in Central Alaska.....	112
5.5 Conclusion	113
Bibliography	116

6. Enhancement of biogenic secondary organic aerosol formation during the 20th century: insights from radiocarbon in organic carbon from a high Alpine glacier	120
Abstract.....	121
6.1 Introduction	122
6.2 Results and Discussion	123
6.2.1 Temporal trends in concentration of carbonaceous aerosols	123
6.2.2 Constraints on BC emissions	126
6.2.3 Sources of enhanced non-fossil OC in late 20th century	128
6.3 Methods	133
6.3.1 Sample selection	133
6.3.2 Sample Preparation	134
6.3.3 WIOC and EC separation and quantification.....	135
6.3.4 WSOC estimation	135
6.3.5 ¹⁴ C analysis.....	136
6.3.6 Radiocarbon based source apportionment	136
6.3.7 Potential emission source regions	138
Bibliography	146
7. Conclusion and Outlook	154
Acknowledgements.....	158
Declaration of consent.....	162
Curriculum Vitae	164

Summary

Global mean surface temperature has been increased 0.85 °C since 1900. With current greenhouse gas emissions, this warming trend will likely continue to reach up to 1.5 °C during 2030-2050. This warming coupled with the corresponding climate consequences has become an important issue for our society. Atmospheric aerosols can modify the earth's radiation balance directly by scattering or absorbing light and indirectly through the interaction with clouds. However, the aerosol radiative forcing is not well understood and quantified at present time largely due to the lack of knowledge about the pre-industrial aerosol, which causes a large fraction of the uncertainty in anthropogenic forcing. Carbonaceous aerosols, consisting of the fractions of Element Carbon (EC) or Black Carbon (BC) depending on the analytical method, Water Insoluble Organic Carbon (WIOC), and Water Soluble Organic Carbon (WSOC), for a major part of fine particles have attracted scientific attention due to their optical properties. Precise reconstructions of pre-industrial natural aerosol background will help to constrain the cloud albedo change due to anthropogenic emissions. High alpine glaciers are valuable archives for past climate and atmospheric compositions. These glaciers are mostly located around densely populated and highly industrialized regions experiencing strong changes by human activities. Aerosols are transport and deposited on glaciers by wet and dry deposition. Major ion records (e.g. sulphate, nitrate, and ammonium) have revealed that human activities caused a major change in the atmospheric composition since the beginning of the industrial revolution. However, regarding to the major fraction of fine aerosols, only very few data of carbonaceous particles (EC, WIOC and WSOC) have been reported from ice cores.

A precise chronology is essential to interpret the climate signal and atmospheric composition preserved in ice cores. Radiocarbon dating of the WIOC fraction has become an important dating tool to constrain the age of ice cores from nonpolar regions. However, in some cases this method is restricted by the low WIOC concentration present in the ice. The WSOC fraction is preserved in ice cores in the dissolved form (DOC) together with organic gases taken up during the snowfall. It holds great potential for ¹⁴C dating since much higher concentration is observed in ice cores. This thesis presents an extraction system for radiocarbon analysis of DOC in ice cores. A photo-oxidation method was applied by means of external UV irradiation of the sample. For an irradiation time of ~30 minutes, catalyzed by addition of Fenton's reagent

Fe^{2+} and H_2O_2 , an efficiency of $96 \pm 6 \%$ on average was achieved. Inert gas working conditions and stringent decontamination procedures enabled a low overall blank of $1.9 \pm 1.6 \mu\text{g C}$ with a F^{14}C value of 0.68 ± 0.13 . The setup can process ice samples of up to 350 g mass and offers ultra-clean working conditions for all extraction steps. This makes it possible to analyse the DOC in ice samples with a carbon content as low as $25 \mu\text{g kg}^{-1}$ ice. The comparison with other devices for ^{14}C analysis of DOC shows the setup performs excellent in terms of low carbon background with the advantage of higher carbon yields while keeping analysis time low. First analysis of firn samples from Piz Zupò (3900 m asl., Swiss Alps) over the period of 1991-1995 resulted in much higher values ($950\text{-}1440 \mu\text{g kg}^{-1}$) compare to previous studies from Col du Dôme (French Alps) with DOC values of around $200 \mu\text{g kg}^{-1}$ at similar time. Furthermore, this analysis also indicated the high risk of DOC contamination in firn samples, at least if the samples had been stored for a longer period of time.

This high performance DOC extraction system for ^{14}C analysis allows for investigating the potential of applying the DOC fraction for ice core dating. Bottom samples from four different high-alpine glaciers (Colle Gnifetti, Belukha, ShuLeNanShan and Chongce) were dated with DO^{14}C in parallel with the well-established WIO^{14}C dating method. ^{14}C ages of the two fractions yielded a comparable probability distribution with WIO^{14}C systematically resulting in a slightly older mean age for samples younger than 1000 years. This could be caused by an incomplete removal of carbonates (^{14}C dead) on the filtered WIOC samples. There is no indication of in-situ ^{14}C production systemically contribution to DOC as reported in a previous studies. This confirms that ^{14}C dating of the ice entrapped DOC fraction is applicable and a valuable future tool for the dating of ice samples. Meanwhile, it clearly demonstrates the benefits of using DOC fraction for dating are not just the reduced required ice amount but also improving the analytical precision. In addition, there is less reservoir effect and no carbonates bias from mineral dust for high dust loaded samples.

The bottom ages of the four glaciers show a decrease with latitude. The northernmost site, Belukha glacier, preserved much older ice close to bedrock than the other sites. A mean age $> 20,000$ year calBP for the deepest sample of the Belukha core was obtained with both, DO^{14}C and WIO^{14}C dating, indicating the Belukha glacier is of late Pleistocene origin. Since the DO^{14}C and the WIO^{14}C fraction yielded the same age for the ice sample just above the bedrock, a bias from mineral dust on the WIO^{14}C fraction can be excluded. Thus, Belukha glacier has a great

potential for reconstruction climate records far back into the Pleistocene in the bottom most few meters. The two glaciers from the Tibetan Plateau (ShuLeNanShan and Chongce) show similar bottom ages around 5500-6000 year BP, which confirmed the previous reported age range of Tibetan Plateau glaciers (Hou et al., 2018). The deepest sample age of DO¹⁴C from Chongce core 1 (5285-5875 calBP) is in the similar age range as the bottom WIO¹⁴C sample (5997-6443 calBP) of Chongce core 2 located about 2km away from core 1 drilling site. The DO¹⁴C dating results shed light on longstanding unresolved questions about the potential WIO¹⁴C dating bias due to the presence of carbonates in the ice, particularly for samples with high loadings of dust. Quantification of this effect based on Ca²⁺ concentrations in the future will be helpful to potential correct WIO¹⁴C dating. Finally, with this new DO¹⁴C method, it may be possible to push radiocarbon dating of ice cores a step forward even to remote and Polar Regions.

The first radiocarbon dated North Pacific/Arctic ice core is shown in this thesis. The chronology of the Mt. Hunter core from the central Alaska Range (62°56'N, 151°5'W, 3900 m asl.) was established by the combination of WIO¹⁴C and DO¹⁴C dating. This core is of great interest, since it may have preserved signals representative of the North Pacific climate. Understanding the climate variability of this region during warm intervals outside of the Common Era is essential for answering the question whether the positive phase of Pacific Decadal Oscillation is persistent and continues contributing to Arctic warming in the future. However, most of the existing ice cores extracted from the Alaska/Yukon region only archived few century because core recovery did not reach bedrock. A 208 m surface to bedrock ice core was retrieved from the summit plateau of Mt. Hunter in central Alaska in the year 2013. The annual layer signal is unambiguous down to a depth of 190 m (152.8 m w.eq), suggesting that the ice is 1203 years old with an uncertainty of about ± 41 years. Below that depth, annual layering could not be identified anymore due to glacier flow induced strong thinning. By applying ¹⁴C dating and a two-parameter flow model, a continuous depth-age relationship was established. For the deepest sample, DO¹⁴C dating was used due to the small ice amount. This is the first time micro radiocarbon dating was applied to ice from an Arctic core, which was achieved by increasing the amount of ice (>1 kg) to obtain the required carbon mass and by using a new technique based on the DOC fraction in ice for ¹⁴C analysis. Calibrated ¹⁴C ages from the two bottom most samples (7946-10226 cal BP and 7018-7975 cal BP) indicate that the Mt. Hunter glacier is of early Holocene origin. The estimated basal ice age from the depth age scale is > 8 kyr. We also noticed that the samples from the depth of 161.0-166.1 m weq

show small changes in ^{14}C ages from 3200 to 3500 BP. This could be due to an increase in accumulation during the regional neoglaciation. As one of few existing ice cores from the North Pacific region covering most of the Holocene, the Mt. Hunter core provides the possibility to investigate the millennial scale hydroclimate variability further back in time.

Besides dating purposes, measurement of the radiocarbon content provides a powerful tool for long-term source apportionment studies of carbonaceous aerosols. The impact of aerosol particles on the Earth's radiation balance remains poorly constrained, leading to considerable uncertainties in predicting the climate sensitivity to greenhouse gases. A large part of these uncertainties is related to the deficient knowledge of the magnitude of pre-industrial emissions, particularly for carbonaceous compounds forming a major fraction of the atmospheric aerosol. Ice core records exist for BC, WIOC and organic tracers, but information is rare for WSOC, forming a major fraction of carbonaceous aerosols. The first WSOC concentration record covering the pre-industrial to industrial time period was obtained in this thesis from DOC analyzed in the high-alpine ice core from Fiescherhorn ($6^{\circ}33'3.2''\text{N}$, $08^{\circ}04'0.4''\text{E}$, 3900 m asl., Swiss Alps) by subtracting the concentrations of formic and acetic acid. A complete 340-year concentration record of all the major carbonaceous aerosol fractions (EC, WIOC and WSOC) was retrieved, whereby each component was separated into fossil and non-fossil contribution using the ^{14}C content. The total carbonaceous aerosol concentration (sum of WIOC, WSOC and EC) increased by a factor of three at the end of 20th century compared to the pre-industrial background and fossil fuel combustion contributed up to ~32% of this increase. EC has highest values in the first half of the 20th century, to a large extent caused by fossil fuel emissions. In contrast, OC (WIOC and WSOC) shows a strong increasing trend between 1940 and 1980, mostly of non-fossil origin, which is not reflected in the potential source region emission estimates of OC. We attribute this trend primarily to enhancement of SOA formation caused by the presence of anthropogenic precursor gases or/and by the increase of the atmospheric oxidative capacity. Thus, bottom-up emission inventories seem to heavily underestimate the atmospheric OC loading by not accounting adequately for SOA formation, limiting the capacity of current models in estimating anthropogenic aerosol forcing.

This thesis demonstrated the great potential of radiocarbon analysis of DOC in ice core studies in two different perspectives: first, applying the DO^{14}C dating to establishing ice core chronologies. The similar age distributions of DO^{14}C and WIO^{14}C ages indicate the potential

for DO^{14}C as dating tool. An advantage of DO^{14}C dating is that carbonates are completely removed during the DOC extraction, even for high mineral dust loading. Secondly, to reconstruct carbonaceous aerosol concentrations for improving the understanding of the natural variations and anthropogenic contributions. This is important to constrain emission estimates used to simulate aerosol forcing in current climate models. The future improvement of the filtration section in the DOC extraction setup will allow the efficient analysis for all three major components of carbonaceous aerosols (WSOC, WIOC, and EC) in the same sample, which in return allows reducing the required amount of ice. Aerosols have very different regional scale distribution due to their short atmospheric lifetime and the uneven distribution of emissions sources. In addition, the onset of anthropogenic emissions varies from region to region. Reconstructing carbonaceous aerosol records from various locations could give more details on the regional and global picture how anthropogenic activities have affected the aerosol concentration and composition. This could help to improve the understanding of the climate sensitivity to anthropogenic emissions at different scales and to reduce the uncertainties in aerosol forcing.

1 Introduction

1.1 Climate change

Observed global mean surface temperature in 2006-2015 was 0.85 °C (range from 0.75 to 0.99 °C) higher compared to the average over the 1850-1900 period [IPCC SR1.5, 2018]. Human activities caused about 1.0 °C of temperature raise above pre-industrial level until now (Figure 1.1). With current greenhouse gas emission, this warming trend is likely continue to reach up to 1.5 °C during 2030-2050. Paleoclimate reconstruction from a range of natural archives (tree ring, ice core, coral, etc.) suggest that there is no evidence of preindustrial coherence of climate cold and warm epochs over the past 2,000 years [Neukom et al., 2019]. However, the ongoing rapid warming trend was observed across larger spatial scales for the past 150 years, underlining its uniqueness. The temperature increase results in further long-term changes in climate system, like sea level rise, glaciers and ice sheet melting, and albedo change. These changes, in return, have a positive impact on the surface radiation balance (positive climate feedback).

The surface temperature increase does not only change the climate system, but also had a strong impact on human society during the last decades in direct and indirect ways. The extreme summer weather in 2003 caused over 14800 deaths and increased mortality in France Dhainaut et al., 2003. The World Health Organization (WHO) estimated that climate change would cause approximately 250`000 additional deaths per year between 2030-2050 [WHO, 2014]. Over the period of 1901-2010, global mean sea level rose by 0.19 m [IPCC AR5, 2013], which is of great concern since a majority of people live in coastal cities and on islands. In addition to economic damage, droughts, flood and extreme events also threaten citizens safety in terms of clean air, safe drinking water sources, food supply and safe shelter.

To project the future climate response to anthropogenic activities, an accurate estimation of natural and anthropogenic radiative forcing is crucial for climate models. Although the greenhouse gas forcing is relatively well constrained, the climate sensitivity remain largely uncertain due to the large uncertainty in anthropogenic aerosol forcing [IPCC AR5, 2013]. The impact of aerosols and aerosol-cloud albedo interactions is highly uncertain, and it is even not fully clear if this is a negative or positive forcing [IPCC AR5, 2013]. This larger uncertainty in

aerosol and aerosol-clouds radiative forcing affects our understanding and the quantification of the sensitivity of the climate system to anthropogenic activities.

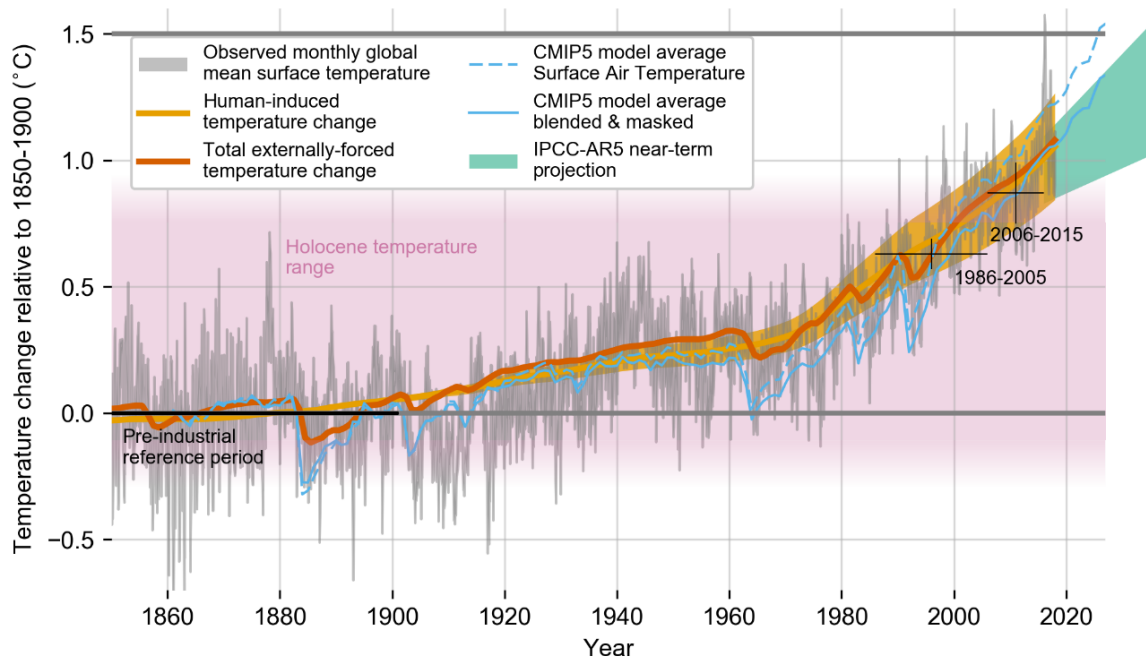


Figure 1.1 Global mean surface temperature (GMST) record. Figure from IPCC SR1.5 (2018). The gray line shows the monthly mean GMST from different observation dataset. The yellow line indicate the human induced temperature changes and the total (human- and naturally-forced) contributions to these GMST changes are shown in orange. The thin blue lines show the modelled global mean surface air temperature (dashed) and blended surface air and sea surface temperature accounting for observational coverage (solid) from the Coupled Model Intercomparison Project phase 5 (CMIP5) historical ensemble average extended with RCP8.5 emission scenario. The pink shading indicates a range for temperature fluctuations over the Holocene. The light green area depicts the AR5 projection for average GMST over 2016–2085.

1.2 The effect of atmospheric aerosols on climate

Atmospheric aerosols modify the earth’s radiation balance directly by scattering or absorbing light and indirectly through the interaction with clouds. The main source of natural aerosols are sea salt, mineral dust, biogenic emissions, volcanic eruptions and wild forest fires. Aerosol

particles emitted from fossil fuel burning, anthropogenic biomass burning and land use are categorized as anthropogenic aerosol. Human activities have resulted in an increase of anthropogenic aerosol emissions since industrial evolution. However, the magnitude of the natural and anthropogenic aerosol effect on climate is still uncertain, largely due to the complex dynamics of aerosols in the climate system. A certain fraction of the aerosol particles can act as cloud condensation nuclei (CCN) or ice-nucleating particle (INP), which affects the cloud albedo and lifetime [Lohmann and Feichter, 2005; DeMott et al., 2010]. Mineral dust is a major component of atmospheric aerosols. It scatters and absorbs both short and long wave length radiation [McCormick and Ludwig, 1967; Miller and Tegen, 1998]. Sulfate aerosol increase reflection of solar radiation back to space [Kiehl and Briegleb, 1993], which could reduce the anthropogenic forcing. Black carbon shows a strong positive radiative forcing with increasing atmospheric burden, whereas organic aerosols cause a direct and indirect negative radiative forcing [Maria et al., 2004]. Biogenic new particle formation might have resulted in a higher pre-industrial aerosol load, which reduced the anthropogenic radiative forcing when included in a global aerosol model [Gordon et al., 2016]. Aerosols not just have an influence on climate, but also threaten people's safety in many different ways. WHO estimates that around 7 million people die every year from diseases (like stroke, heart disease and lung cancer) caused by the exposure to fine particles in the polluted air [WHO 2018].

Organic aerosols significantly contribute to fine particles and account for 20-50% of the fine aerosol mass at mid latitudes and up to 90% in tropical forest regions [Andreae and Crutzen, 1997; Putaud et al., 2004]. Depending on how they formed, organic aerosols commonly categorize into primary organic aerosol (POA) and secondary organic aerosol (SOA). POA is emitted directly from natural sources (vegetation, micro-organisms and wild forest fires) and by anthropogenic activities (like incomplete combustion, agriculture). Gas phase organic compounds may become oxidized in the atmosphere, resulting in less volatile species, which then partition into the solid phase to generate aerosol phase organic particles as SOA. Volatile organic compounds (VOCs) are ubiquitous as the main gas phase organic compounds. Biogenic VOCs are emitted into the atmosphere from natural sources like marine phytoplankton, terrestrial vegetation and soil micro-organisms. In contrast to greenhouse gases, on the global basis, anthropogenic VOCs (AVOCs) emissions are 5-10 times lower than biogenic VOCs (BVOCs) emission [Kanakidou et al., 2005].

Carbonaceous aerosol particles are the dominant component of atmospheric aerosols and compose ~40% of the total aerosol mass in Europe [Yttri et al., 2007]. They consist of two major fractions, black carbon (BC) or element carbon (EC) and organic carbon (OC) based on the physical and chemical properties. The terminology of BC or EC has originated from the measurement techniques used: BC is determined using optical methods as the fraction is optically absorptive and EC refers to the fraction measured through thermal combusting in an oxygenated helium atmosphere. BC/EC are directly emitted from combustion of fossil fuel and biomass. The sources, chemical composition and morphology of OC have a large spatial and temporal variability. OC is composed of two main fractions, water insoluble organic carbon (WIOC) and water soluble organic carbon (WSOC) based on their solubility. Different to WIOC, which mainly consists of primary organic aerosol from direct emissions, water soluble organic carbon (WSOC) contains to a large part secondary organic aerosols (SOAs) formed in the atmosphere from volatile organic precursor compounds [Gelencsér et al., 2007]. WSOC typically contributed 20-80% of the total organic carbon depending on the season and region [Decesari et al., 2001; Ram and Sarin, 2010; Khare et al., 2011]. At the alpine high elevation site of Sonnblick (3106 m asl.), the ratio of WSOC/WIOC was about 1.5 [Pio et al., 2007]. WSOC is a major fraction of organic aerosols in the atmosphere, however, its sources are not well constrained. Recently carbonaceous aerosol have attracted a lot of attention because of their optical properties. BC/EC absorb solar radiation and heat up the atmosphere, whereas organic aerosols mostly cool the atmosphere [Japar et al., 1986; Penner et al., 1998; Maria et al., 2004]. In addition, when BC/EC is deposited on bright surfaces, like snow and ice, it can change the surface albedo and lead to warming.

An accurate estimation of climate forcing from carbonaceous aerosols requires good knowledge of temporal and spatial, fraction resolved emissions. Modelled aerosol climate forcing is highly uncertain and strongly depends on the pre-industrial aerosol loading [Carslaw et al., 2013]. The cloud albedo has a non-linear relationship with anthropogenic emissions (Figure 1.2). As consequence, the global mean cloud albedo of the pristine pre-industrial atmosphere was very sensitive to changes in emissions, with strong implications for the estimation of anthropogenic aerosol forcing [Carslaw et al., 2013]. Precise reconstructions of pre-industrial natural aerosol background will help to constrain the cloud albedo change due to anthropogenic emissions. Which in return could narrow down the uncertainty of radiative forcing due to anthropogenic aerosol emissions.

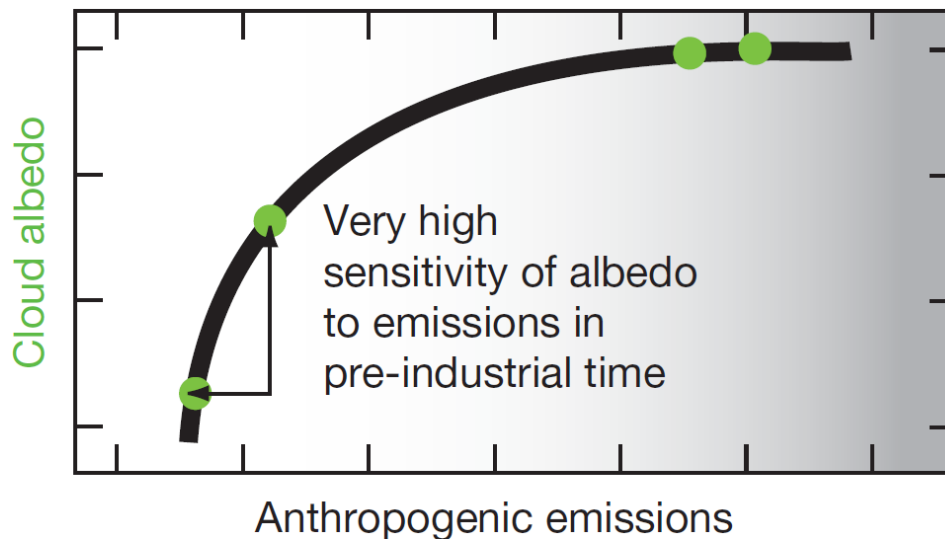


Figure 1.2 Cloud albedo changes in dependence of anthropogenic emissions. Due to the non-linear relationship, the cloud albedo is much more sensitive to changes in anthropogenic emissions in pre-industrial times compared to the industrial period. Figure adapted from Carslaw et al., 2013.

1.3 Glacier archives

There are many valuable climate archives (for example historical documents, tree rings, ice cores, lake and ocean sediments and peat bogs), which record the past climate related parameters (proxies) in different way. Tree rings and sediments can provide information about temperature and precipitation further back in time compared to historical documents. However, only ice cores preserve the atmospheric composition. Glaciers in mid and low latitudes and ice sheets in Polar Regions are natural archives of past precipitation, temperature, atmospheric composition and circulation. Snow deposits and accumulates on glaciers and is transformed into firn and ice through snow metamorphism. Inert gases are entrapped in air bubbles, from which they can be measured directly. Particles and soluble gases are taken up during cloud formation and snowfall (Figure 1.3). Records of atmospheric CO₂ concentration have been obtained back to 800,000 years ago from the European Project for Ice Coring in Antarctic (EPICA) Dome C ice core [Lüthi et al., 2008; Bereiter et al., 2015]. While these global

syntheses continue to make excellent use of individual polar records, there is also recognition of significant regional-scale variability that needs to be understood and reconciled with the broad view of insolation being the key driver of Holocene climate change, particularly in the high latitude Northern Hemisphere [Renssen et al., 2009].

Atmospheric aerosol particles incorporate into snow through in-cloud and below-cloud scavenging and are subsequently deposited on glaciers [Baltensperger et al., 1998]. Therefore, one of the most important approaches (the only direct approach) to constrain the pre-industrial aerosol burden is to obtain records from ice cores. However, Polar ice sheets are located far away from the source regions. On the other hand, high-alpine ice cores can provide paleoclimate and atmospheric information on decadal to millennial time scales, which allow reconstruction of climate and atmospheric composition from the most interesting transition period of pre-industrial to industrial [for example Schwikowski, 2004; Uglietti et al., 2016; Eyrikh et al., 2017]. In addition to that, these ice cores are from most densely populated regions, which are directly impacted by anthropogenic activities. Alpine glaciers offer the possibility to derive information on past changes in emission sources, atmospheric loading and composition of aerosols in Europe.

Major ion records (e.g. sulphate, nitrate, and ammonium) and trace element records from alpine glaciers have revealed that human activities have significant impact on atmospheric composition [Schwikowski, 2004; Eichler et al., 2012; Eyrikh et al., 2017]. Long-term high-resolution BC/EC records have been reported from multiple locations from Greenland to alpine glaciers [Ruppel et al., 2014; Osmont et al., 2018; Sigl et al., 2018], but pre-industrial records of OC aerosols are very rare [Lavanchy et al., 1999; Jenk et al., 2006; Legrand et al., 2007; May et al., 2013]. The very first historical records of carbonaceous aerosol (EC, WIOC, TC) were reconstructed from Colle Gnifetti, Swiss Alps [Lavanchy et al., 1999]. This record indicated the WIOC concentration had increased by factor of two to three times in 1980s compare to pre-industrial level. This increasing trend of OC in the 20th century was confirmed by another record from Col du Dôme ice core, French Alps later on [Legrand et al., 2007; Legrand et al., 2013]. Also the major fraction of organic aerosol, WSOC, which is analyzed in the ice as DOC and It may also contain organic gases taken up during snowfall, was for the first time measured in the same core. The average WSOC/WIOC concentration ratio is ~three in ice [Legrand et al., 2013]. To the best of our knowledge, however, there are no complete continuous high resolution

records of the three major fractions of carbonaceous aerosols (WIOC, WSOC, EC) from one ice, covering the whole period of pre-industrial up to modern time.

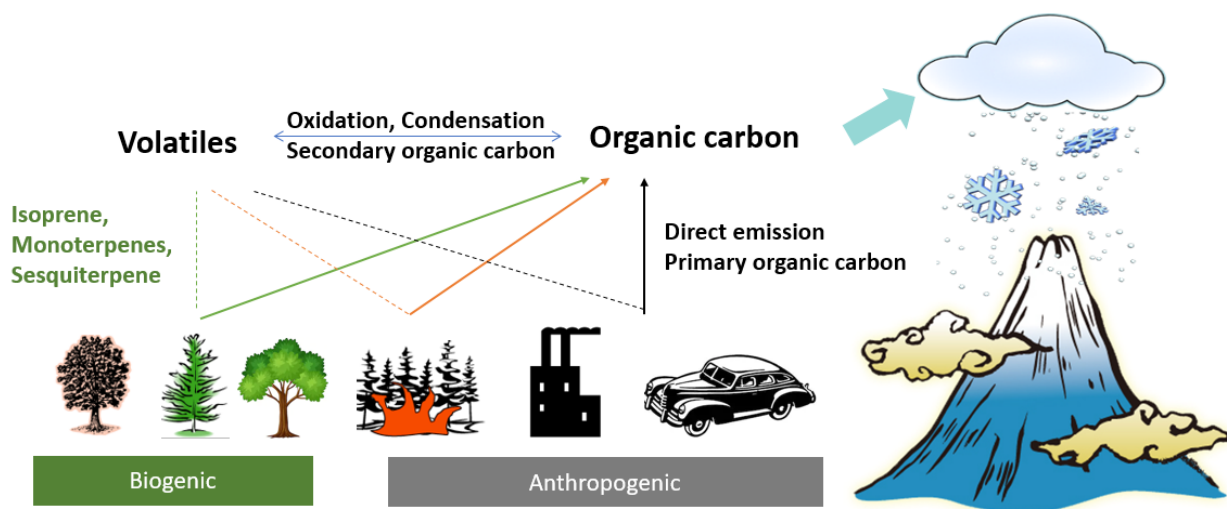


Figure 1.3 Sources of OC preserved in ice cores. Secondary organic carbon formed from biogenic and anthropogenic volatile compound emissions through chemical oxidation in the atmosphere. Together with primary organic carbon transport to higher altitude due to convection. Part of the organic aerosol deposited on the glacier through wet and dry deposition.

1.4 ^{14}C dating of ice cores

In order to interpret the climate record archived in glaciers, establishing a precise chronology is essential. Annual layer counting is one of the fundamental methods used for ice core dating. Which is based on seasonal variability in chemical and physical signals, like ammonium, water isotopes and conductivity. However, this method is only available down to a certain depth for Alpine ice cores due to the strong thinning in the deep part. Meanwhile, missed years or miscounting leads to accumulating errors with depth. Therefore, independent absolute dating is required for the validation of ice chronology. Absolute time horizons are helpful to pin down the age of the ice. The most profoundly identified event is the bomb test peak in 1963 (Figure 1.4). This signal is documented in multiple proxies, like the tritium and cesium peak. Besides that, volcano eruptions also are commonly used as time markers. They are indicated as peaks in sulfate, chloride and conductivity. During the 19th and 20th century, Katmai in 1912 and

Tambora in 1815 were observed in ice cores [Cole - Dai et al., 2009; Jenk et al., 2009]. The eruptions from 18th century (Laki eruption in 1783 and Pavlof in 1763) are also used for chronology validation [Winski et al., 2017]. Additionally, Saharan dust events are well documented during the 20th century, which can be easily identified in Alpine ice cores. The most common events are from 2000, 1977, 1947 and 1901 AD. However, all these Horizons are limited to a time length of hundred years.

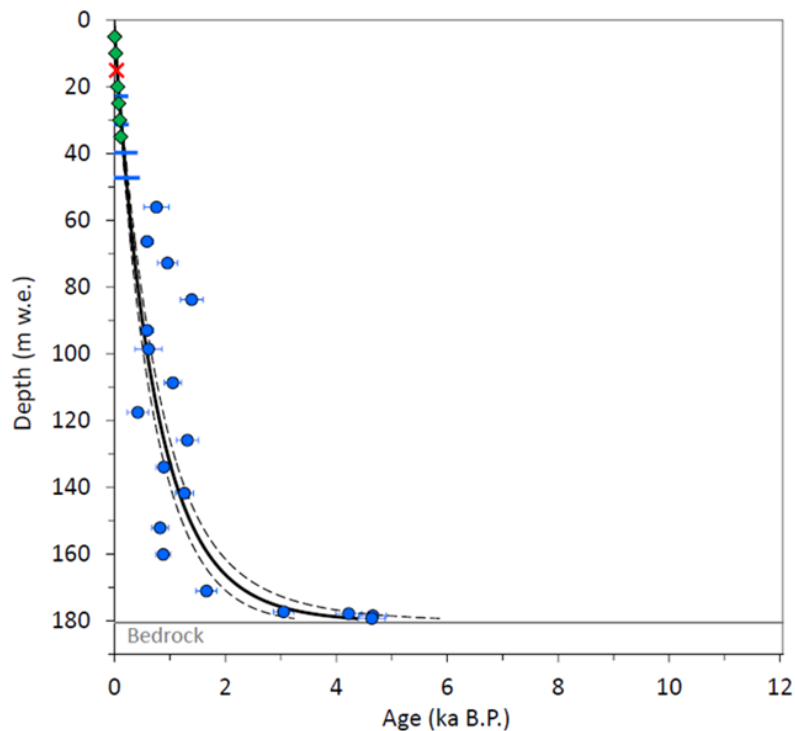


Figure 1.4 Depth age scale from Chongce core 4 from the north-western Tibetan Plateaus. Figure from Hou et al., 2018. The red cross stands for the tritium horizon (1963), green diamonds for ^{210}Pb ages, and the blue dots for calibrated ^{14}C ages of WIOC with 1σ error bar. The dashed lines represent the 1σ confidence interval of the $2p$ model fit (solid black line).

Radioactive elements contained in the ice offers another opportunity to obtain absolute dates from ice samples. The concentrations of ^{39}Ar and ^{32}Si are both very low requiring several kg of ice sample for dating [Morgenstern et al., 2010; Feng et al., 2019]. ^{210}Pb and ^{14}C are the most promising radioactive dating techniques. With the half-life of 22.3 years, ^{210}Pb can be used to date ice back to 200 years [Hou et al., 2018; Gägger et al., 2020]. But for the millennial

scale ice cores, ^{14}C dating is the ideal isotope, having a half-life of 5370 years which allows dating up to 26000 years [Godwin, 1960], which covers most of the time range for alpine glaciers [Uglietti et al., 2016]. To establish a completed depth age scale extrapolate down to the bedrock, ice flow models are typically used. The Figure 1.4 show an example of depth-age scale based on the combination of all these dating methods. Ice flow models require many basic assumptions like constant accumulation, which we know do not represent real conditions. All these assumptions introduce more bias into the bottom most part. Even with 3D models, which require complex geometry data, is still challenging to simulate the bottom age [Licciulli et al., 2020]. Meanwhile this underlines the importance to have absolute dating in the bottom part of the core.

The ^{14}C -dating method using the WIOC fraction has been applied for multiple mid-latitude ice cores, for example [Jenk et al., 2009; Sigl et al., 2009; Aizen et al., 2016; Uglietti et al., 2016; Hou et al., 2018]. Before the industrial period, carbonaceous aerosols were mainly emitted from the living biosphere and biomass burning as well as being produced by secondary organic aerosol formation from gaseous precursors. Consequently, this carbon reflects the contemporary atmospheric ^{14}C content. After deposition, the WIOC is incorporated into glacier snow, firn and ice and undergoes radioactive decay with a half-life of 5730 years [Godwin, 1962]. The Figure 1.5 demonstrates the location of samples dated with WIO ^{14}C worldwide. The improvement of ^{14}C measurement instrument precision reduced the required ice sample size. With a carbon amount larger than 10 μg a reasonable dating precision of 10-20% was obtained [Uglietti et al., 2016]. However, the low WIOC concentration in glaciers remote from sources, e.g. glaciers in the Polar Regions, puts a limit to this application.

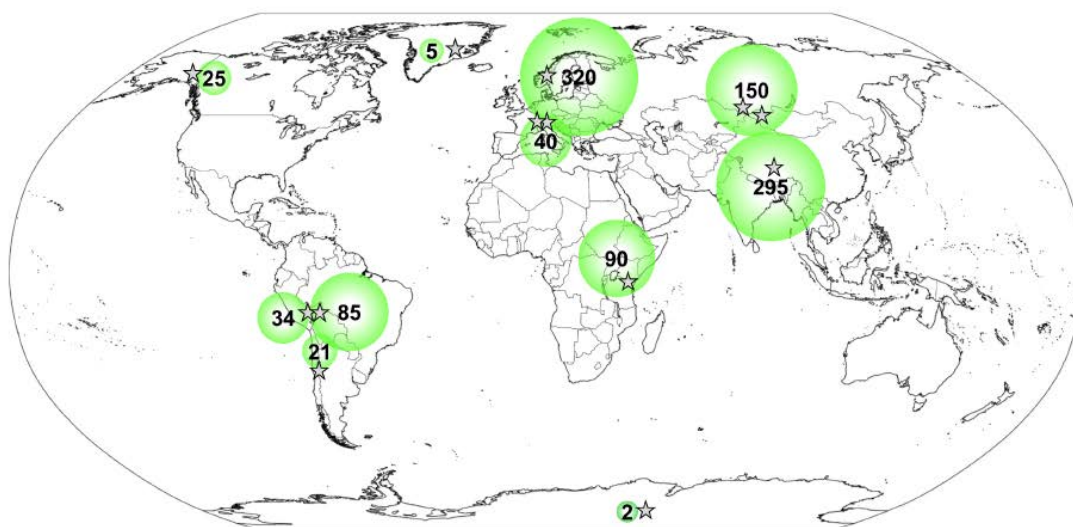


Figure 1.5 WIOC sample concentrations from worldwide samples. The location of samples indicated as star. Figure from Uglietti et al., 2016.

The relative higher concentrations of DOC compared to WIOC of around a factor of 5, i.e. 10 to 100 ppbC [Legrand et al., 2013; May et al., 2013], could allow dating of ice with too low WIOC concentration and may reach the achievable analytical (dating) uncertainty. The basic assumption of applying the DOC fraction for ^{14}C dating is similar to the WIOC dating approach [Jenk et al., 2009; Sigl et al., 2009], with DOC originating from the biosphere before anthropogenic fossil fuel contribution. The first attempt of DO^{14}C dating of ice cores was conducted by B. May, at the University of Heidelberg, who built a system for both DOC and WIOC fraction radiocarbon microanalysis [May, 2009]. However, in that work only super modern F^{14}C values were obtained, suggesting possible in-situ ^{14}C production. Since also the first ^{14}C dating results using the WIOC were rather questionable in May (2009) and in such cases conflicting with previous and proven findings from the pioneering studies in this field. The question how the in-situ produced ^{14}CO and $^{14}\text{CO}_2$ should interfere with organic species in the ice is still not resolved, unless there is carbon exchange between different reservoirs. This encourages the re-evaluation the possibility of DOC ^{14}C dating.

^{14}C analysis additionally could be used as tracer for the fossil fuel burning contribution to carbonaceous aerosol. Fossil carbon (like coal, natural gas, and petroleum) do not contain any ^{14}C and on the contrary biogenic carbon has a modern atmospheric ^{14}C content. Based on isotope mass balance, fossil fuel contribution to organic matter can be estimated [Zhang et al.,

2012]. There is only one record presenting long-term trends of WIOC and EC concentrations along with their corresponding fractions of modern carbon ($F^{14}C$, find definition in the Method section) which exists to date [Jenk et al., 2006]. This record indicated that fossil fuel significantly contributes to EC and OC since the 1850s. This core was only analyzed back to 1950 due to technical limitations at that time. ^{14}C -based source apportionment was applied to DOC in the Col du Dôme ice core, suggesting that 85% of the DOC increase from 1920 to 1990 is related to non-fossil origin [May et al., 2013]. Nevertheless, a complete ice core concentration record of the different bulk carbonaceous particle fractions WIOC, WSOC, and EC, along with their fossil and non-fossil contributions covering the preindustrial time to the present would be a fundamental help to constrain source contributions, emission estimates, and the effect of atmospheric aerosols on global and/or regional climate

1.5 Objectives

There are two main objectives for this thesis are: To obtain the first complete ice core record of all carbonaceous aerosol fractions (EC, WIOC and WSOC) including the historical fossil and non-fossil contributions over the pre-industrial to industrial transition period. These carbonaceous aerosol records could help narrow down the uncertainty of aerosol radiative forcing in climate models. Secondary, to re-evaluate the feasibility of using ^{14}C analysis on DOC fraction for ice core dating. To reach these goals:

1. Optimize the DOC extraction method for the PSI DOC extraction setup which was built by Schindler [J Schindler, 2017].
2. Applying the DOC extraction technique for ^{14}C analysis to multiple bottom ice samples that are independently dated by WIO ^{14}C dating from different alpine glaciers to investigate the possibility of applying the ^{14}C analysis on DOC fraction for dating purpose.
3. Complete the atmospheric carbonaceous aerosol (EC, WIOC, and WSOC) records including the fossil and non-fossil sources over the pre-industrial to industrial transition period from Fiescherhorn ice cores. The WIOC/EC records have been published from 1650 to 1940 [Jenk et al., 2006]. The new decontamination analytical

method for firn samples could allow extending the WIOC/EC records up to 2000s [Cao et al., 2013]. In addition, it combined with the new DOC extraction method to estimate WSOC record.

4. To obtain the natural organic carbon background variation before the industrial revolution
5. To quantify the impact of the anthropogenic emissions on organic aerosol by comparing these ice core carbonaceous records with atmospheric loading estimates based on emission databases.

All these goals are based on the technique to extract DOC from large ice cores sample for ^{14}C analysis. Therefore, this thesis composed of two main parts, optimizing the DOC extraction setup and applying it to ice core samples. The thesis is structured as follows:

Chapter 2 gives an overview on the methodology we used in this study, the instrument and the analytical setup applied to ice core samples.

Chapter 3 is the optimization of the DOC extraction setup for ^{14}C analysis in ice cores. The focus is on the method development of radiocarbon analysis for low carbon content ice core samples. We try to minimize the contamination, the blank and to establish a reliable method to reconstruct the DOC concentration and ^{14}C measurement.

Chapter 4 is dedicated to the application of an optimized DOC extraction setup for ice core dating. The study of mid-latitude and tropical mountain glaciers is limited by the lack of dating techniques due to complex bedrock geometry and strong annual layer thinning. Water-insoluble organic carbon (WIOC) in glacier ice has been used for radiocarbon dating for years. However, in some cases this method is restricted by the low WIOC concentration. The majority of organic carbon is preserved in water soluble form. To investigate the suitability of DOC for ice core dating, we applied both the DOC extraction setup and the WIOC filtration setup to four glaciers in different location.

As a case study of ice core dating based on both WIOC and DOC analysis is shown in Chapter 5. A 208 m core was drilled in 2013 from Mt. Hunter, Alaska. The upper 190m was well dated by Annual Layer Counting and horizons. But in the deeper part, the seasonal signal vanish due to the strong thinning and low sample resolution. To obtain the chorology of whole

core, ^{14}C analysis of organic carbon is applied to the bottom 20m. We established the depth age scale for the Mt. Hunter core by the combination of ALC, ^{14}C dating and the 2p flow model.

Chapter 6 describes the complete high-resolution carbonaceous aerosol records with corresponding ^{14}C values from the Fiescherhorn ice core, a 340-year concentration record of WSOC, EC and WIOC from the pre-industrial to the industrial transition period. Each component is separated into fossil and non-fossil contributions based on the ^{14}C analysis. Combined with the inorganic aerosol concentration records from the Fiescherhorn ice core to reconstruct the variability of aerosol over the last 340 years and evaluating the impact to aerosol due to anthropogenic activities.

Finally, conclusion and outlook are provided in Chapter 7.

An accurate estimation of climate forcing from carbonaceous aerosols requires good knowledge of historical, fraction resolved emissions. Systematically established historical records of carbonaceous particles for long-term abundance and fossil/non-fossil contributions would be helpful to understand the impact of atmospheric aerosols on global and/or regional climate, which is a prerequisite for a reasonable implementation of air pollution and climate mitigation measures. An accurate age is also crucial for the interpretation of these ice core records. ^{14}C analysis of organic carbon preserved in ice provides an important tool for dating the ice cores. This thesis is dedicated to investigating the potential of ^{14}C analysis of carbonaceous aerosols in ice cores.

Bibliography

Aizen, E. M., V. B. Aizen, N. Takeuchi, P. A. Mayewski, B. Grigholm, D. R. Joswiak, S. A. Nikitin, K. Fujita, M. Nakawo and A. Zapf. Abrupt and moderate climate changes in the mid-latitudes of Asia during the Holocene. *Journal of Glaciology* **62**, 411-439, (2016).

Andreae, M. O. and P. J. Crutzen. Atmospheric aerosols: Biogeochemical sources and role in atmospheric chemistry. *Science* **276**, 1052-1058, (1997).

Baltensperger, U., M. Schwikowski, D. Jost, S. Nyeki, H. Gäggeler and O. Poulida. Scavenging of atmospheric constituents in mixed phase clouds at the high-alpine site Jungfrauoch part I: Basic concept and aerosol scavenging by clouds. *Atmospheric Environment* **32**, 3975-3983, (1998).

Bereiter, B., S. Eggleston, J. Schmitt, C. Nehrass-Ahles, T. F. Stocker, H. Fischer, S. Kipfstuhl and J. Chappellaz. Revision of the EPICA Dome C CO₂ record from 800 to 600 kyr before present. *Geophysical Research Letters* **42**, 542-549, (2015).

Cao, F., Y.-L. Zhang, S. Szidat, A. Zapf, L. Wacker and M. Schwikowski. Microgram level radiocarbon determination of carbonaceous particles in firn samples: pre-treatment and OC/EC separation. *Radiocarbon* **55**, 383-390 (2013). 10.2458/azu_js_rc.55.16291

Carslaw, K., L. Lee, C. Reddington, K. Pringle, A. Rap, P. Forster, G. Mann, D. Spracklen, M. Woodhouse and L. Regayre. Large contribution of natural aerosols to uncertainty in indirect forcing. *Nature* **503**, 67-71, (2013).

Cole-Dai, J., D. Ferris, A. Lanciki, J. Savarino, M. Baroni and M. H. Thiemens. Cold decade (AD 1810–1819) caused by Tambora (1815) and another (1809) stratospheric volcanic eruption. *Geophysical Research Letters* **36**, (2009).

Decesari, S., M. Facchini, E. Matta, F. Lettini, M. Mircea, S. Fuzzi, E. Tagliavini and J.-P. J. A. E. Putaud. Chemical features and seasonal variation of fine aerosol water-soluble organic compounds in the Po Valley, Italy. **35**, 3691-3699, (2001).

DeMott, P. J., A. J. Prenni, X. Liu, S. M. Kreidenweis, M. D. Petters, C. H. Twohy, M. Richardson, T. Eidhammer and D. Rogers. Predicting global atmospheric ice nuclei distributions and their impacts on climate. *Proceedings of the National Academy of Sciences* **107**, 11217-11222, (2010).

Dhainaut, J.-F., Y.-E. Claessens, C. Ginsburg and B. Riou. Unprecedented heat-related deaths during the 2003 heat wave in Paris: consequences on emergency departments. *Critical care* **8**, 1, (2003).

Eichler, A., L. Tobler, S. Eyrikh, G. Gramlich, N. Malygina, T. Papina and M. Schwikowski. Three centuries of Eastern European and Altai lead emissions recorded in a Belukha ice core. *Environmental science & technology* **46**, 4323-4330, (2012).

Eyrikh, S., A. Eichler, L. Tobler, N. Malygina, T. Papina and M. Schwikowski. A 320 year ice-core record of atmospheric Hg pollution in the Altai, central Asia. *Environmental science & technology* **51**, 11597-11606, (2017).

Feng, Z., P. Bohleber, S. Ebser, L. Ringena, M. Schmidt, A. Kersting, P. Hopkins, H. Hoffmann, A. Fischer and W. Aeschbach. Dating glacier ice of the last millennium by quantum technology. *Proceedings of the National Academy of Sciences* **116**, 8781-8786, (2019).

Gäggeler H., Tobler L., Schwikowski M., and Jenk T., Application of the radionuclide ²¹⁰Pb in glaciology- an overview. *Journal of Glaciology*, (2020).

Gelencsér, A., B. May, D. Simpson, A. Sánchez-Ochoa, A. Kasper-Giebl, H. Puxbaum, A. Caseiro, C. Pio and M. Legrand. Source apportionment of PM_{2.5} organic aerosol over Europe: Primary/secondary, natural/anthropogenic, and fossil/biogenic origin. *Journal of Geophysical Research: Atmospheres* **112**, (2007).

Godwin, H. J. N. Half-life of radiocarbon. **195**, 984, (1962).

Gordon, H., K. Sengupta, A. Rap, J. Duplissy, C. Frege, C. Williamson, M. Heinritzi, M. Simon, C. Yan and J. Almeida. Reduced anthropogenic aerosol radiative forcing caused by biogenic new particle formation. *Proceedings of the National Academy of Sciences* **113**, 12053-12058, (2016).

Hou, S., T. M. Jenk, W. Zhang, C. Wang, S. Wu, Y. Wang, H. Pang and M. J. T. C. Schwikowski. Age ranges of the Tibetan ice cores with emphasis on the Chongce ice cores, western Kunlun Mountains. **12**, 2341-2348, (2018).

Japar, S., W. Brachaczek, R. Gorse Jr, J. Norbeck and W. Pierson. The contribution of elemental carbon to the optical properties of rural atmospheric aerosols. *Atmospheric Environment (1967)* **20**, 1281-1289, (1986).

Jenk, T. M., S. Szidat, D. Bolius, M. Sigl, H. W. Gaeggeler, L. Wacker, M. Ruff, C. Barbante, C. F. Boutron and M. J. J. o. G. R. A. Schwikowski. A novel radiocarbon dating technique applied to an ice core from the Alps indicating late Pleistocene ages. **114**, (2009).

Jenk, T. M., S. Szidat, M. Schwikowski, H. W. Gaggeler, S. Brutsch, L. Wacker, H. A. Synal and M. Saurer. Radiocarbon analysis in an Alpine ice core: record of anthropogenic and biogenic contributions to carbonaceous aerosols in the past (1650-1940). *Atmospheric Chemistry and Physics* **6**, 5381-5390, (2006).

Kanakidou, M., J. Seinfeld, S. Pandis, I. Barnes, F. Dentener, M. Facchini, R. Van Dingenen, B. Ervens, A. Nenes and C. Nielsen. Organic aerosol and global climate modelling: a review. (2005).

Khare, P., B. Baruah, P. J. T. B. C. Rao and P. Meteorology. Water-soluble organic compounds (WSOCs) in PM_{2.5} and PM₁₀ at a subtropical site of India. **63**, 990-1000, (2011).

Kiehl, J. and B. Briegleb. The relative roles of sulfate aerosols and greenhouse gases in climate forcing. *Science* **260**, 311-314, (1993).

Lavanchy, V., H. Gäggeler, S. Nyeki and U. Baltensperger. Elemental carbon (EC) and black carbon (BC) measurements with a thermal method and an aethalometer at the high-alpine research station Jungfraujoch. *Atmospheric Environment* **33**, 2759-2769, (1999).

Legrand, M., S. Preunkert, B. Jourdain, J. Guilhermet, X. Fain, I. Alekhina and J. R. Petit. Water-soluble organic carbon in snow and ice deposited at Alpine, Greenland, and Antarctic sites: a critical review of available data and their atmospheric relevance. *Climate of the Past* **9**, 2195-2211, (2013). DOI 10.5194/cp-9-2195-2013

Legrand, M., S. Preunkert, B. May, J. Guilhermet, H. Hoffman and D. Wagenbach. Major 20th century changes of the content and chemical speciation of organic carbon archived in Alpine ice cores: Implications for the long-term change of organic aerosol over Europe. *Journal of Geophysical Research: Atmospheres* **118**, 3879-3890, (2013).

Legrand, M., S. Preunkert, M. Schock, M. Cerqueira, A. Kasper-Giebl, J. Afonso, C. Pio, A. Gelencsér and I. Dombrowski-Etchevers. Major 20th century changes of carbonaceous aerosol components (EC, WinOC, DOC, HULIS, carboxylic acids, and cellulose) derived from Alpine ice cores. *Journal of Geophysical Research* **112**, (2007). 10.1029/2006jd008080

Licciulli, C., P. Bohleber, J. Lier, O. Gagliardini, M. Hoelzle and O. Eisen. A full Stokes ice-flow model to assist the interpretation of millennial-scale ice cores at the high-Alpine drilling site Colle Gnifetti, Swiss/Italian Alps. *Journal of Glaciology* **66**, 35-48, (2020).

Lohmann, U. and J. Feichter. Global aerosol indirect effects: A review. *Atmos. Chem. Phys* **5**, 715-737, (2005).

Lüthi, D., M. Le Floch, B. Bereiter, T. Blunier, J.-M. Barnola, U. Siegenthaler, D. Raynaud, J. Jouzel, H. Fischer and K. Kawamura. High-resolution carbon dioxide concentration record 650,000–800,000 years before present. *Nature* **453**, 379-382, (2008).

Maria, S. F., L. M. Russell, M. K. Gilles and S. C. Myneni. Organic aerosol growth mechanisms and their climate-forcing implications. *Science* **306**, 1921-1924, (2004).

May, B., D. Wagenbach, H. Hoffmann, M. Legrand, S. Preunkert and P. Steier. Constraints on the major sources of dissolved organic carbon in Alpine ice cores from radiocarbon analysis over the bomb-peak period. *Journal of Geophysical Research: Atmospheres* **118**, 3319-3327, (2013).

May, B. L. Radiocarbon microanalysis on ice impurities for dating of Alpine glaciers, PhD dissertation, University of Heidelberg (2009).

Morgenstern, U., L. K. Fifield, S. G. Tims and R. G. Ditchburn. Progress in AMS measurement of natural ³²Si for glacier ice dating. *Nuclear Instruments and Methods in Physics Research Section B: Beam Interactions with Materials and Atoms* **268**, 739-743, (2010).

- McCormick, R. A. and J. H. Ludwig. Climate modification by atmospheric aerosols. *Science* **156**, 1358-1359, (1967).
- Miller, R. and I. Tegen. Climate response to soil dust aerosols. *Journal of climate* **11**, 3247-3267, (1998).
- Neukom, R., N. Steiger, J. J. Gómez-Navarro, J. Wang and J. P. Werner. No evidence for globally coherent warm and cold periods over the preindustrial Common Era. *Nature* **571**, 550-554, (2019).
- Osmont, D., I. A. Wendl, L. Schmidely, M. Sigl, C. Vega, E. Isaksson and M. Schwikowski. An 800-year high-resolution black carbon ice core record from Lomonosovfonna, Svalbard. *Atmospheric Chemistry and Physics* **18**, 12777-12795, (2018).
- Penner, J., C. Chuang and K. Grant. Climate forcing by carbonaceous and sulfate aerosols. *Climate Dynamics* **14**, 839-851, (1998).
- Pio, C. A., M. Legrand, T. Oliveira, J. Afonso, C. Santos, A. Caseiro, P. Fialho, F. Barata, H. Puxbaum and A. J. J. o. G. R. A. Sanchez-Ochoa. Climatology of aerosol composition (organic versus inorganic) at nonurban sites on a west-east transect across Europe. **112**, (2007).
- Putaud, J.-P., F. Raes, R. Van Dingenen, E. Brüggemann, M.-C. Facchini, S. Decesari, S. Fuzzi, R. Gehrig, C. Hüglin and P. Laj. A European aerosol phenomenology—2: chemical characteristics of particulate matter at kerbside, urban, rural and background sites in Europe. *Atmospheric Environment* **38**, 2579-2595, (2004).
- Ram, K. and M. Sarin. Spatio-temporal variability in atmospheric abundances of EC, OC and WSOC over Northern India. *Journal of Aerosol Science* **41**, 88-98, (2010).
- Renssen, H., H. Seppä, O. Heiri, D. Roche, H. Goosse and T. Fichefet. The spatial and temporal complexity of the Holocene thermal maximum. *Nature geoscience* **2**, 411-414, (2009).
- Ruppel, M. M., I. Isaksson, J. Strom, E. Beaudon, J. Svensson, C. A. Pedersen and A. Korhola. Increase in elemental carbon values between 1970 and 2004 observed in a 300-year ice core from Høltedahlfonna (Svalbard). *Atmospheric Chemistry and Physics* **14**, 11447-11460, (2014). 10.5194/acp-14-11447-2014
- Schindler, J. An Extraction System for Radiocarbon Microanalysis of Dissolved Organic Carbon in Glacier Ice, PhD dissertation, Universität Bern,(2017).
- Schwikowski, M. Reconstruction of European air pollution from Alpine ice cores. *Earth Paleoenvironments: records preserved in mid-and low-latitude glaciers*, Springer: 95-119. (2004).
- Sigl, M., N. Abram, J. Gabrieli, T. M. Jenk, D. Osmont and M. Schwikowski. 19th century glacier retreat in the Alps preceded the emergence of industrial black carbon deposition on high-alpine glaciers. (2018).

Sigl, M., T. M. Jenk, T. Kellerhals, S. Szidat, H. W. Gäggeler, L. Wacker, H.-A. Synal, C. Boutron, C. Barbante and J. Gabrieli. Towards radiocarbon dating of ice cores. *Journal of Glaciology* **55**, 985-996, (2009).

Uglietti, C., A. Zapf, T. M. Jenk, M. Sigl, S. Szidat, G. A. Salazar Quintero and M. Schwikowski. Radiocarbon dating of glacier ice: overview, optimisation, validation and potential. *The Cryosphere* **10**, 3091-3105, (2016).

IPCC, 2013: Climate Change 2013: The Physical Science Basis. Contribution of Working Group I to the Fifth Assessment Report of the Intergovernmental Panel on Climate Change [Stocker, T.F., D. Qin, G.-K. Plattner, M. Tignor, S.K. Allen, J. Boschung, A. Nauels, Y. Xia, V. Bex and P.M. Midgley (eds.)]. Cambridge University Press, Cambridge, United Kingdom and New York, NY, USA, 1535 pp, doi:10.1017/CBO9781107415324

IPCC, 2018: Global warming of 1.5°C. An IPCC Special Report on the impacts of global warming of 1.5°C above pre-industrial levels and related global greenhouse gas emission pathways, in the context of strengthening the global response to the threat of climate change, sustainable development, and efforts to eradicate poverty [V. Masson-Delmotte, P. Zhai, H. O. Pörtner, D. Roberts, J. Skea, P.R. Shukla, A. Pirani, W. Moufouma-Okia, C. Péan, R. Pidcock, S. Connors, J. B. R. Matthews, Y. Chen, X. Zhou, M. I. Gomis, E. Lonnoy, T. Maycock, M. Tignor, T. Waterfield (eds.)]. In Press.

Winski, D., E. Osterberg, D. Ferris, K. Kreutz, C. Wake, S. Campbell, R. Hawley, S. Roy, S. Birkel and D. Introne. Industrial-age doubling of snow accumulation in the Alaska Range linked to tropical ocean warming. *Scientific reports* **7**, 1-12, (2017).

World Health Organization. Quantitative risk assessment of the effects of climate change on selected causes of death, 2030s and 2050s. World Health Organization (2014).

World Health Organization. Global Ambient Air Quality Database (2018).

Yttri, K. E., W. Aas, A. Bjerke, D. Ceburnis, C. Dye, L. Emblico, M. Facchini, C. Forster, J. Hanssen and H. Hansson. Elemental and organic carbon in PM 10: a one year measurement campaign within the European Monitoring and Evaluation Programme EMEP. (2007).

Zhang, Y. L., N. Perron, V. G. Ciobanu, P. Zotter, M. C. Minguillón, L. Wacker, A. S. H. Prévôt, U. Baltensperger and S. Szidat. On the isolation of OC and EC and the optimal strategy of radiocarbon-based source apportionment of carbonaceous aerosols. *Atmospheric Chemistry and Physics* **12**, 10841-10856, (2012).

2 Methodology

2.1 Separation of the particulate organic and elemental carbon fraction

For ice core samples the particulate organic carbon (POC) is considered to represent the water insoluble organic carbon (WIOC) fraction, since the water soluble fraction (WSOC) will dissolve into water as dissolved organic carbon (DOC) during melting. Sample preparation and decontamination followed the protocol in [Uglietti et al., 2016]. All sample cutting was carried out in a cold room (-20°C). To decontaminate the sample, surface layer ($\sim 3\text{mm}$) of ice was cut away in the cold room. Sections were combined, aiming for an overall ice mass of 200-700 g to yield enough carbon for radiocarbon analysis, and stored in 1 L pre-cleaned PETG containers (Semadeni, Switzerland). Samples were further decontaminated by removing the outer layer through rinsing with ultra-pure water in a laminar flow box, melted at room temperature and acidified with 20 ml 1M HCl. Melted ice samples were sonicated for 5 min, before vacuum filtration using pre-heated quartz fiber filters (Pallflex Tissuquartz™, 2500QAO-UP, ~ 11 mm diameter, pre-heated for 5h at 800°C). Particles on the filters were subsequently acidified with ~ 50 μL of 0.2 M HCl for 1 h to remove carbonates. After rinsing with 5ml ultra-pure water to remove HCl, filters were again placed for ~ 1 h in a class 100 laminar flow-box until completely dry. The filters were packed in aluminium foil and kept frozen until analysis.

WIOC and EC were separated with a recently developed thermal-optical method (Swiss_4S), quantified with a non-dispersive infrared (NDIR) detector using a commercial OC/EC analyzer (Sunset Laboratory Inc., USA) and evolving CO_2 was individually trapped cryogenically and finally sealed in glass ampoules for ^{14}C analysis [Zhang et al., 2012; Cao et al., 2013]. The Sunset Laboratory Carbon Aerosol Analyzer applies a proven thermal-optical method to analyze organic and elemental carbon aerosols collected on quartz filters and has been used to analyze a wide variety of aerosol samples to determine the aerosol composition and sources. The particles are thermally desorbed from the filter medium under an inert helium atmosphere followed by an oxidizing atmosphere, using carefully controlled heating ramps. The Swiss_4S protocol has four temperature steps from 375°C to 475°C for OC and 650°C to

completed remove remaining OC then heat up to 760 °C for EC (Figure 2.1). The filter transmittance is monitored by a 660 nm laser shown as the red line in Figure 2.1. This is used for correcting the loss or formation EC by charring during the thermal heating. The resulting CO₂ gas is quantified by the NDIR cell. In contrast to the previously used purely thermal method [Szidat et al., 2004; Jenk et al., 2007], losses or artificial formation (charring) of EC during the thermal treatment was evaluated by monitoring the optical transmittance of the filter samples. This Swiss_4S protocol allowed to significantly suppress charring, which on average accounted for less than 10% EC only [Zhang et al., 2012].

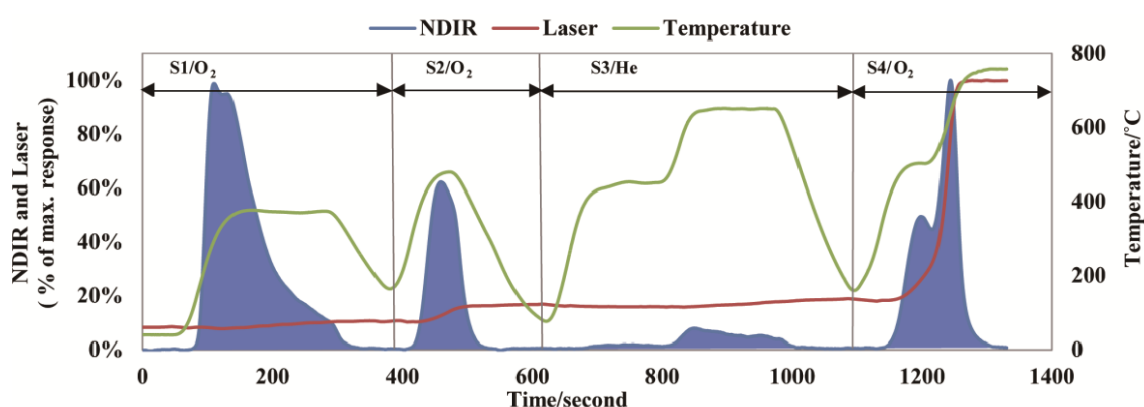


Figure 2.1 Thermal and optical program of water extracted aerosol samples using the Swiss_4S protocol. Laser signal and temperature are indicated as red and green lines, respectively. The blue areas are the NDIR detected CO₂ peaks. Figure from Zhang et al., 2012.

2.2 DOC extraction for ¹⁴C analysis

The analysis of the WSOC aerosol related DOC fraction has been more challenging due to higher potential of contamination by gases ubiquitously present in lab air such as formic and acetic acid. Further, DOC extraction efficiency is generally low from 64 to 96% and time consuming with oxidation time up to 2hours [May et al., 2013; Steier et al., 2013] or not suitable for ice core ¹⁴C analysis with low carbon content [Preunkert et al., 2010; Lang et al., 2016]. A new setup, as show in the Figure 2.2, was designed and built in our laboratory for DOC oxidation under inert gas conditions. DOC is photochemically oxidized to CO₂ gas by ultraviolet (UV) light and the produced CO₂ is purified, quantified with a manometer, and

collected in a glass ampoule for ^{14}C analysis. Details about the development and improvements are presented in chapter 3. Sample preparation followed the instructions in Fang et al., 2019. The outer layer (~3mm) of the ice samples was removed in the cold room at -20°C , similar to the samples for WIOC/EC analysis. After transfer to the laboratory, samples were further decontaminated by rinsing with ultrapure water under helium atmosphere in the melting vessel of the extraction setup, where they were also melted under helium flow. There is an extra decontamination step to remove the potential system contamination before filtrating the sample into the reactor. 50 mL ultra-pure water injected into the reactor and acidified with 1mL of 85% H_3PO_4 . To enhance the oxidation efficiency, 2 mL of 100 ppm FeSO_4 and 1mL of 50 mM H_2O_2 (Fenton's reagent) are also injected into the base water based on the study from Hsueh et al., 2005 and Kušić et al., 2006. UV irradiation for ~20-30mins is used to prepare a clean system and base water. After the ice had melted, the meltwater was filtrated using a pre-baked (heated at 800°C for 5 hours) quartz fibre filter. Filtration was also performed under helium gas flow, always preserving a little overpressure to prevent ambient air from leaking into the setup. The sample volume was determined by measuring the reactor fill level. The filtrate was acidified by mixing with the base water. After the degassing of inorganic carbon (IC), 1 mL of 50 mM H_2O_2 was injected into reactor right before the irradiation started. During UV oxidation, water vapor was removed by cryogenic trapping at -60°C and produced CO_2 was trapped in liquid nitrogen. The sample CO_2 was further cleaned from residual water vapor and quantified manometrically. In the end, CO_2 was sealed into a glass vial for ^{14}C analyses. The setup can process ice samples of up to 350 g mass and offers ultra-clean working conditions for all extraction steps. For an irradiation time of 30 minutes with catalyzation by addition of Fenton's reagent, an average efficiency of $96 \pm 6\%$ was achieved. Inert gas working conditions and stringent decontamination procedures resulted in a low overall blank of $1.9 \pm 1.6 \mu\text{g C}$ with an F^{14}C value of 0.68 ± 0.13 . This makes it possible to analysis the DOC in ice samples with a carbon content of as low as $25 \mu\text{g kg}^{-1}$ ice. The comparison with other devices for ^{14}C analyses of DOC shows the setup performs excellent in terms of low carbon background with the advantage of higher carbon yields while keeping analysis time low. This was achieved thanks to sample treatment under inert gas conditions, a thorough decontamination procedure of the system prior to sample loading and an enhanced UV oxidation efficiency by taking advantage of the Fenton catalytic reaction.

DOC concentrations were calculated from measured CO₂ pressure and sample volume. However, the DOC present in ice samples is not just formed by the WSOC fraction in the aerosol, but also includes organic gases scavenged from the atmosphere. Legrand et al., 2007 proposed using DOC, after subtracting monoacids and formaldehyde, as proxy of WSOC preserved in ice cores. For the reconstruction of historical carbonaceous aerosol concentrations, in this work the WSOC fraction was estimated by subtracting the concentrations of the most abundant monoacids, formic acid and acetic acid from the DOC concentration. Concentrations of formic acid and acetic acid were analyzed with ion chromatography. For other organic gases (like formaldehyde) no correction was applied, but their overall effect is estimated to be small, i.e. in the range of a few ppbC, due to their low concentrations in ice (< 5% of DOC in 1990s) [Legrand et al., 2013].

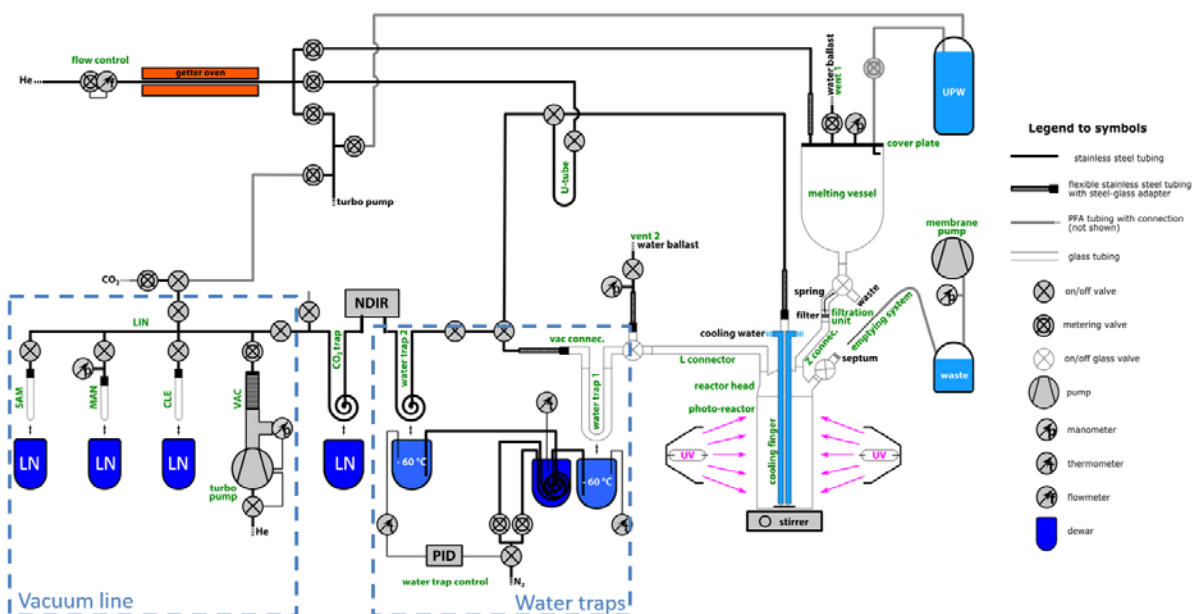
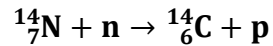


Figure 2.2 Scheme of the DOC extraction setup. Green text labels individual components. UPW (ultra-pure water), LN (liquid nitrogen), NDIR (CO₂ detector), LN (liquid nitrogen, vacuum manifold), VAC (pump manifold), CLE (cleaning tube), MAN (manometry cell), SAM (sampling tube). The detail see in Chapter 3. Figure from Fang et al., 2019.

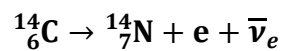
2.3 Radiocarbon analysis

2.3.1 General concept

Although there are 15 carbon isotopes, only three (^{12}C , ^{13}C and ^{14}C) are widely distributed in nature [Lide, 2007]. ^{12}C and ^{13}C are stable carbon isotopes, and ^{14}C is radioactive. ^{14}C is naturally produced by the spallation reaction of nitrogen with a neutron originating from cosmic rays mainly in the lower stratosphere through the following reaction [Libby 1946]:



Where n is a neutron and p is a proton. The cosmic ray neutrons flux depends on the solar activity, solar magnetic field and Earth's magnetic field resulting in a natural temporal and spatial variation of the atmospheric ^{14}C concentration [Usoskin, 2017]. Produced ^{14}C is rapidly oxidized to ^{14}CO and $^{14}\text{CO}_2$. The latter takes part in the global carbon cycle, which is the exchange between atmospheric, oceanic, terrestrial and biosphere carbon reservoirs. When a living plant, animal or phytoplankton dies, it no longer exchanges with CO_2 . This starts the radioactive decay "clock." ^{14}C decays by emitting an electron, which transforms a neutron into a proton, converting ^{14}C back to its original stable ^{14}N form. ^{14}C is unstable and undergoes beta decay [Calvin et al., 1949] with a half-life of 5730 years [Godwin, 1962]:



Where e is an electron and $\bar{\nu}_e$ is an electron anti-neutrino. One neutron from ^{14}C decays to a proton and releases an electron and an anti-neutrino.

2.3.2 ^{14}C measurement

The initial ^{14}C measurements were based on counting of beta decays [Libby et al., 1952]. This is time consuming and large sample masses are required due to the low decay rate of ^{14}C . Accelerator mass spectrometry (AMS) allows directly detecting ^{14}C based on the atom mass instead of beta decay [Bennett et al., 1977; Nelson et al., 1977; Muller et al., 1978], thereby reducing the required sample sizes by a factor of about one thousand. A tabletop AMS system only aimed at ^{14}C analysis with dimensions of only $2.5 \times 3 \text{ m}^2$ was designed, built and tested at the Laboratory of Ion Beam Physics, ETH Zürich, Switzerland [Synal et al., 2007]. This MIni

Carbon Dating System (MICADAS) is based on a vacuum insulated acceleration unit that uses a commercially available 200 kV power supply to generate acceleration fields in a tandem configuration. The scheme of MICADAS is shown in the Figure 2.3 [Synal et al., 2007]. Although this systems application is limited to ^{14}C , the reduced the instrument size and avoidance of high voltage platforms fosters the operation at common laboratory environments. ^{14}C measurements in this thesis were carried out at the Laboratory for the Analysis of Radiocarbon at the Bern University (LARA) using a MICADAS equipped with a gas ion source (GIS) interface [Wacker et al., 2013; Szidat et al., 2014]. GIS is the interface for preparing and injection of the CO_2 gas sample to the Cs ion source of MICADAS. In LARA, the GIS can operate between different sample prepare systems, like Sunset OC/EC analyzer, Cracker and Elemental analyzer. The obtained filter samples from filtration are combusted with Sunset OC/EC analyzer that is directly connect to MICADAS though GIS. On the other hand, the glass vial sealed CO_2 gas produced from DOC is injected into MICADAS by the cracker system. This system is designed to break the glass vials mechanically under vacuum and deliver CO_2 gas to the Cs ion source with helium flow.

With the MICADAS, the ^{14}R ($^{14}\text{C}/^{12}\text{C}$) and ^{13}R ($^{13}\text{C}/^{12}\text{C}$) ratios are measured instead of radioactivity. Stable carbon isotope measurements are commonly reported compared to the ratio of $^{13}\text{C}/^{12}\text{C}$ in a standard:

$$\delta^{13}\text{C} = \left(\frac{^{13}\text{R}_{\text{sample}}}{^{13}\text{R}_{\text{standard}}} - 1 \right) \times 1000$$

Where $^{13}\text{R}_{\text{sample}}$ and $^{13}\text{R}_{\text{standard}}$ are the $^{13}\text{C}/^{12}\text{C}$ ratios of sample and standard, respectively. All the ^{14}C measurements have to be corrected with the ^{13}C values for fractionation effects in the AMS [Stuiver and Polach, 1977]:

$$^{14}\text{R}_{\text{SN}} = ^{14}\text{R} \times \left(1 - 2 \times \left(\frac{\delta^{13}\text{C} + 25}{1000} \right) \right)$$

Where $^{14}\text{R}_{\text{SN}}$ is the sample normalized to $\delta^{13}\text{C} = -25\text{‰}$ and the ^{14}R is the measurement ratio. All ^{14}C results are expressed as F^{14}C which is originally defined as the fraction of the normalized specific activity of sample A_{SN} to normalized radiocarbon standard A_{ON} in the year 1950 [Stuiver and Polach, 1977].

$$F^{14}C = \frac{A_{SN}}{A_{ON}}$$

However, for the measurements from MICADAS are the isotope ratios. $F^{14}C$ values are calculated following the equation proposed in Reimer et al., 2004. All the $F^{14}C$ values of filter samples were corrected for constant contamination ($0.91 \pm 0.18 \mu\text{g}$ with $F^{14}C$ of 0.72 ± 0.11) and cross contamination (0.2 % from the previous sample) for the Sunset-GIS-MICADS system. $F^{14}C$ values of DOC samples were corrected for constant ($0.06 \pm 0.18 \mu\text{g}$ with $F^{14}C$ of 0.50 ± 0.11) and cross contamination (0.2 % from the previous sample) from MICADAS and the cracker system. In addition to the instrument related corrections, $F^{14}C$ of WIOC was corrected for the filtration procedural blanks with a carbon mass of $1.26 \pm 0.59 \mu\text{g}$ and an $F^{14}C$ value of 0.69 ± 0.15 (average of 76 values over last 16 years). The blank contribution for $F^{14}C$ of EC is small because the carbon mass of the EC blank ($0.42 \pm 0.36 \mu\text{g}$) with an estimated $F^{14}C$ value of $\sim 0.30 \pm 0.30$ is around 10 times lower than the ^{14}C -AMS limit of detection ($\sim 3\text{-}5 \mu\text{g}$, Ruff et al., 2010). For the DOC extraction setup, $1.9 \pm 1.6 \mu\text{g}$ with $F^{14}C$ of 0.68 ± 0.13 is used for total blank correction (average of 26 values and 2 years). All these uncertainties were propagated throughout whole data processing until final ^{14}C calibration.

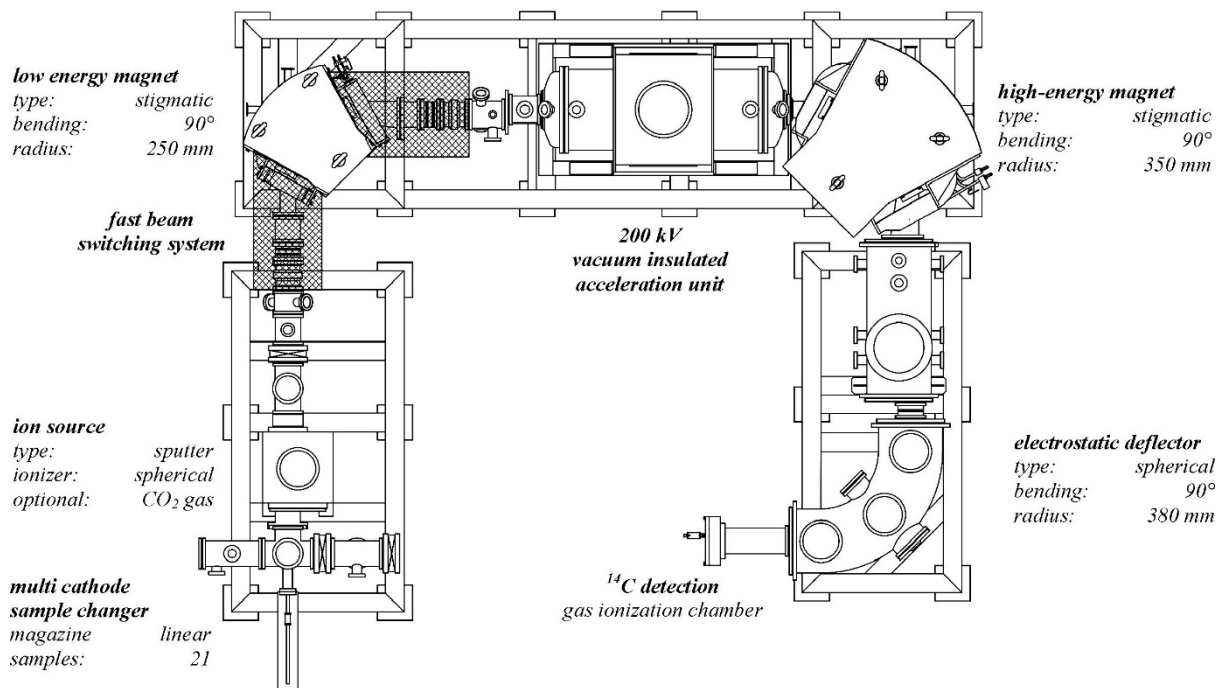


Figure 2.3 Scheme of MICADAS from Synal et al., 2007.

2.3.3 ¹⁴C applications

2.3.3.1 Dating

¹⁴C has been used widely as timer in archeology, geology, geochemistry and other scientific studies because of the well-determined half-life. The carbon clock starts when the material is isolated from the environment and there is no carbon exchange anymore. From then on ¹⁴C slowly decays. By determining how many ¹⁴C isotopes are left, the time when this material became isolated from environment can be estimated by the radioactive decay law:

$$A(t) = A_0 e^{-\lambda t}$$

$A(t)$ is the activity at the time t and A_0 is the initial activity in the sample. λ is the decay constant and t gives the age. The conventional ¹⁴C age also defined as:

$$t = -8033 \ln\left(\frac{A_{SN}}{A_{ON}}\right)$$

$A_{SN}/A_{ON} = F^{14}C$. There the t is given as the year before present (BP), which refers to the year 1950AD. The 8033 is the mean radiocarbon lifetime. However, atmospheric ¹⁴C is not constant due to changes in cosmic ray flux caused by changes in solar activity and the Earth's magnetic field. In addition to that, anthropogenic activities (like nuclear bomb tests, fossil fuel burning) have disturbed the atmospheric ¹⁴C background significantly. Fossil fuel burning releases ¹⁴C depleted CO₂ gas into the atmosphere [Suess, 1955]. In the period 1950-1965, the nuclear bomb tests raised atmospheric ¹⁴C concentrations almost twice. To correct for all these variations, calibration curves are established based on well-dated archives, like tree rings, speleothems, and marine corals [Reimer et al., 2013]. Applying the calibration curves, the ¹⁴C age (BP) is converted into calendar age (calBP) using the OxCal v4.3.2 program (Figure 2.4).

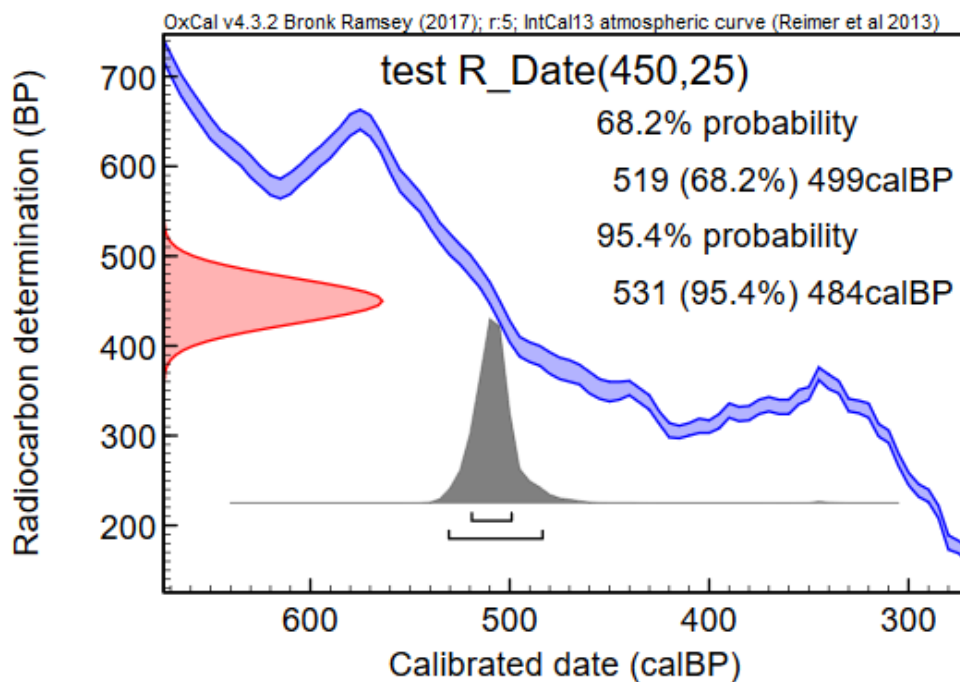


Figure 2.4 Example for the OxCal v4.3.2 calibration output. The blue thick curve is the IntCal13 Northern Hemisphere atmospheric ^{14}C calibration curve. The red area is the ^{14}C age distribution and the grey area is the calibrated ^{14}C age distribution with Intcal13. The bars below give the 1σ and 2σ intervals.

2.3.3.2 Source apportionment

Radiocarbon is also a unique biogeochemical tracer to investigate the sources and sinks of organic matter. Based on the mass balance of ^{14}C , the fossil fuel contribution to an organic reservoir can be estimated from the ^{14}C concentration after correction for the radioactive decay. Note that since 1955, the $F^{14}\text{C}$ value of contemporary carbon from biogenic sources and biomass burning (i.e., $F^{14}\text{C}_{\text{bio}}$ and $F^{14}\text{C}_{\text{bb}}$, respectively) is larger than $F^{14}\text{C} = 1$, the theoretical modern level of contemporary carbon, due to the input from nuclear-bomb testings in the 1950s and 1960s [Szidat et al., 2006; Levin et al., 2010]. For source apportionment, the obtained $F^{14}\text{C}$ is converted to the fraction of non-fossil (f_{NF}) using the following equation [Zhang et al., 2012]:

$$f_{\text{NF}} = \frac{F^{14}\text{C}}{f_{\text{NF}}(\text{ref})}$$

$f_{\text{NF}}(\text{ref})$ is the reference value representing $F^{14}\text{C}$ of non-fossil sources at the time when the particles were deposited on the glacier (i.e. age of surrounding ice layer as defined by the dating of the core). It includes biogenic (bio) and biomass-burning (bb) sources and assumes contributions from other non-fossil sources (e.g. cooking emissions) to be negligible. Accordingly, $f_{\text{NF}}(\text{ref})$ is obtained by:

$$f_{\text{NF}}(\text{ref}) = p_{\text{bio}} \times F^{14}\text{C}_{\text{bio}}(\text{ref}) + (1 - p_{\text{bio}}) \times F^{14}\text{C}_{\text{bb}}(\text{ref})$$

where p_{bio} refers to the fraction of the biogenic sources to the total non-fossil sources. The value of $F^{14}\text{C}_{\text{bb}}$ was estimated by a tree-growth model [Mohn et al., 2008]. Based on mass balance, fossil and non-fossil source contribution to each carbonaceous species WSOC, WIOC and EC can be determined, respectively. For example:

$$[\text{WIOC}_{\text{nf}}] = [\text{WIOC}] \times f_{\text{NF}}(\text{WIOC})$$

$$[\text{WIOC}_{\text{f}}] = [\text{WIOC}] \times (1 - f_{\text{NF}}(\text{WIOC}))$$

Bibliography

Bennett, C. L., R. P. Beukens, M. R. Clover, H. E. Gove, R. B. Liebert, A. Litherland, K. H. Purser and W. E. Sondheim. Radiocarbon dating using electrostatic accelerators: negative ions provide the key. *Science* **198**, 508-510, (1977).

Calvin, M., C. Heidelberger, J. C. Reid, B. M. Tolbert, P. E. Yankwich and C. J. Collins. Isotopic Carbon. *The Journal of Physical Chemistry* **53**, 1139-1140, (1949).

Cao, F., Y.-L. Zhang, S. Szidat, A. Zapf, L. Wacker and M. Schwikowski. Microgram level radiocarbon determination of carbonaceous particles in firn samples: pre-treatment and OC/EC separation. *Radiocarbon* **55**, 383-390 (2013). 10.2458/azu_js_rc.55.16291

Fang, L., J. Schindler, T. Jenk, C. Uglietti, S. Szidat and M. J. R. Schwikowski. Extraction of Dissolved Organic Carbon from Glacier Ice for Radiocarbon Analysis. **61**, 681-694, (2019).

Godwin, H. J. N. Half-life of radiocarbon. **195**, 984, (1962).

Hsueh, C., Y. Huang, C. Wang and C.-Y. Chen. Degradation of azo dyes using low iron concentration of Fenton and Fenton-like system. *Chemosphere* **58**, 1409-1414, (2005).

Jenk, T., S. Szidat, M. Schwikowski, H. Gaggeler, L. Wacker, H. Synal and M. Saurer. Microgram level radiocarbon (¹⁴C) determination on carbonaceous particles in ice. *Nuclear Instruments and Methods in Physics Research Section B: Beam Interactions with Materials and Atoms* **259**, 518-525, (2007). 10.1016/j.nimb.2007.01.196

Kušić, H., N. Koprivanac, A. L. Božić and I. Selanec. Photo-assisted Fenton type processes for the degradation of phenol: a kinetic study. *Journal of Hazardous Materials* **136**, 632-644, (2006).

Lang, S. Q., C. P. McIntyre, S. M. Bernasconi, G. L. Früh-Green, B. M. Voss, T. I. Eglinton and L. Wacker. Rapid ¹⁴C analysis of dissolved organic carbon in non-saline waters. *Radiocarbon* **58**, 505-515, (2016).

Legrand, M., S. Preunkert, B. Jourdain, J. Guilhermet, X. Fain, I. Alekhina and J. R. Petit. Water-soluble organic carbon in snow and ice deposited at Alpine, Greenland, and Antarctic sites: a critical review of available data and their atmospheric relevance. *Climate of the Past* **9**, 2195-2211, (2013). DOI 10.5194/cp-9-2195-2013

Levin, I., T. Naegler, B. Kromer, M. Diehl, R. J. Francey, A. J. Gomez-Pelaez, L. P. Steele, D. Wagenbach, R. Weller and D. E. Worthy. Observations and modelling of the global distribution and long-term trend of atmospheric $^{14}\text{CO}_2$. *Tellus Series B* **62**, 26-46, (2010). DOI 10.1111/j.1600-0889.2009.00446.x

Libby, W. F. Atmospheric helium three and radiocarbon from cosmic radiation. *Physical Review* **69**, 671, (1946).

Libby, W. F. Radiocarbon Dating, University of Chicago Press, Chicago, Illinois (1952).

Lide, D. R. CRC Handbook of chemistry and physics, Internet version. (2007).

May, B., D. Wagenbach, H. Hoffmann, M. Legrand, S. Preunkert and P. Steier. Constraints on the major sources of dissolved organic carbon in Alpine ice cores from radiocarbon analysis over the bomb - peak period. *Journal of Geophysical Research: Atmospheres* **118**, 3319-3327, (2013).

Mohn, J., S. Szidat, J. Fellner, H. Rechberger, R. Quartier, B. Buchmann and L. Emmenegger. Determination of biogenic and fossil CO_2 emitted by waste incineration based on $^{14}\text{CO}_2$ and mass balances. *Bioresource Technology* **99**, 6471-6479, (2008). DOI 10.1016/j.biortech.2007.11.042

Muller, R. A., E. J. Stephenson and T. S. Mast. Radioisotope dating with an accelerator: a blind measurement. *Science* **201**, 347-348, (1978).

Nelson, D. E., R. G. Korteling and W. R. Stott. Carbon-14: direct detection at natural concentrations. *Science* **198**, 507-508, (1977).

Preunkert, S., M. Legrand, P. Stricker, S. Bulat, I. Alekhina, J. Petit, H. Hoffmann, B. May, B. J. E. s. Jourdain and technology. Quantification of dissolved organic carbon at very low levels in natural ice samples by a UV-induced oxidation method. **45**, 673-678, (2010).

Reimer, P., T. Brown and R. Reimer. Discussion: reporting and calibration of post-bomb ^{14}C Data. *Radiocarbon* **46**, 1299-1304, (2004). 10.1017/S0033822200033154

Reimer, P. J., E. Bard, A. Bayliss, J. W. Beck, P. G. Blackwell, C. B. Ramsey, H. C. Caitlin E Buck, R. L. Edwards, M. Friedrich, P. M. Grootes, T. P. Guilderson, H. Haflidason, I. Hajdas, C. Hatté, T. J. Heaton, D. L. Hoffmann, A. G. Hogg, K. A. Hughen, K. F. Kaiser, B. Kromer, S. W. Manning, M. Niu, R. W. Reimer, D. A. Richards, E. M. Scott, J. R. Southon, R. A. Staff, C. S. M. Turney and J. v. d. Plicht. Intcal13 and Marine13 radiocarbon age calibration curves 0-50,000 years cal BP. *Radiocarbon* **55**, 1869-1887, (2013).

Ruff, M., S. Fahrni, H. Gäggeler, I. Hajdas, M. Suter, H. Synal, S. Szidat and L. Wacker. On-line radiocarbon measurements of small samples using elemental analyzer and MICADAS gas ion source. *Radiocarbon* **52**, 1645-1656, (2010).

Steier, P., C. Fasching, K. Mair, J. Liebl, T. Battin, A. Priller and R. Golser. A new UV oxidation setup for small radiocarbon samples in solution. *Radiocarbon* **55**, 373-382, (2013).

Stuiver, M. and H. A. Polach. Discussion reporting of ^{14}C data. *Radiocarbon* **19**, 355-363, (1977).

Suess, H. E. Radiocarbon concentration in modern wood. *Science* **122**, 415-417, (1955).

Synal, H.-A., M. Stocker and M. Suter. MICADAS: a new compact radiocarbon AMS system. *Nuclear Instruments and Methods in Physics Research Section B: Beam Interactions with Materials and Atoms* **259**, 7-13, (2007).

Szidat, S., T. M. Jenk, H. W. Gäggeler, H.-A. Synal, I. Hajdas, G. Bonani and M. Saurer. THEODORE, a two-step heating system for the EC/OC determination of radiocarbon (^{14}C) in the environment. *Nuclear Instruments and Methods in Physics Research Section B: Beam Interactions with Materials and Atoms* **223-224**, 829-836, (2004). 10.1016/j.nimb.2004.04.153

Szidat, S., T. M. Jenk, H.-A. Synal, M. Kalberer, L. Wacker, I. Hajdas, A. Kasper-Giebl and U. Baltensperger. Contributions of fossil fuel, biomass-burning, and biogenic emissions to carbonaceous aerosols in Zurich as traced by ^{14}C . *Journal of Geophysical Research* **111**, D07206, (2006). 10.1029/2005jd006590

Szidat, S., G. A. Salazar, E. Vogel, M. Battaglia, L. Wacker, H. A. Synal and A. Turler. C-14 Analysis and Sample Preparation at the New Bern Laboratory for the Analysis of Radiocarbon with Ams (Lara). *Radiocarbon* **56**, 561-566, (2014). 10.2458/56.17457

Uglietti, C., A. Zapf, T. M. Jenk, M. Sigl, S. Szidat, G. A. Salazar Quintero and M. Schwikowski. Radiocarbon dating of glacier ice: overview, optimisation, validation and potential. *The Cryosphere* **10**, 3091-3105, (2016).

Usoskin, I. G. A history of solar activity over millennia. *Living Reviews in Solar Physics* **14**, 3, (2017).

Wacker, L., S. M. Fahrni, I. Hajdas, M. Molnar, H. A. Synal, S. Szidat and Y. L. Zhang. A versatile gas interface for routine radiocarbon analysis with a gas ion source. *Nuclear*

Instruments & Methods in Physics Research Section B-Beam Interactions with Materials and Atoms **294**, 315-319, (2013). DOI 10.1016/j.nimb.2012.02.009

Zhang, Y., N. Perron, V. G. Ciobanu, P. Zotter, M. C. Minguillón, L. Wacker, A. S. Prévôt, U. Baltensperger and S. Szidat. On the isolation of OC and EC and the optimal strategy of radiocarbon-based source apportionment of carbonaceous aerosols. *Atmospheric Chemistry and Physics* **12**, 10841-10856, (2012).

Zhang, Y. L., N. Perron, V. G. Ciobanu, P. Zotter, M. C. Minguillón, L. Wacker, A. S. H. Prévôt, U. Baltensperger and S. Szidat. On the isolation of OC and EC and the optimal strategy of radiocarbon-based source apportionment of carbonaceous aerosols. *Atmospheric Chemistry and Physics* **12**, 10841-10856, (2012).

3 Extraction of dissolved organic carbon from glacier ice for radiocarbon analysis

L. Fang^{1,2,3}, J. Schindler^{1,2,3}, T.M. Jenk^{1,3}, C. Uglietti^{1,2,3}, S. Szidat^{2,3}, M. Schwikowski^{1,2,3}

¹Laboratory for Environmental Chemistry, Paul Scherrer Institute, CH-5232 Villigen PSI, Switzerland

²Department of Chemistry and Biochemistry, University of Bern, CH-3012 Bern, Switzerland

³Oeschger Centre for Climate Change Research, University of Bern, CH-3012 Bern, Switzerland

Corresponding author: M. Schwikowski

Manuscript published in

Radiocarbon, 61(3), 681-694, 2019

Abstract

Alpine glaciers are valuable archives for the reconstruction of human impact to the environment. Besides dating purposes, measurement of radiocarbon content provides a powerful tool for long-term source apportionment studies on the carbonaceous aerosols incorporated in ice cores. In this work, we present an extraction system for radiocarbon analyses of dissolved organic carbon (DOC) in ice cores. The setup can process ice samples of up to 350 g mass and offers ultra-clean working conditions for all extraction steps. A photo-oxidation method is applied by means of external UV irradiation of the sample. For an irradiation time of 30 minutes with catalyzation by addition of Fe^{2+} and H_2O_2 , we achieve an efficiency of $96 \pm 6\%$ on average. Inert gas working conditions and stringent decontamination procedures enable a low overall blank of $1.9 \pm 1.6 \mu\text{g C}$ with a F^{14}C value of 0.68 ± 0.13 . This makes it possible to analysis the DOC in ice samples with a carbon content of as low as $25 \mu\text{g C kg}^{-1}$ ice. For a first validation, the new method was applied to ice core samples from Swiss Alps. The average DOC concentration and F^{14}C values for the Fiescherhorn ice core samples show good agreement with previously reported data for the investigated period of 1925-1936AD.

KEYWORDS: dissolved organic carbon, ice core, method development, UV oxidation

3.1 Introduction

For meaningful interpretation of the recorded signals in ice cores from glacier archives, accurate dating is essential. Radiocarbon (^{14}C) is a powerful tool for dating widely applied in different fields [Libby, 1954; Stuiver and Suess, 1966; Reimer et al., 2013]. For ice cores from high-alpine glaciers ^{14}C -dating is particularly valuable for the ice in the bottom part, where strong thinning of annual layers prevents the use of annual layer counting or the assignment of reference horizons for dating [Thompson et al., 1998; Schwikowski et al., 1999]. The ^{14}C half-life of 5730 years allows covering the typical age range of alpine ice cores. Radiocarbon dating of water insoluble organic carbon (WIOC) from glacier ice has been well established. Samples of 10 μg WIOC can now be dated with reasonable uncertainty, requiring less than 1 kg of ice from typical mid-latitude and low-latitude glaciers [Jenk et al., 2007; Jenk et al., 2009; Sigl et al., 2009; Uglietti et al., 2016]. However, the low WIOC concentration in glaciers remote from sources, e.g. glaciers in the Polar Regions, puts a limit to this application. Because the concentrations of dissolved organic carbon (DOC) are around a factor 5 higher [10 to 100 ppbC, Legrand et al., 2013; Legrand et al., 2013], using this fraction promises to allow an extension of this approach to new sites and generally reducing the achievable analytical (dating) uncertainty.

In addition to dating, ^{14}C has proved to be a powerful tool for source apportionment studies, i.e. to distinguish biogenic and fossil source contributions [Szidat et al., 2006; Zhang et al., 2012]. Alpine ice cores allow access to continuous records of atmospheric pollution back to the pre-industrial era in the regions where the majority of humans live [Schwikowski et al., 1999; Eichler et al., 2012; Eichler et al., 2015]. A first long-term trend in concentrations separated into the contribution from fossil fuel and biogenic sources of atmospheric organic carbonaceous particles was reconstructed from an ice core at the Fiescherhorn glacier [Swiss Alps; Jenk et al., 2006; Cao et al. 2018 submitted]. Different to WIOC, which mainly consists of primary organic aerosol from direct emissions, water soluble organic carbon (WSOC) originates to a large part from secondary organic aerosols (SOAs) formed in the atmosphere from volatile organic precursor compounds [Gelencsér et al., 2007]. WSOC is a major fraction of organic aerosols in the atmosphere; however, its sources are not well constrained [Pio et al., 2007]. WSOC in snow and ice is only one part of the DOC which is analysed and additionally contains gaseous organics taken up during snowfall [Legrand et al., 2013]. Studying DOC along

with its ^{14}C content in samples from ice cores will allow additional insight into historical natural and anthropogenic contributions to the organic carbon content of atmospheric aerosols.

Only very few long-term records of DOC concentrations, and even fewer in combination with the ^{14}C content exist to date. To our knowledge all of these records were derived from ice cores [Preunkert et al., 2010; Legrand et al., 2013; May et al., 2013]. For studies of DOC in ice cores, one of the major limitations is the rather large demand of sample amount along with relatively low extraction efficiency and the threat of sample contamination [Preunkert et al., 2010; Legrand et al., 2013; May et al., 2013]. With the current state of the art of ^{14}C analysis with accelerator mass spectrometry (AMS) that allows the direct measurement of gaseous CO_2 samples, carbon sample masses of as low as $3\ \mu\text{g}$ are sufficient [Ruff et al., 2007]. Still, this translates to typical ice sample masses of several hundred grams for DO^{14}C analyses. However, preceding AMS analysis, DOC has to be oxidized to CO_2 . In contrast to high-temperature combustion or wet-chemical oxidation techniques, the use of Ultra-violet (UV) photochemical oxidation has the advantage of being suitable for large volumes of sample with low carbon content [Beaupré et al., 2007]. It was applied by Singer et al. (2012) to determine the DO^{14}C content of ice samples from different glaciers in the European Alps. However, their method has a limited carbon yield of 50 % [Steier et al., 2013]. May (2009) and May et al. (2013) developed a setup for ^{14}C microanalysis of glacier ice and applied it to several ice core samples, but unexpected super-modern ^{14}C values led to inconclusive results. It should be noted that a straightforward analysis of DOC is challenging due to its vulnerability to contamination [Legrand et al., 2013]. Ice cores can potentially be contaminated during drilling, storage, and sample processing. Besides, DOC consists to a large part of mono- and di-carboxylic acids that are ubiquitous in ambient and laboratory air [Legrand et al., 2013]. Therefore, it is vital to ensure ultra-clean sample preparation and extraction with a low and stable process blank for reliable ^{14}C analysis of DOC. Here, we present such an approach with a new extraction setup for DOC concentration and ^{14}C analysis in low-concentration ice core samples. Our extraction system is designed for samples with volumes of up to $\sim 350\ \text{mL}$ and concentrations as little as 25 ppbC DOC (equals to $25\ \mu\text{g C kg}^{-1}$ ice).

3.2 Experimental

3.2.1 Extraction Setup

Figure 3.1 shows an overview scheme of the complete DOC extraction setup [Schindler, 2017]. This setup allows handling of the entire sample treatment under inert gas conditions ($\geq 99.999\%$ helium gas, further purified by a home-made getter oven) in order to extract carbon masses of as little as a few micrograms, while aiming to avoid potential contamination during analysis. The getter oven consists of an insulated, resistively heated Inconel (a high temperature resistant nickel-chromium-based super-alloy) tube filled with 15 g tantalum wire. Helium is used as carrier gas in the entire setup. Furthermore, all parts in contact with the sample when in its liquid form were fabricated modularly from either glass or quartz glass to allow thorough cleaning and reduction of memory effects compared to stainless steel. To minimise outgassing or out-washing of organic carbon into the sample, no lubricants are used. The major system components, highlighted in green text in Figure 3.1, are described in detail in the following:

The glass melting vessel (custom made by GlasKeller AG, Switzerland) with an inner diameter with an inner diameter of 100 mm has a volume of around 1.3 L (Figure 3.2a). A support holds the vessel and fixes the stainless steel cover plate to the vessel by spring tension. The flange connection is sealed by a PFA coated O-ring. As illustrated in the sketch, the cover plate gives access to four thread connectors (1/4 inch): i) the helium supply, ii) a metering valve (SS-BNTS6MM, Swagelok, USA) with a bubble counter (GlasKeller AG, Switzerland) that acts as a vent with water ballast (vent 1), iii) a manometer for pressure monitoring (PBMN-25B11AA14402201000, Baumer Electric AG, Switzerland) and iv) the ultra-pure water (UPW) supply. The UPW dispenser system consists of a glass bottle filled with UPW (Sartorius, 18.2 M Ω ×cm) and connected by PFA tubes to both the helium supply and the cover plate. Applying pressure via the helium supply allows pushing the desired amount of UPW to the melting vessel.

The filtration unit is shaped as an adapter piece from glass spherical joint (SJ) 41/25 to SJ 19/7 (Figure 3.2a). In the center, a 8 mm diameter frit (160-250 μ m) acts as support for a pre-cleaned quartz fiber filter that was baked at 800°C for 2 h (20 mm diameter, PALLFLEX Tissuquartz, 2500QAO-UP) and fixed onto the frit by a metal spring. The filter used for the separation of POC from the liquid sample is similar to the procedure for WIO¹⁴C analysis described in Jenk et al. (2006). However, in contrast to the commonly used lab filtration unit described therein, this setup allows filtration under inert gas conditions, avoiding potential

Table 3.1 Performances of different DOC extraction setups for ice or non-saline water samples.

References	Method	Sample / size	¹⁴ C analysis	Oxidation blank	Total blank	Efficiency (%)	Oxidation time (min)
This study	UV(H ₂ O ₂ , Fe ²⁺)	Ice / 350 mL	yes	0.67 ± 0.26 µg C	1.9 ± 1.6 µg C	96±6	30
Federer et al., 2008	CFA ¹ -UV	Ice / ~1 mL/min	no	--	50 ppbC	86-139*	2
May et al., 2013	UV	Ice / 300 mL	yes	1.9 ± 0.2 µg C	6 ± 3 µg C	81-96	40
Preunkert et al., 2010	UV	Ice / 4mL	no	--	25±1.5 ppbC	85-125*	10
Steier et al., 2013	UV	Water / 1 mL	yes	--	1.1±0.7 µg C	64±17	120
Lang et al., 2016	WCO ²	Non-saline water / 7 mL	yes	--	0.68-1.05 µg C	87-128	60

-- no data available, ¹ Continuous Flow Analysis, ² Wet Chemical Oxidation, *TOC standard (phthalate) set as 100%

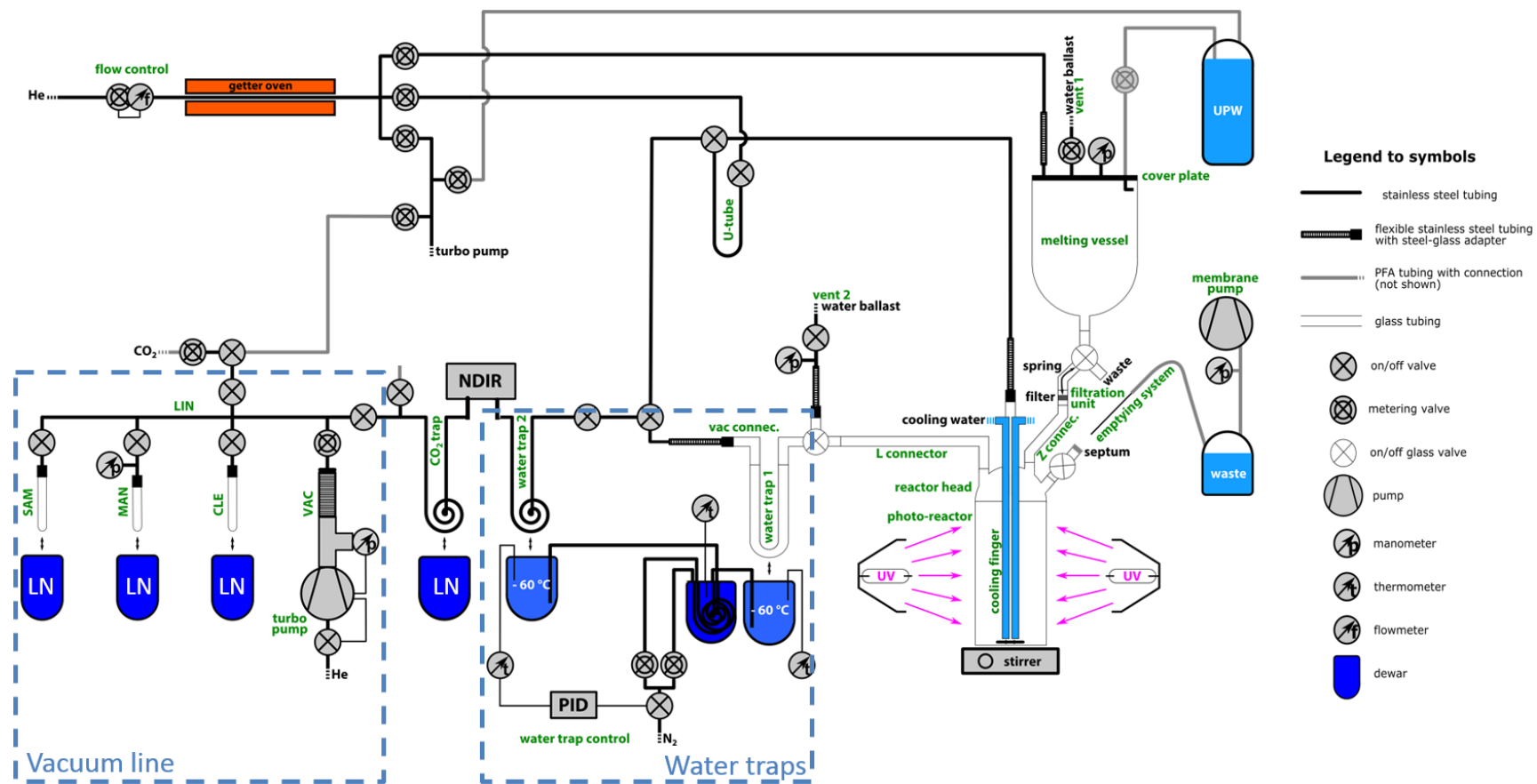


Figure 3.1 Schematic of the complete DOC extraction setup. Green text labels individual components. UPW (ultra-pure water), LN (liquid nitrogen), NDIR (CO₂ detector), LIN (vacuum manifold), VAC (pump manifold), CLE (cleaning tube), MAN (manometry cell), SAM (sampling tube).

sample contamination from take-up and mixing of ambient air with the liquid sample during the filtration step.

The photo-reactor is a cylindrical quartz glass vessel (Qsil GmbH, Germany) (Figure 3.2b), and allows introduction of the filtered solution via a glass connector (Z connector). In the center of the reactor head, the cooling finger is inserted via a glass SJ 41/25 connection and reaches close to the base of the photo-reactor. The cooling finger has several functions and is constructed from three concentric glass tubes. The inner tube is connected to the helium supply. The outer two tubes serve for cooling water circulation in the cooling finger and in combination with external cooling of the photo-reactor by air ventilation is essential to control the sample temperature during photo-oxidation. For sample mixing, the promotion of homogeneous oxidation and efficient degassing, a magnetic stirrer is used. The magnetic stir bar is encapsulated in glass to avoid contamination (Beaupré et al., 2007). Two UV lamps (MH-Module 250W Hg XL, Heraeus, Germany) are installed opposite of each other and enclose the reactor in a distance of 3 cm to the reactor walls. A box surrounds the UV lamps and reactor to prevent user-exposure to UV irradiation and ozone. This protection box further enhances the photon-yield because of its reflective aluminum construction. The emptying system consists of a long stainless steel needle, a glass bottle, and a membrane pump. For sample removal the stainless steel needle is introduced through a septum to the reactor and the sample is pumped out with a membrane pump.

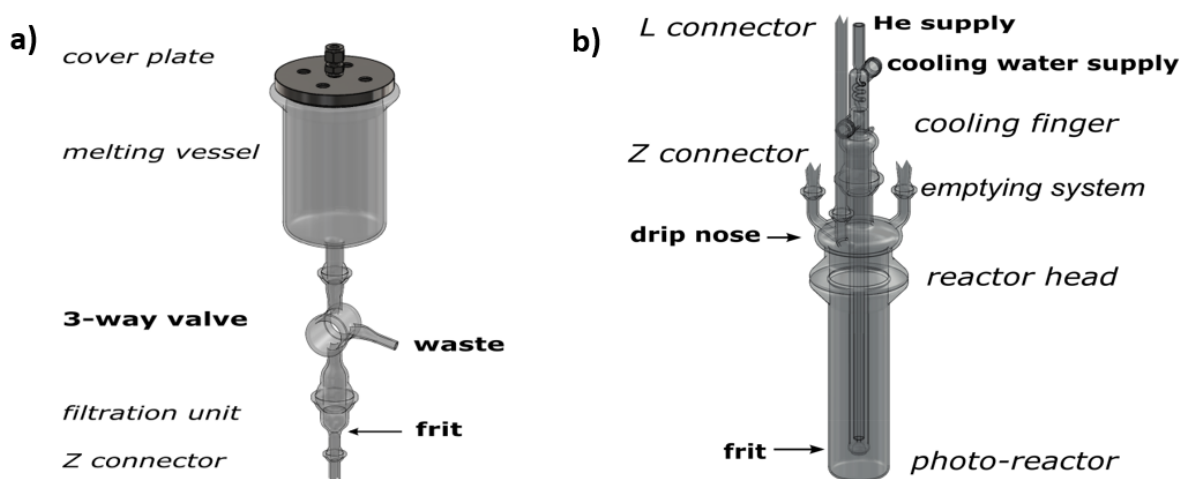


Figure 3.2 View of a) melting vessel, filtration valve and filtration unit, b) the photo-reactor, reactor head and cooling finger. Italic text refers to the labeling introduced in Figure 3.1, bold text refers to connections or emphasizes special features.

Despite cooling with the cool finger, the liquid sample heats up to around 50 °C during UV irradiation, resulting in an enhanced content of water vapor. For water removal, two cryogenic water traps are therefore added in front of the CO₂ trap that is cooled with liquid nitrogen (LN). Water trap 1 (Figure 3.1) is a U-shaped glass tube (20 cm length, 10 mm inner diameter) filled with glass capillaries and water trap 2 is made from stainless steel tube bent to a coil (2 m length, ¼ inch outer diameter (OD), Swagelok). A PID temperature controller (Eurotherm Produkte AG, Switzerland) is used to stabilize both water traps at -60 °C by a controlled nitrogen gas transfer from a LN reservoir into the Dewar around the water traps, similar in principle to the system described in Jenk et al. (2016).

All components of the vacuum line (indicated as blue dashed box in Figure 3.1) are made from stainless steel tubes (¼ inch OD) and stainless steel fittings (Swagelok) allowing operation at high vacuum of about 10⁻⁷ mbar. A turbo-molecular pump (HiCube 80 Eco, Pfeiffer Vacuum AG, Germany) is connected to the vacuum line through a dosing valve (SS-6BMRG-MM-SC11, Swagelok). The vacuum line for CO₂ sample purification and collection is similar to the one described in Szidat et al. (2004) and consists of a cleaning tube for CO₂ purification ('CLE', glass tube, 200 mm length, 8 mm OD) with a removable ethanol-dry ice cooling bath (-72 °C), the manometry cell ('MAN', glass tube, 150 mm length, 6 mm OD) with a removable LN bath (-196 °C) and connected to a pressure gauge for CO₂ quantification (Baumer Electric AG), and the sampling tube for CO₂ transfer and sample flame sealing ('SAM', glass tube, 150 mm length, 4 mm OD) connected to the vacuum line by a steel-glass adapter (homemade) to allow easy removal and replacement.

3.2.2 Sample Preparation and Decontamination

Prior to the extraction of DOC from ice samples and subsequent ¹⁴C analyses, several steps are required. First, ice samples are cut and decontaminated by removing 5 mm from the surface using a band saw in a cold lab (-20°C). Ice samples are then transferred in pre-cleaned PETG containers (1000 mL, Semadeni, Switzerland; soaked three times overnight in UPW) from the cold room to the analytical laboratory. After tempering in the laboratory, ice blocks are inserted into the melting vessel, which is closed and then flushed with helium during rinsing of the ice block with UPW to remove approximately 20% of the ice volume, with the rinsing water then being discarded through the waste outlet (Figure 3.2a).

Before introducing a sample, the DOC extraction set-up is decontaminated by running a procedure to remove potential sources of carbon contamination: After flushing the vacuum line with helium and zeroing the nondispersive infrared CO₂ detector (NDIR, LI-820A, LI-COR, USA, modified to allow in-line operation by improved connection seals), the glass setup is pressurized with helium slightly above atmospheric pressure (1.04 bar) to create the inert gas atmosphere. In the next step, the melting vessel is filled with about 50 mL UPW, which is subsequently drained to the photo-reactor to remove potential contamination from the melting vessel, quartz fiber filter, and reactor glass surfaces. 1 mL of 85% H₃PO₄ (Merck KGaA) is then added via a septum into the reactor using a glass syringe to acidify the water (pH ~1) while it is continuously purged with helium to remove dissolved CO₂ and the CO₂ evolving from the solvation of inorganic carbon (IC). To enhance the oxidation efficiency, 2 mL of 100 ppm FeSO₄ (ACS reagent, ≥99.0%, Sigma-Aldrich) and 1 mL of 50 mM H₂O₂ (≥30%, Sigma-Aldrich) are additionally injected into the reactor (Hsueh et al., 2005; Kušić et al., 2006). With the reactor also being irradiated with UV light, this cleaning process is monitored by continuous measurement of the emerging CO₂ being flushed through the NDIR CO₂ detector by the helium carrier (flow rate 100 mL/min). Once the CO₂ signal drops asymptotically below a set threshold, indicating that cleaning is finished, the UV lamps are turned off. In Figure 3.3, a typical CO₂ detector scan is shown.

3.2.3 DOC extraction

After the ice has been rinsed, it is melted, thereby slightly enhancing the melt rate by heating with an infrared lamp and a hot air gun. The liquid sample is then transferred from the melting vessel to the photo-reactor passing a quartz fibre filter, both pre-cleaned as described earlier. To keep the filter in place, it is fixed with the help of a stainless steel spring, the only metal part in contact with the liquid sample. Filtration is performed at inert gas conditions, always preserving a little overpressure to prevent ambient air from leaking into the setup. After transfer, the sample volume is determined by measuring the reactor fill level. By mixing with the previously cleaned solution, the filtrate gets acidified. After the degassing of CO₂ from IC, again 1 mL of 50 mM H₂O₂ is injected into the reactor right before the UV irradiation is started. During UV oxidation, CO₂ is continuously degassed by the helium carrier gas stream and led through three cryogenic traps (Figure 3.1). The first two traps (water trap 1 & 2) operate at –60 °C and retain water vapour, while a further cryogenic trap in a LN bath (CO₂ trap) is used

to freeze out the CO₂ from the carrier gas stream. Once the oxidation has finished, as monitored by the CO₂-detector (see Figure 3.3), the cryogenic trap is isolated and evacuated to remove helium and volatile gases while still being cooled by LN to keep the CO₂ sample frozen. After subsequent cryotransfer of the sample CO₂ to the CLE with LN, the CLE is closed-off towards the vacuum and the vacuum-lines are again evacuated. The CLE is heated up to room temperature. Afterwards, potential small amounts of remaining water vapour is frozen out using an ethanol-dry ice bath for 4 minutes before the CO₂ is then cryotransferred and collected in the MAN while water vapour is kept frozen in CLE by the ethanol-dry ice bath. In MAN, the sample CO₂ is quantified manometrically after the valve towards the vacuum line is closed and the tube reached room temperature. Finally the CO₂ is transferred to SAM and flame sealed in the glass tube. For ¹⁴C analysis in the AMS laboratory, the glass vial is cracked in the gas interface system and the CO₂ sample is injected into the AMS (MICADAS, University of Bern, Switzerland; Ruff et al., 2007; Szidat et al., 2014).

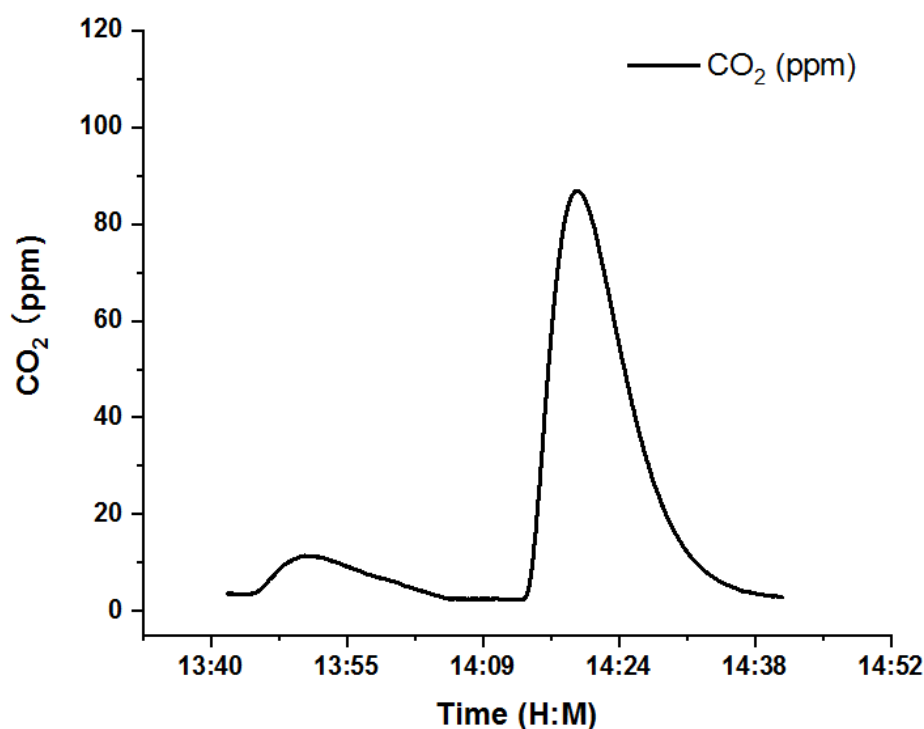


Figure 3.3 Typical NDIR CO₂ scan of the decontamination step (first peak) followed by the oxidation of a 5 μM sodium acetate standard solution (Sigma-Aldrich, No. 71180) at a helium flowrate of 100 ml/min.

3.3 Characterization

To characterise the setup and procedure in terms of its oxidation efficiency, procedural blanks and accuracy, various standard and blank measurements have been carried out. For a first validation by comparison with other published DOC data, environmental ice samples from Piz Zupò and Fiescherhorn [both Swiss Alps; Jenk et al., 2006; Sodemann et al., 2006; Mariani et al., 2014; Cao et al., submitted) were analysed.

3.3.1 Oxidation Efficiency

For determination of the oxidation efficiency, multiple standard solutions covering a range of concentrations were prepared from different organic substances using UPW for dissolution which had previously additionally been cleaned from DOC and IC in our photo-reactor as described earlier. The liquid solutions were then added with a syringe via a septum to the UV reactor containing the pre-oxidised water and then were oxidised following the procedure described earlier to quantify their carbon content. The efficiency was then calculated from the determined carbon yield of the initial substrate after subtraction of the oxidation blank which will be discussed in the next section. Using an initial setup with a fixed oxidation time of 45 minutes; average oxidation efficiencies of 82%, 105%, 79% and 54% for oxalate, formate, phthalate and acetate were observed, respectively (Figure 3.4a). With installing the NDIR CO₂ detector in-line in the modified set-up (Figure 3.1) allowing for continuous monitoring of the oxidation progress, sample specific adjustment of the oxidation time became possible allowing reaching higher efficiencies of up to 90±6% (Figure 3.4b). However, the optimised, much longer oxidation times (up to 120 minutes) limit sample throughput and are thus not favourable. Based on the study of photo-assisted Fenton-type processes for the degradation of phenol, Fe²⁺ and H₂O₂ was used to facilitate oxidation in a further improvement aimed at the reduction of the analytical time (Hsueh et al., 2005; Kušić et al., 2006). As described, 2 mL of 100 ppm FeSO₄ and 1 mL of 50 mM H₂O₂ solution were therefore added to the reactor at the beginning of the pre-cleaning step and an additional 1 mL H₂O₂ right before the sample UV irradiation. As a result, the average oxidation efficiency was improved again significantly to 96±6% (n=8, various compounds) while strongly shortened irradiation times of 20-30 minutes depending on the compound could be achieved (Figure 3.4c). This is an advancement compared to other existing systems for the analysis of DOC and its ¹⁴C content (Table 3.1). With this set-up

optimised both for oxidation efficiency and irradiation time, the analysis of one blank and three samples can be performed per day.

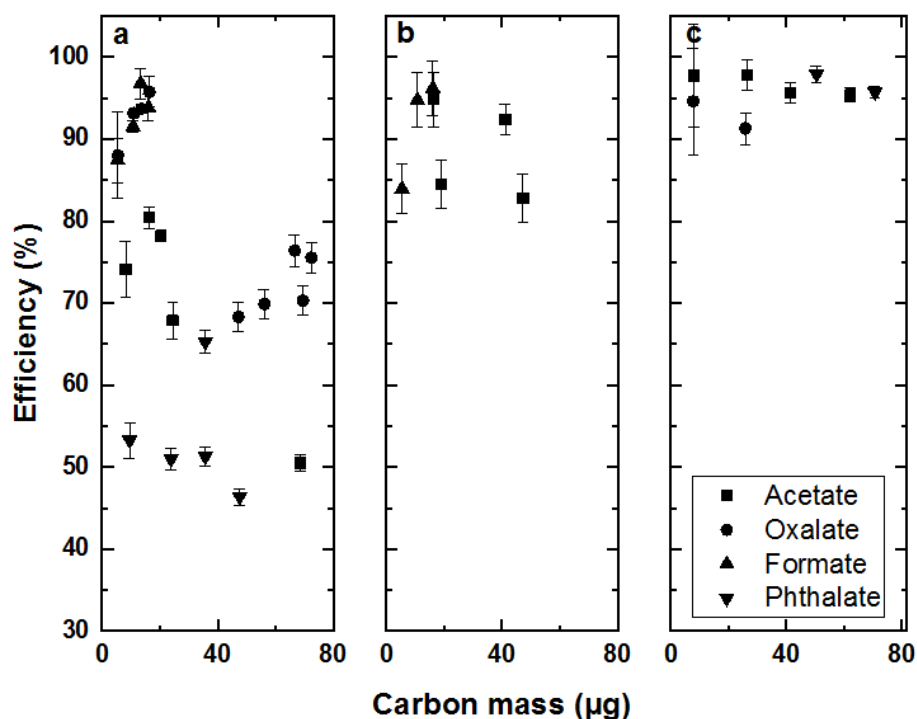


Figure 3.4 Oxidation efficiency for different organic compounds. a) initial setup with fixed oxidation time at 45 min; b) modified setup allowing compound specific optimisation of the oxidation time (60-120 min); c) modified setup with added Fe^{2+} and H_2O_2 for a catalysed oxidation reaction (20-30 min).

3.3.2 Standards and Blank

We assume the oxidation step to be the most crucial step of the entire procedure since potential contaminations are oxidised and detected along with the sample. To determine the blank mass (m_{COx}) and the blank ^{14}C activity ($F^{14}\text{COx}$) of the oxidation step, solutions were prepared from the standard reference material (NIST oxalic acid II, SRM 4990C, $F^{14}\text{C} = 1.3407 \pm 0.0005$) and sodium acetate (Sigma-Aldrich, No. 71180, $F^{14}\text{C} = 0.0018 \pm 0.0005$, Szidat et al., 2014) over a range of concentrations and with different $F^{14}\text{C}$ activity. In Figure 3.5, the ^{14}C results measured for these two standard samples are shown as a function of the carbon mass. Based on these values and assuming constant contamination, m_{COx} and $F^{14}\text{COx}$ can be estimated by applying

isotopic mass balance calculations (Hwang and Druffel 2005). The resulting values for the oxidation blank are $mC_{OX} = 0.67 \pm 0.26 \mu\text{g C}$ with $F^{14}C_{OX} = 0.76 \pm 0.18$ with the uncertainties being derived from a full error propagation including the analytical uncertainty for both, mC and $F^{14}C$. In reverse, when these values are now applied for a blank correction of the measured standards, good agreement within the uncertainties is found compared to the expected $F^{14}C$ values (Figure 3.5). This suggests a correction based on the determined blank values under the assumption of a constant contamination is valid. As shown in Figure 3.5 it can be applied over a wide range of sample sizes, however it does result in an increase of the overall uncertainty for small samples ($<10 \mu\text{g C}$) due to the uncertainty of the blank.

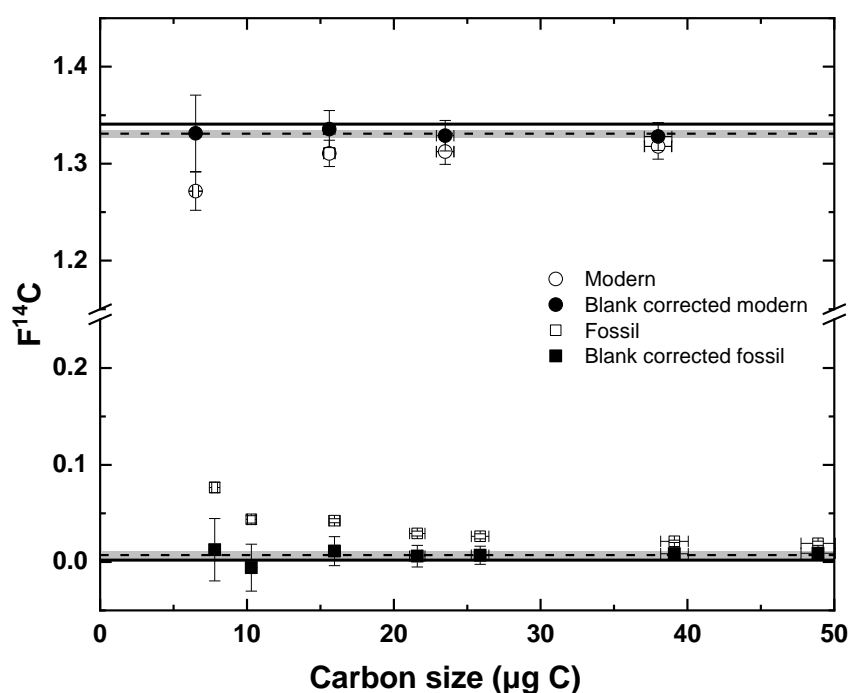


Figure 3.5 $F^{14}C$ of radiocarbon standards before (open symbols) and after correction for the oxidation blank (black symbols) with analytical and fully propagated uncertainties (1σ), respectively. Solid horizontal lines indicate the reference values for a fossil standard with $F^{14}C=0.0018 \pm 0.0005$ (sodium acetate) and a modern standard with $F^{14}C=1.3407 \pm 0.0005$ (NIST oxalic acid II), respectively. Dashed lines indicate the here determined mean values (1σ uncertainty band in gray) of $F^{14}C=0.007 \pm 0.006$ and $F^{14}C=1.331 \pm 0.003$ for the fossil and modern standard, respectively.

Going one step further, the overall process blank including all pre-treatment steps such as ice cutting, melting, and filtration was determined using frozen UPW for the simulation of blank ice (UPIce). As expected, this overall process blank was found to be higher in carbon mass and higher in variability compared to the above discussed oxidation blank alone (Figure 3.6). Measurements of 26 individual UPIce blanks resulted in a mean carbon mass of $m_{C_P} = 1.9 \pm 1.6 \mu\text{g C}$ ($n=26$) with 8 samples giving masses below the detection limit ($0.5 \mu\text{g C}$; to calculate the mean, the oxidation blank value was considered in these cases). Due to the generally small carbon masses, only a few of these blanks could be measured for radiocarbon resulting in a mean $F^{14}C_P = 0.68 \pm 0.13$ ($n=7$). To check the water quality, UPW from the water system have been measured routinely, also shown in Figure 3.6. Considering all the results shown in this figure, a the trend to higher blanks with increasing water/ice volumes can be observed making it apparent that at least a fraction of the determined carbon mass and variability in m_{C_P} can be assigned to changing water quality. Similarly set-up and method unrelated, a contribution from potential contamination occurring during the freezing process of the UPIce blocks cannot be excluded. With the current data set, a quantitative distinction of these different contribution factors is however not possible and both size and uncertainty of the determined overall process blank can be considered to be rather conservative estimates. Nevertheless, our method still performs excellent in terms of low carbon background if compared to other set-ups, with our values being at the low end (Table 3.1).

Considering the effect of blank correction on the uncertainty, the conventional approximation is that samples with a carbon content of around 5 times the blank mass still allows obtaining reliable results. In our case, this would require a minimal sample mass of $9.5 \mu\text{g C}$. Considering a maximum sample size of about 350 mL, our setup can thus be expected to reliably allow analysis of samples with concentrations as low as $\sim 25 \text{ ppbC}$ ($= 25 \mu\text{g C kg}^{-1} \text{ ice}$). This makes our method applicable for the analysis of typical high-alpine ice core samples and potentially Greenland samples [Legrand et al., 2013].

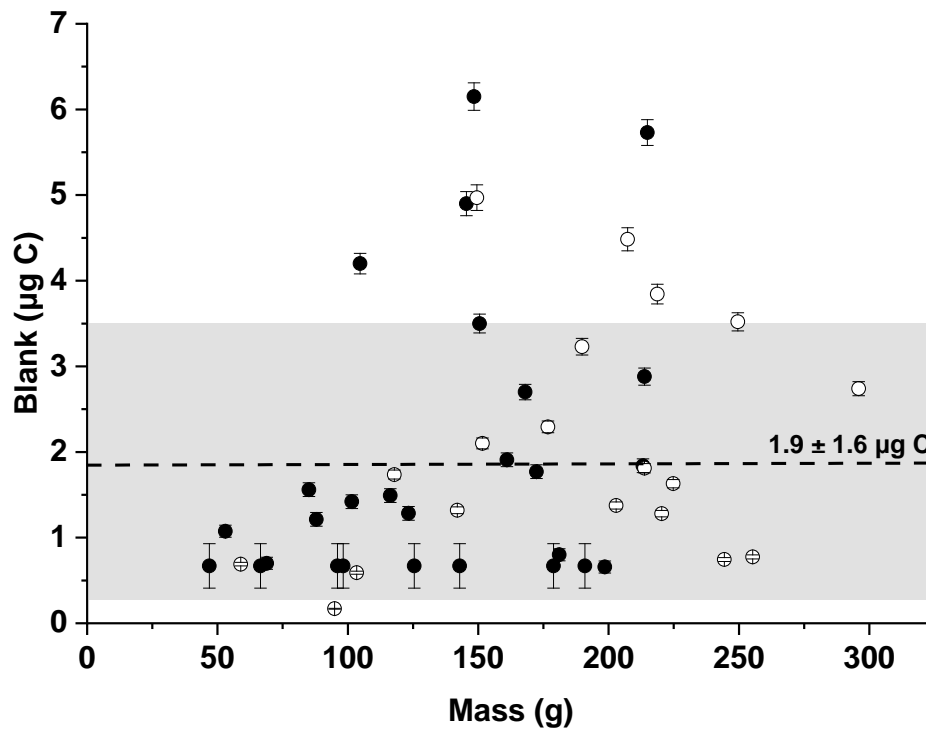


Figure 3.6 Process blank including all method steps. Open circles indicate blanks using ultra-pure water samples (UPW blank) and closed circles artificial ice blanks prepared by freezing ultra-pure water (UPIce blank). The UPIce blank mean is indicated by the dashed line with the 1σ uncertainty band in gray.

3.3.3 Natural Ice Samples

In order to apply the described set-up and method to natural ice samples in a first attempt, sections of a 43 m long ice core from Piz Zupò (3900 m asl., Swiss Alps), drilled in 2002 were selected. The high mean annual accumulation rate of 2.6 ± 0.8 m w.e. [Sodemann et al., 2006] allows investigating the seasonal variation of DOC. Samples from a depth of 29-41 m (corresponding to the period of 1991-1995) that consisted of porous firn were cut and analysed. Our results, however, show no clear seasonal DOC trend, but extremely high DOC concentrations of about 950-1400 ppbC with depleted $F^{14}C$ values ($\sim 0.15-0.22$) especially in the top part of this core, assigned to the years 1994-1995 AD. These high concentrations are unexpected based on available results of similar age from Col du Dôme (French Alps) with DOC values of around 200 ppbC [Legrand et al., 2013]. Thus, contamination of this porous firn part of the core has to be assumed. This is supported by the fact that the observed DOC concentrations show significant increase with decreasing density of the firn. An estimate of the mean density at which bubbles are closed-off in the firn can be calculated [Martinerie et al., 1992; Martinerie et al., 1994] and is around 0.81 kg/L for the conditions at Piz Zupò. With decreasing densities (i.e. depth), the open porous space in the firn increases and is connected to the atmosphere. Core sections from these depths thus do not contain enclosed bubbles but open pores connected to the ambient air allowing potential contaminants to diffuse into the core with the possibility of subsequent deposition. This process is active from the time of drilling, over the entire time of storage until final sample handling. The $F^{14}C$ results of around 0.2 gives further indication of the contamination, pointing to a source being dead in ^{14}C if considering the expected $F^{14}C$ range of around 0.8-1.1 [May et al., 2013; Cao et al. submitted]. We thus assume the contamination sources to be related to indoor (cold room) storage and packing material (e.g. outgassing plastic bags and isolation foams). Based on these first results, one should be very cautious when analysing and interpreting DOC data from firn samples, at least if stored for a long time, since this source of contamination cannot be removed by decontamination procedures.

In a second attempt, we selected samples from the Fiescherhorn ice core using sections from greater depth and ice densities of around 0.9 kg/L (i.e. solid ice samples). We analyzed samples from the period 1925-1936 AD, because annual mean DOC concentrations were previously reported for the Alps for that period (Legrand et al. 2013a). The average DOC

concentration we found was 66 ± 19 ppbC with an $F^{14}\text{C}$ of 0.74 ± 0.05 ($n=9$), which is in good agreement with the concentrations of 70 ppbC at Col du Dôme [Legrand et al., 2013]. $F^{14}\text{C}$ values are comparable to the values measured in WIOC in the Fiescherhorn ice core ($F^{14}\text{C} = 0.70 \pm 0.08$, Cao et al. submitted, note that values there are given as f_{NF} and for comparison were converted to $F^{14}\text{C}$ here).

3.4 Conclusions

We present a new set-up for the analysis of DOC and its ^{14}C content. The comparison with other devices for ^{14}C analysis of DOC shows our setup performs excellent in terms of low carbon background with the advantage of higher carbon yields while keeping analysis time low. This was achieved thanks to sample treatment under inert gas conditions, a thorough decontamination procedure of the system prior to sample loading and an enhanced UV oxidation efficiency by taking advantage of the Fenton catalytic reaction. With the current setup, samples with DOC concentrations as low as ~ 25 ppbC can be reliably analysed for ^{14}C when using the maximal applicable volume of 350 mL of ice. First analysis of samples from two Alpine ice cores (Fiescherhorn and Piz Zupò, Switzerland) resulted in values comparable to previous studies using different setups. Furthermore, this analysis also indicated the high risk of DOC contamination in firn samples, at least if stored for a longer period of time. In the near future, this system will allow increasing the number of available long-term DOC records covering the pre-industrial period, which is an important constrain for emission estimates used to simulate aerosol forcing in current climate models.

ACKNOWLEDGMENTS

We thank the Laboratory for the Analysis of Radiocarbon with AMS (LARA), especially Gary Salazar, for support with radiocarbon measurements. Also we thank Steven Beaupré for his sharing of knowledge and experience with DOC systems resulting in invaluable technical advice and Alexander Vogel for helping with ice cutting in the cold room.

Bibliography

Beaupré, S. R., E. R. Druffel and S. Griffin. A low-blank photochemical extraction system for concentration and isotopic analyses of marine dissolved organic carbon. *Limnology and Oceanography: Methods* **5**, 174-184, (2007).

Eichler, A., G. Gramlich, T. Kellerhals, L. Tobler and M. Schwikowski. Pb pollution from leaded gasoline in South America in the context of a 2000-year metallurgical history. *Science advances* **1**, e1400196, (2015).

Eichler, A., L. Tobler, S. Eyrikh, G. Gramlich, N. Malygina, T. Papina and M. Schwikowski. Three centuries of Eastern European and Altai lead emissions recorded in a Belukha ice core. *Environmental science & technology* **46**, 4323-4330, (2012).

Federer, U., P. R. Kaufmann, M. A. Hutterli, S. Schüpbach and T. F. Stocker. Continuous flow analysis of total organic carbon in polar ice cores. *Environmental science & technology* **42**, 8039-8043, (2008).

Gelencsér, A., B. May, D. Simpson, A. Sánchez-Ochoa, A. Kasper-Giebl, H. Puxbaum, A. Caseiro, C. Pio and M. Legrand. Source apportionment of PM_{2.5} organic aerosol over Europe: Primary/secondary, natural/anthropogenic, and fossil/biogenic origin. *Journal of Geophysical Research: Atmospheres* **112**, (2007).

Hsueh, C., Y. Huang, C. Wang and C.-Y. Chen. Degradation of azo dyes using low iron concentration of Fenton and Fenton-like system. *Chemosphere* **58**, 1409-1414, (2005).

Jenk, T., S. Szidat, M. Schwikowski, H. Gäggeler, S. Brüttsch, L. Wacker, H.-A. Synal and M. Saurer. Radiocarbon analysis in an Alpine ice core: record of anthropogenic and biogenic contributions to carbonaceous aerosols in the past (1650–1940). *Atmospheric Chemistry and Physics* **6**, 5381-5390, (2006).

Jenk, T. M., M. Rubino, D. Etheridge, V. G. Ciobanu and T. Blunier. A new set-up for simultaneous high-precision measurements of CO₂, delta C-13-CO₂ and delta O-18-CO₂ on small ice core samples. *Atmospheric Measurement Techniques* **9**, 3687-3706, (2016).

Jenk, T. M., S. Szidat, D. Boliu, M. Sigl, H. W. Gaeggeler, L. Wacker, M. Ruff, C. Barbante, C. F. Boutron and M. Schwikowski. A novel radiocarbon dating technique applied to an ice core from the Alps indicating late Pleistocene ages. *Journal of Geophysical Research: Atmospheres* **114**, (2009).

Jenk, T. M., S. Szidat, M. Schwikowski, H. Gäggeler, L. Wacker, H.-A. Synal and M. Saurer. Microgram level radiocarbon (¹⁴C) determination on carbonaceous particles in ice. *Nuclear*

Instruments and Methods in Physics Research Section B: Beam Interactions with Materials and Atoms **259**, 518-525, (2007).

Kušić, H., N. Koprivanac, A. L. Božić and I. Selanec. Photo-assisted Fenton type processes for the degradation of phenol: a kinetic study. *Journal of Hazardous Materials* **136**, 632-644, (2006).

Lang, S. Q., C. P. McIntyre, S. M. Bernasconi, G. L. Früh-Green, B. M. Voss, T. I. Eglinton and L. Wacker. Rapid ^{14}C analysis of dissolved organic carbon in non-saline waters. *Radiocarbon* **58**, 505-515, (2016).

Legrand, M., S. Preunkert, B. Jourdain, J. Guilhermet, I. Alekhina and J. Petit. Water-soluble organic carbon in snow and ice deposited at Alpine, Greenland, and Antarctic sites: a critical review of available data and their atmospheric relevance. *Climate of the Past* **9**, 2195-2211, (2013).

Legrand, M., S. Preunkert, B. May, J. Guilhermet, H. Hoffman and D. Wagenbach. Major 20th century changes of the content and chemical speciation of organic carbon archived in Alpine ice cores: Implications for the long-term change of organic aerosol over Europe. *Journal of Geophysical Research: Atmospheres* **118**, 3879-3890, (2013).

Libby, W. F. Chicago radiocarbon dates V. *Science* **120**, 733-742, (1954).

Mariani, I., A. Eichler, T. Jenk, S. Brönnimann, R. Auchmann, M. Leuenberger and M. Schwikowski. Temperature and precipitation signal in two Alpine ice cores over the period 1961-2001. *Climate of the Past* **10**, 1093-1108, (2014).

Martinerie, P., V. Y. Lipenkov, D. Raynaud, J. Chappellaz, N. Barkov and C. Lorius. Air content paleo record in the Vostok ice core (Antarctica): A mixed record of climatic and glaciological parameters. *Journal of Geophysical Research: Atmospheres* **99**, 10565-10576, (1994).

Martinerie, P., D. Raynaud, D. M. Etheridge, J.-M. Barnola and D. Mazaudier. Physical and climatic parameters which influence the air content in polar ice. *Earth and Planetary Science Letters* **112**, 1-13, (1992).

May, B., D. Wagenbach, H. Hoffmann, M. Legrand, S. Preunkert and P. Steier. Constraints on the major sources of dissolved organic carbon in Alpine ice cores from radiocarbon analysis over the bomb-peak period. *Journal of Geophysical Research: Atmospheres* **118**, 3319-3327, (2013).

May, B. L. Radiocarbon microanalysis on ice impurities for dating of Alpine glaciers, University of Heidelberg,(2009).

Pio, C., M. Legrand, T. Oliveira, J. Afonso, C. Santos, A. Caseiro, P. Fialho, F. Barata, H. Puxbaum, A. Sanchez-Ochoa, A. Kasper-Giebl, A. Gelencsér, S. Preunkert and M. Schock. Climatology of aerosol composition (organic versus inorganic) at nonurban sites on a west-east transect across Europe. *Journal of Geophysical Research: Atmospheres* **112**, (2007).

Preunkert, S., M. Legrand, P. Stricker, S. Bulat, I. Alekhina, J. Petit, H. Hoffmann, B. May and B. Jourdain. Quantification of dissolved organic carbon at very low levels in natural ice samples by a UV-induced oxidation method. *Environmental science & technology* **45**, 673-678, (2010).

Reimer, P. J., E. Bard, A. Bayliss, J. W. Beck, P. G. Blackwell, C. B. Ramsey, C. E. Buck, H. Cheng, R. L. Edwards, M. Friedrich, P. Grootes, T. Guilderson, H. Haflidason, I. Hajdas, C. Hatté, T. Heaton, D. L. Hoffmann, A. G. Hogg, K. A. Hughen, K. Felix Kaiser, B. Kromer, S. W. Manning, M. Niu, R. W. Reimer, D. A. Richards, E. M. Scott, J. R. Southon, R. A. Staff, C. S. Turney and J. van der Plicht. IntCal13 and Marine13 radiocarbon age calibration curves 0–50,000 years cal BP. *Radiocarbon* **55**, 1869-1887, (2013).

Ruff, M., L. Wacker, H. Gäggeler, M. Suter, H.-A. Synal and S. Szidat. A gas ion source for radiocarbon measurements at 200 kV. *Radiocarbon* **49**, 307-314, (2007).

Schindler, J. An Extraction System for Radiocarbon Microanalysis of Dissolved Organic Carbon in Glacier Ice, Universität Bern,(2017).

Schwikowski, M., S. Brütsch, H. Gäggeler and U. Schotterer. A high-resolution air chemistry record from an Alpine ice core: Fiescherhorn glacier, Swiss Alps. *Journal of Geophysical Research: Atmospheres* **104**, 13709-13719, (1999).

Schwikowski, M., A. Döscher, H. Gäggeler and U. Schotterer. Anthropogenic versus natural sources of atmospheric sulphate from an Alpine ice core. *Tellus B: Chemical and Physical Meteorology* **51**, 938-951, (1999).

Sigl, M., T. M. Jenk, T. Kellerhals, S. Szidat, H. W. Gäggeler, L. Wacker, H.-A. Synal, C. Boutron, C. Barbante and J. Gabrieli. Towards radiocarbon dating of ice cores. *Journal of Glaciology* **55**, 985-996, (2009).

Singer, G. A., C. Fasching, L. Wilhelm, J. Niggemann, P. Steier, T. Dittmar and T. J. Battin. Biogeochemically diverse organic matter in Alpine glaciers and its downstream fate. *Nature Geoscience* **5**, 710, (2012).

Sodemann, H., A. Palmer, C. Schwierz, M. Schwikowski and H. Wernli. The transport history of two Saharan dust events archived in an Alpine ice core. *Atmospheric Chemistry and Physics* **6**, 667-688, (2006).

Steier, P., C. Fasching, K. Mair, J. Liebl, T. Battin, A. Priller and R. Golser. A new UV oxidation setup for small radiocarbon samples in solution. *Radiocarbon* **55**, 373-382, (2013).

Stuiver, M. and H. E. Suess. On the relationship between radiocarbon dates and true sample ages. *Radiocarbon* **8**, 534-540, (1966).

Szidat, S., T. Jenk, H. Gäggeler, H.-A. Synal, I. Hajdas, G. Bonani and M. Saurer. THEODORE, a two-step heating system for the EC/OC determination of radiocarbon (^{14}C) in the environment. *Nuclear Instruments and Methods in Physics Research Section B: Beam Interactions with Materials and Atoms* **223**, 829-836, (2004).

Szidat, S., T. M. Jenk, H. A. Synal, M. Kalberer, L. Wacker, I. Hajdas, A. Kasper-Giebl and U. Baltensperger. Contributions of fossil fuel, biomass-burning, and biogenic emissions to carbonaceous aerosols in Zurich as traced by ^{14}C . *Journal of Geophysical Research: Atmospheres* **111**, (2006).

Szidat, S., G. A. Salazar, E. Vogel, M. Battaglia, L. Wacker, H.-A. Synal and A. Türlér. ^{14}C analysis and sample preparation at the new Bern Laboratory for the Analysis of Radiocarbon with AMS (LARA). *Radiocarbon* **56**, 561-566, (2014).

Thompson, L. G., M. E. Davis, E. Mosley-Thompson, T. Sowers, K. A. Henderson, V. S. Zagorodnov, P.-N. Lin, V. N. Mikhalenko, R. K. Campen and J. F. Bolzan. A 25,000-year tropical climate history from Bolivian ice cores. *Science* **282**, 1858-1864, (1998).

Uglietti, C., A. Zapf, T. M. Jenk, M. Sigl, S. Szidat, G. A. Salazar Quintero and M. Schwikowski. Radiocarbon dating of glacier ice: overview, optimisation, validation and potential. *The Cryosphere* **10**, 3091-3105, (2016).

Zhang, Y., N. Perron, V. Ciobanu, P. Zotter, M. Minguillón, L. Wacker, A. Prévôt, U. Baltensperger and S. Szidat. On the isolation of OC and EC and the optimal strategy of radiocarbon-based source apportionment of carbonaceous aerosols. *Atmospheric Chemistry and Physics* **12**, 10841-10856, (2012).

4 Radiocarbon dating of alpine ice cores with the dissolved organic carbon (DOC) fraction

Ling Fang^{1,2,3}, Thomas Singer^{1,2,3}, Shugui Hou⁴, M. Schwikowski^{1,2,3}, Theo M. Jenk^{1,3}

¹Laboratory for Environmental Chemistry, Paul Scherrer Institute, CH-5232 Villigen PSI, Switzerland

²Department of Chemistry and Biochemistry, University of Bern, CH-3012 Bern, Switzerland

³Oeschger Centre for Climate Change Research, University of Bern, CH-3012 Bern, Switzerland

⁴School of Geographic and Oceanographic Sciences, Nanjing University, Nanjing, 210023, China

Manuscript to be submitted to

The Cryosphere

Abstract

Alpine glaciers are valuable archives for paleoclimate records. A precise chronology is essential to interpret the climate signal preserved in ice cores. Radiocarbon dating of Water-insoluble organic carbon (WIOC) fraction has become an important dating tool to constrain the age of ice cores from nonpolar region. However, in some cases this method is restricted by the low WIOC concentration present in the ice. In this work, we present first comprehensive ^{14}C dating results using the dissolved organic carbon (DOC) fraction, evaluating this new approach by comparison to the established WIO ^{14}C dating based on parallel sample sections from four different glaciers. ^{14}C dated ages of the two fractions yield a comparable probability distribution with WIO ^{14}C systematically resulting in a slightly older mean age for samples younger than around 1000 years. Our data suggests this to be caused by an incomplete removal of carbonates (^{14}C dead) on the filtered WIOC samples while a potential reservoir effect from aged aerosols in the WIOC being negligible considering the analytical uncertainties currently achieved. This study confirms that ^{14}C dating of the ice entrapped DOC fraction is applicable and a valuable future tool for the dating of ice samples. There is no indication of in-situ production systematically contributing to DO ^{14}C as reported in a previous study. The benefits to use the DOC fraction is not just reducing the required ice mass, but also improving the analytical precision. Finally, with this new DO ^{14}C method, it may be possible to push radiocarbon dating of ice a step forward even to remote and Polar Regions.

4.1 Introduction

For a meaningful interpretation of the recorded paleoclimate signals in ice cores from glacier archives, an accurate chronology is essential. Annual layer counting, supported and tied to independent time markers such as the 1963 horizon evident by a peak maximum in tritium or other radioisotopes, or distinct signals from known volcano eruptions in the past is the fundamental and most accurate technique used for ice core dating. However, for ice cores from high alpine glaciers this approach is limited up to a few centuries only, because of the exceptional strong thinning of annual layers with increasing depth and thus a loss of the sampling resolution required for the detection of seasonal fluctuations or the detection of distinct single events. Ice flow models (e.g. Nye's model) are widely used to retrieve a full depth age scale [Nye, 1963; Bolzan, 1985; Thompson et al., 2006]. However, due to the complex bedrock geometry of high-alpine glaciers, ice flow models can also not be applied for the entire length of the core. Even with a 3D model, which requires complex geometry data, it is challenging to simulate the bottom age [Licciulli et al., 2020]. This emphasizes the need for an absolute dating tool applicable to the oldest, bottom part of cores from these sites.

Radioactive isotopes contained in the ice offer the opportunity to obtain absolute ages of an ice sample. The concentrations of ^{39}Ar and ^{32}Si are both very low requiring several kg of ice for dating [Morgenstern et al., 2010; Feng et al., 2019]. ^{210}Pb and ^{14}C are the most promising radioactive isotopes for dating. With the half-life of 22.3 years, ^{210}Pb can be used to date ice back to 200 years [Gäggeler et al., 2020]. However, for millennial scale ice cores, ^{14}C dating is the technique of choice. With a half-life of 5370 years dating up to 26000 years is possible [Godwin, 1962], which covers most of time ranges of alpine glaciers [Uglietti et al., 2016]. ^{14}C dating of water insoluble organic carbon (WIOC) from glacier ice has become an established technique for ice core dating. Samples of $>10\ \mu\text{g}$ WIOC can now be dated with reasonable uncertainty (10-20%), requiring less than 1 kg of ice from typical mid-latitude and low-latitude glaciers [Jenk et al., 2007; Jenk et al., 2009; Sigl et al., 2009; Uglietti et al., 2016]. However, the low WIOC concentration in some glaciers and in Polar Regions together with the large demands of ice mass puts a limit to this application.

Considering previously reported dissolved organic carbon (DOC) concentrations in ice being a factor of about 5 higher compared to typical WIOC concentrations [Legrand et al., 2007; Legrand et al., 2013; May et al., 2013], applying ^{14}C analysis to DOC fraction could

reduce the required ice amount. This may allow an extension of ^{14}C dating to new sites and generally reducing the achievable analytical (dating) uncertainty. The underlying hypothesis of applying the DOC fraction for ^{14}C dating is similar to WIOC dating approach [Jenk et al., 2007; Sigl et al., 2009]. DOC stored in ice is composed of atmospheric water soluble organic carbon (WSOC) contained in carbonaceous aerosol particles and organic gases taken up during precipitation [Legrand et al., 2013]. WSOC is formed in the atmosphere by oxidation of gases emitted from the biosphere, followed by condensation of the less volatile products. Carbonaceous aerosols are transported in the atmosphere and eventually deposited on the glacier by wet and dry deposition. Before the industrial revolution, these organic carbon species contained the corresponding atmospheric ^{14}C signal when the snow deposited on the glacier. For analysing of DO^{14}C in ice cores, one of the major limitations is the relatively low extraction efficiency ranging from 64% to 96%, [Steier et al., 2013 and May et al., 2013], respectively and the high risk of sample contamination [Legrand et al., 2013]. In contrast to high-temperature combustion or wet-chemical oxidation techniques, the use of ultraviolet (UV) photochemical oxidation has the advantage of being suitable for large volumes of sample with low carbon content [Beaupré et al., 2007]. Ice cores can potentially be contaminated during drilling, storage, and sample processing.

A first attempt to use DOC for ^{14}C dating of ice samples was conducted by May (2009) using a set-up for a combined analysis of both the DOC and WIOC fraction with subsequent radiocarbon microanalysis. However, their results were not entirely conclusive, also suggesting potential in-situ production of ^{14}C in the DOC fraction based on derived $F^{14}\text{C}$ values indicating super modern origin. Building on these initial findings, May (2009) questioned the applicability of the DOC fraction for radiocarbon dating. It should be noted, that although the in-situ ^{14}C production of ^{14}CO and $^{14}\text{CO}_2$ has been studied thoroughly and is rather well understood (Van de Wal et al., 1994; Lal et al., 1997; Smith et al., 2000), the potential processes and mechanisms of ^{14}C in-situ formation in organic compounds seem far less likely and not investigated to date (Woon, 2002). Also the first ^{14}C dating results using the WIOC fraction were rather questionable in May (2009) and in cases conflicting with previous and proven findings from the pioneering studies in this field. Therefore, a DOC extraction setup for radiocarbon analyses was designed and built at PSI for further investigation of the potential of DO^{14}C for dating ice (Fang et al., 2019). The PSI extraction system can handle samples with volumes of up to ~350 mL and DOC concentrations as low as 25 ppbC. In this study, we will investigate the DOC ^{14}C

dating of samples from selected ice cores and compare the DOC ^{14}C age with ages obtained using the well established WIOC ^{14}C dating method.

4.2 Sample preparation and ^{14}C analysis

To validate the DOC ^{14}C dating technique, the deep part of ice cores from the four glaciers Colle Gnifetti, Belukha, Chongce core 1, and Shu Le Nan Shan (SLNS) were selected (Figure 4.1). The high-alpine glacier Colle Gnifetti is located in the Monte Rosa massif in the Swiss Alps close to the Italian border. A 76 m long core down to the bedrock was retrieved from the glacier saddle in September 2015 at an altitude of 4450 m asl. ($45^{\circ}55'45.7''\text{N}$, $7^{\circ}52'30.5''\text{E}$). Four samples were selected from the bottom 4 m (72-76 m) right above the bedrock. The Belukha core was drilled in 2018 from the saddle between the two summits of Belukha ($49^{\circ}48'27.7''\text{N}$, $86^{\circ}34'46.5''\text{E}$, 4055 m asl.), the highest in the Altai mountain range, which is of particular interest due to the proximity to Eastern Europe. The bedrock was reached and the total length of the core is 163 m. Three samples were analyzed from the deeper part (158-163 m). Seven and three samples were analyzed from the deep parts of SLNS and Chongce, respectively. The SLNS ice core was retrieved in May 2010 from the south slope of the Shulenanshan Mountain ($38^{\circ}42'19.35''\text{N}$, $97^{\circ}15'59.70''\text{E}$, 5336.5 m asl.). The bedrock was reached and the total length of the ice core is 81.05 m. The Chongce ice cap is located in the western Kunlun Mountains on the northwestern Tibetan Plateau, covering an area of 163.06 km^2 with a volume of 38.16 km^3 . The ice cap faces south with a mean equilibrium line altitude of 5900 m asl. A 134.03 m long core down to the bedrock was retrieved from this ice cap in October 2012 at an altitude of 6010 m asl. ($35^{\circ}14'5.77''\text{N}$, $81^{\circ}7'15.34''\text{E}$).

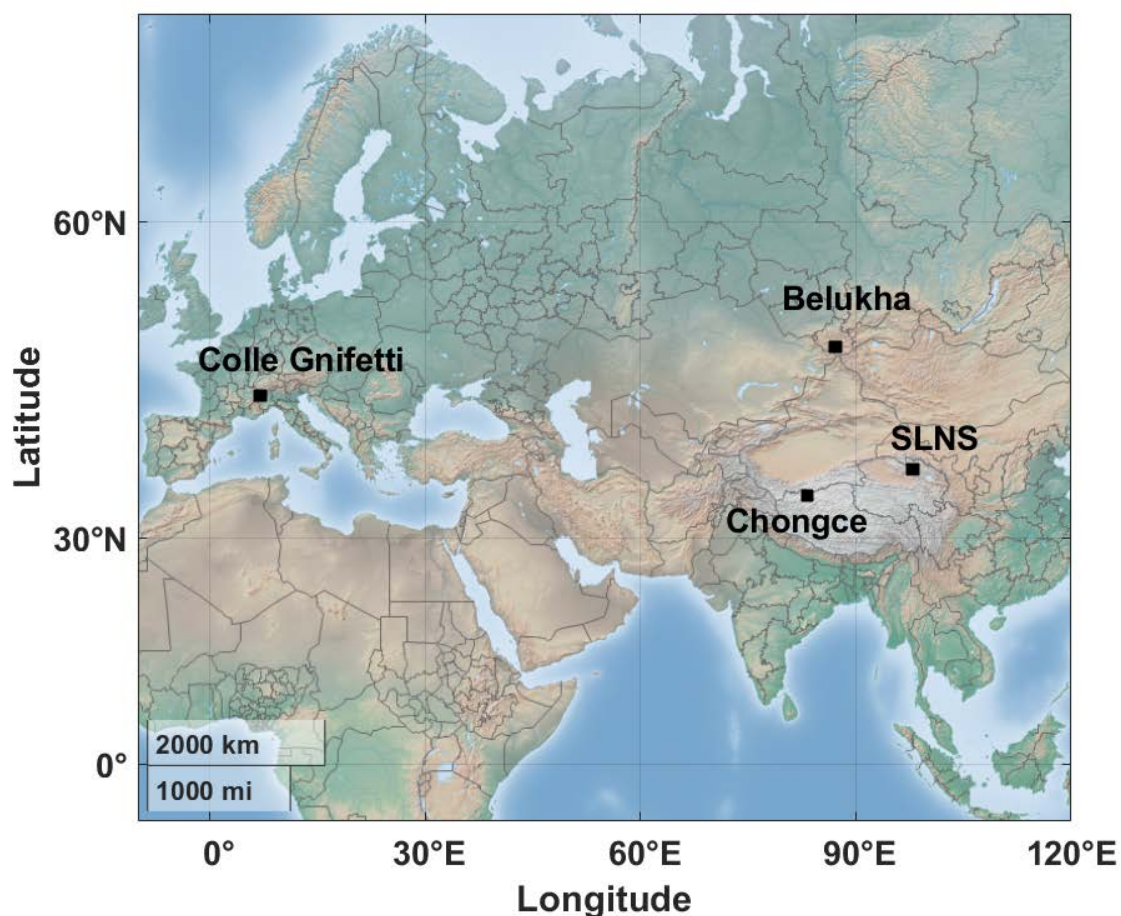


Figure 4.1 Location of the four glaciers Colle Gnifetti, Belukha, Chongce, and Shu Le Nan Shan (SLNS). Map made from Matlab R2019b geobasemap. Colle Gnifetti is located in the Monte Rosa massif in the Swiss Alps, Belukha glacier in the Altai mountain range, Russia, the Chongce ice cap on the northwestern Tibetan Plateau, China, and the SLNS at the south slope of the Shulenanshan Mountain, China.

All sample were decontaminated in a cold room (-20°C) by cutting off the surface layer (~ 3 mm). Each sample was split into two parallel sections to perform both WIOC and DOC ^{14}C analysis. Samples for WIOC ^{14}C -daing were prepared following the protocol described in Uglietti et al. (2016), a brief summary is provided in the following. In order to remove potential contamination in the outer layer of the ice core, pre-cut samples from the inner part of the core were additionally rinsed with ultra-pure water. After melting, the contained particles were filtered onto prebaked quartz fibre filters (Pallflex Tissueqtz-2500QAT-UP). These initial steps were performed in a class 100 laminar flow box to ensure clean conditions.

For DO¹⁴C analysis, sample preparation follows the procedure in Fang et al. (2019). After transfer to the laboratory, samples were further decontaminated by rinsing with ultrapure water under helium atmosphere in the melting vessel of the extraction setup, where they were also melted under helium flow. An extra decontamination step was applied to clean the system before filtering the sample into the reactor. For this 50 mL ultra-pure water was injected into the reactor and acidified with 1 mL of 85% H₃PO₄. To enhance the oxidation efficiency, 2 mL of 100 ppm FeSO₄ and 1 mL of 50 mM H₂O₂ (Fenton's reagent) was also injected into the base water following the study from Hsueh et al. (2005) and Kušić et al. (2006). Switching on the UV lights for ~20 to 30 min to remove all potential contamination and monitoring the resulting CO₂ by the online non-dispersive infrared (NDIR) analyzer. After the ice melted, the meltwater was filtrated using a pre-baked (heated at 800 °C for 5 h) in-line quartz fibre filter under helium gas flow. The sample volume was determined by measuring the reactor fill level. The filtrate was acidified by mixing with the base water containing H₃PO₄ from the extra decontamination step. After the degassing of CO₂ from inorganic carbon (IC) based on the NDIR signal, 1 mL of 50 mM H₂O₂ was injected into reactor right before the irradiation started. During UV oxidation, water vapor was removed by cryogenic trapping at – 60 °C and produced CO₂ was trapped in liquid nitrogen. The sample CO₂ was further cleaned from residual water vapor and quantified manometrically. Finally, CO₂ was sealed into a glass vial for ¹⁴C analyses. ¹⁴C measurements were carried out at the University of Bern in the Laboratory for the Analysis of Radiocarbon with AMS (LARA laboratory). The obtained WIOC samples were combusted in a thermo-optical OC/EC analyzer (Model4L, Sunset Laboratory Inc, USA) equipped NDIR cell to quantify the CO₂ produced, using the well-established Swiss 4S protocol for OC/EC separation (Zhang et al., 2012). Being coupled to a 200 kV compact accelerator mass spectrometer (AMS, mini radiocarbon dating system MICADAS) equipped with a gas ion source and a Gas Interface System (GIS, Synal et al., 2007; Ruff et al., 2010; Wacker et al., 2013; Szidat et al., 2014), the LARA Sunset-GIS-AMS system (Agrios et al., 2017) then allowed for final, direct online ¹⁴C measurements of the CO₂ produced from the WIOC fraction. Resulting CO₂ gas from DOC in the glass vial was directly injected into the MICADAS using a cracker system, which is designed for cracking glass vials under vacuum and carrying the CO₂ gas with a helium flow to the Cs ion source [Wacker et al., 2013].

All ¹⁴C results are expressed as fraction modern (F¹⁴C), which is the fractionation corrected ¹⁴C/¹²C ratio of the sample divided by the same ratio of the modern standard (NIST

standard oxalic acid II, SRM 4990C). The $F^{14}C$ results shown in Table 4.1 are corrected for the MICADAS system constant contamination ($0.91 \pm 0.18 \mu\text{g}$ with $F^{14}C$ of 0.72 ± 0.11 for the Sunset-GIS-AMS system and $0.06 \pm 0.18 \mu\text{g}$ with $F^{14}C$ of 0.50 ± 0.11 for the cracker system), cross contamination (0.2 % from the previous sample), and procedure blanks ($1.26 \pm 0.59 \mu\text{g}$ with $F^{14}C$ of 0.69 ± 0.15 for WIOC samples and $1.9 \pm 1.6 \mu\text{g}$ with a $F^{14}C$ value of 0.68 ± 0.13 for DOC samples). All these uncertainties were propagated throughout whole data processing until final ^{14}C calibration. These corrections have a stronger effect on low carbon mass samples, resulting in a larger dating uncertainty. Therefore, we only discuss samples with a carbon mass $> 10 \mu\text{g}$ as recommended in Uglietti et al. (2016). We calculated the conventional ^{14}C age based on the mean lifetime of 8033 years [Stuiver and Polach, 1977], and given in years before present (BP, BP=1950) in Table 4.1. The conventional ^{14}C ages were calibrated using OxCal 4.3.2 software with the IntCal13 calibration curve (Reimer et al., 2013; Ramsey, 2017). Calibrated mean ages are given in years before present (cal BP) with $\pm 1\sigma$ range in Table 4.2. We also calibrated our data with the sequence deposition model (Ramsey, 2008), which are given as cal BP in Table 4.2.

4.3 Results

4.3.1 DOC and WIOC concentration

DOC concentrations are generally higher than the corresponding WIOC concentrations (Figure 4.2). The average DOC/WIOC concentration ratio is 1.9 ± 0.6 for the four glaciers (Table 4.1). This is lower than the previously reported average DOC to WIOC ratio of about 5 in three discontinuous samples over the time period of 1568-1854 from Colle Gnifetti, Swiss Alps [Legrand et al., 2007; Legrand et al., 2013]. The difference maybe the result of spatial and temporal natural variation. DOC related WSOC typically contributed 20-80% of the total organic carbon depending on the season and region [Decesari et al., 2001; Ram et al., 2010; Khare et al., 2011]. At the alpine high elevation site of Sonnblick (3106 m asl), the ratio of WSOC/WIOC is about 1.5 [Pio et al., 2007]. Consider about the uptake of organic gaseous, the slightly enriched ratio we observed in ice is consistent with atmospheric observation about DOC related WSOC to WIOC. Legrand et al., (2007) suggested estimate WSOC from DOC by subtracting the monocarboxylic acids and formaldehyde. The formaldehyde concentration in

Table 4.1 WIOC samples analyzed for Colle Gnifetti, Belukha, SLNS and Chongce ice cores

Core section	Depth (m)	WIOC (μg)	Concentration ($\mu\text{g}/\text{kg}$)	Be Nr.	F ¹⁴ C ($\pm 1\sigma$)	¹⁴ C age (BP, $\pm 1\sigma$)
CG110	72.1-72.7	35.2	61.9 \pm 3.3	11770.1.1	0.875 \pm 0.011	1088 \pm 96
CG111	72.7-73.4	38.7	71.8 \pm 3.8	11771.1.1	0.848 \pm 0.010	1334 \pm 93
CG112	73.4-73.9	23.7	44.1 \pm 2.4	11772.1.1	0.852 \pm 0.014	1306 \pm 129
CG113	73.9-74.6	39.8	72.4 \pm 3.8	11773.1.1	0.786 \pm 0.010	1949 \pm 102
Belukha412	160.2-160.9	37.8	85.2 \pm 4.5	11766.1.1	0.368 \pm 0.009	8055 \pm 189
Belukha414	161.7-162.5	27.8	82.6 \pm 4.4	11768.1.1	0.213 \pm 0.012	12448 \pm 460
Belukha415	162.5-163.0	39.3	123.3 \pm 6.5	11769.1.1	0.102 \pm 0.009	18398 \pm 766
SLNS101	56.8-57.5	41.5	98.9 \pm 2.1	12325.1.1	0.906 \pm 0.048	792 \pm 424
SLNS113	64.7-65.4	45.3	106.1 \pm 2.5	12324.1.1	0.856 \pm 0.047	1245 \pm 439
SLNS122	68.9-69.7	58.5	138.0 \pm 3.6	12323.1.1	0.810 \pm 0.046	1689 \pm 457
SLNS127	71.8-72.5	50.9	105.3 \pm 2.5	12322.1.1	0.701 \pm 0.046	2851 \pm 525
SLNS136	76.7-77.5	50.6	135.2 \pm 3.0	12321.1.1	0.530 \pm 0.045	5104 \pm 685
SLNS139	78.9-79.6	61.2	126.3 \pm 3.6	12320.1.1	0.528 \pm 0.045	5124 \pm 685
SLNS141-142	80.3-81.0	61.7	149.5 \pm 3.8	12319.1.1	0.496 \pm 0.045	5633 \pm 729
CC237	126.0-126.7	22.4	63.7 \pm 1.8	12328.1.1	0.718 \pm 0.050	2662 \pm 558
CC244	130.2-130.8	29.8	95.9 \pm 2.2	12327.1.1	0.650 \pm 0.048	3455 \pm 588
CC252	133.4-133.8	23.8	136.7 \pm 4.3	12326.1.1	0.341 \pm 0.046	8646 \pm 1086

Table 4.2 DOC samples analyzed for Colle Gnifetti, Belukha, SLNS and Chongce ice cores.

Core section	Depth (m)	DOC (μg)	Concentration ($\mu\text{g}/\text{kg}$)	Be Nr.	F ¹⁴ C ($\pm 1\sigma$)	¹⁴ C age (BP, $\pm 1\sigma$)	DOC/WIOC
CG110	72.1-72.7	18.9	110.0 \pm 2.7	11575.1.1	0.943 \pm 0.030	474 \pm 259	1.8
CG111	72.7-73.4	25.5	122.9 \pm 3.0	11576.1.1	0.901 \pm 0.021	836 \pm 190	1.7
CG112	73.4-73.9	23.6	95.0 \pm 2.3	11577.1.1	0.889 \pm 0.021	943 \pm 192	2.2
CG113	73.9-74.6	29.5	119.4 \pm 2.9	11578.1.1	0.849 \pm 0.016	1312 \pm 151	1.7
Belukha412	160.2-160.9	28.5	165.0 \pm 4.0	11581.1.1	0.315 \pm 0.024	9284 \pm 623	1.9
Belukha414	161.7-162.5	41.9	327.4 \pm 7.9	11584.1.1	0.239 \pm 0.019	11505 \pm 648	4.0
Belukha415	162.5-163.0	23.7	231.0 \pm 5.6	11585.1.1	0.144 \pm 0.041	15584 \pm 2298	1.9
SLNS101	56.8-57.5	44.0	184.9 \pm 4.5	12458.1.1	0.972 \pm 0.016	227 \pm 131	1.9
SLNS113	64.7-65.4	39.4	185.2 \pm 4.5	12459.1.1	0.942 \pm 0.016	484 \pm 137	1.7
SLNS122	68.9-69.7	57.9	248.0 \pm 6.0	12460.1.1	0.773 \pm 0.010	2073 \pm 101	1.8
SLNS127	71.8-72.5	57.8	229.7 \pm 5.5	12461.1.1	0.730 \pm 0.009	2527 \pm 101	2.2
SLNS136	76.7-77.5	48.3	219.1 \pm 5.3	12462.1.1	0.657 \pm 0.009	3380 \pm 112	1.6
SLNS139	78.9-79.6	48.1	230.8 \pm 5.6	12463.1.1	0.580 \pm 0.010	4381 \pm 131	1.8
SLNS141-142	80.3-81.0	43.8	177.5 \pm 4.3	12464.1.1	0.550 \pm 0.025	4809 \pm 151	1.2
CC237	126.0-126.7	28.5	136.6 \pm 3.3	12454.1.1	0.980 \pm 0.023	161 \pm 185	2.1
CC244	130.2-130.8	21.7	129.8 \pm 3.1	12455.1.1	0.800 \pm 0.018	1789 \pm 185	1.4
CC252	133.4-133.8	24.3	202.5 \pm 4.9	12456.1.1	0.546 \pm 0.016	4854 \pm 239	1.5

snow is negligible and monocarboxylic acids are account for about 15% to 25% of DOC from Col du Dôme, Colle Gnifetti and Fiescherhorn [Legrand et al., 2007; Fang et al., 2020]. Using the WSOC/WIOC of 1.5 to estimate the DOC/WIOC in the ice is about 1.7-1.9, which is in the ideal range of our results. It's also interesting to notice that average DOC/ WIOC ratio from Belukha (2.5) is higher compare to other sites (Colle Gnifetti, SLNS and Chongce is 1.8, 1.7 and 1.6, respectively). Belukha glacier is surround by Siberian Forest, the higher ratio may indicate higher WSOC formation from biogenic volatile organic compounds. DOC and WIOC concentrations at Colle Gnifetti ($112 \pm 12 \mu\text{g/kg}$ and $63 \pm 13 \mu\text{g/kg}$, respectively) are slightly lower compared to the other three glaciers. It also interesting to notice that not just the DOC/WIOC ratio is highest at Belukha, but also the DOC concentrations ($241 \pm 82 \mu\text{g/kg}$) (Figure 4.2). Belukha glacier is surrounded by Siberian Forests, a strong source of WSOC forming biogenic precursor gases. Mean DOC and WIOC concentrations from cores retrieved from Tibetan Plateau are $211 \pm 28 \mu\text{g/kg}$ and $123 \pm 19 \mu\text{g/kg}$ at SLNS and $156 \pm 40 \mu\text{g/kg}$ and $99 \pm 37 \mu\text{g/kg}$ at Chongce, respectively. In general, these values are higher compared with European Alpine glaciers in the pre-industrial period.

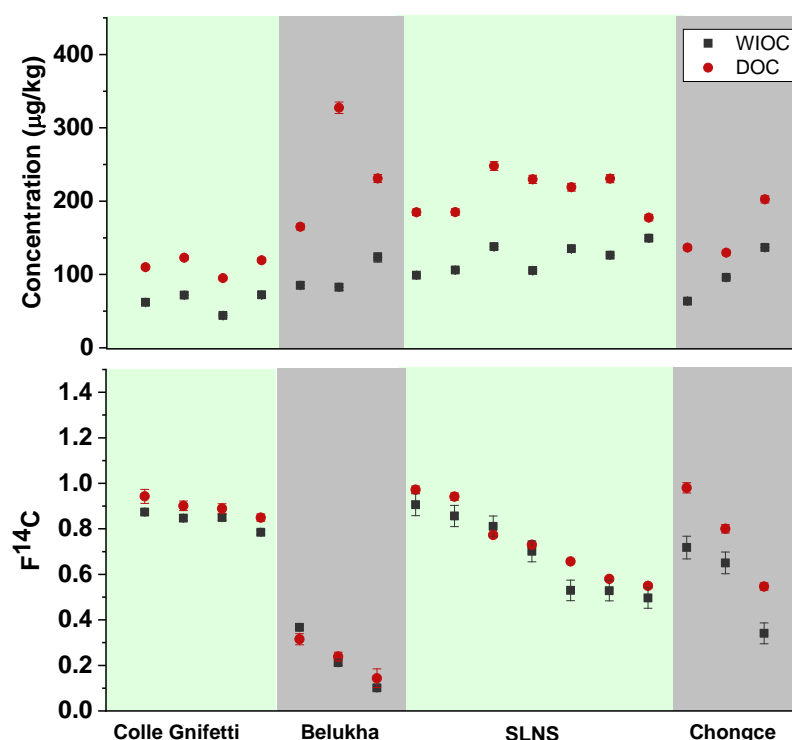


Figure 4.2: Comparison of concentrations (a) and $F^{14}C$ (b) of the WIOC and DOC fractions.

4.3.2 ^{14}C results

$F^{14}\text{C}$ values from DOC fraction is generally following the same trend as WIOC but except the site from Chongce. The DOC $F^{14}\text{C}$ fall far below the corresponding WIOC $F^{14}\text{C}$ values. Generally the corresponding DOC and WIOC fractions yielded within the uncertainties the same $F^{14}\text{C}$ values as illustrated by the scatter plot in Figure 4.3. Values scatter along the 1:1 ratio line and these two dataset are significantly correlated (Pearson correlation coefficient $r=0.96$, $p<0.01$, $n=19$). However, as we expected, three sample from Chongce are fall far above the 1:1 ratio line (Figure 4.3a). Previous ^{14}C ages from the upper part of the Chongce core 2 (80-180 m), less than 2km away from core1, did not show a clear increase with depth and it was suggested that the observed larger uncertainties were caused by a high mineral dust load (Hou et al., 2018). During filtration, we also noticed a higher dust loading for these samples. Therefore, we exclude these samples from Chongce for the linear regression shown in the Figure 4.3a. The slope of the linear regression (1.03 ± 0.04 , $R^2=0.97$, $n=16$ exclude the three sample from Chongce) show these two method comparable but the intercept of 0.02 indicates that $F^{14}\text{C}$ -DOC values are systemically higher compare to the corresponding $F^{14}\text{C}$ -WIOC values (see also Figure 4.3).

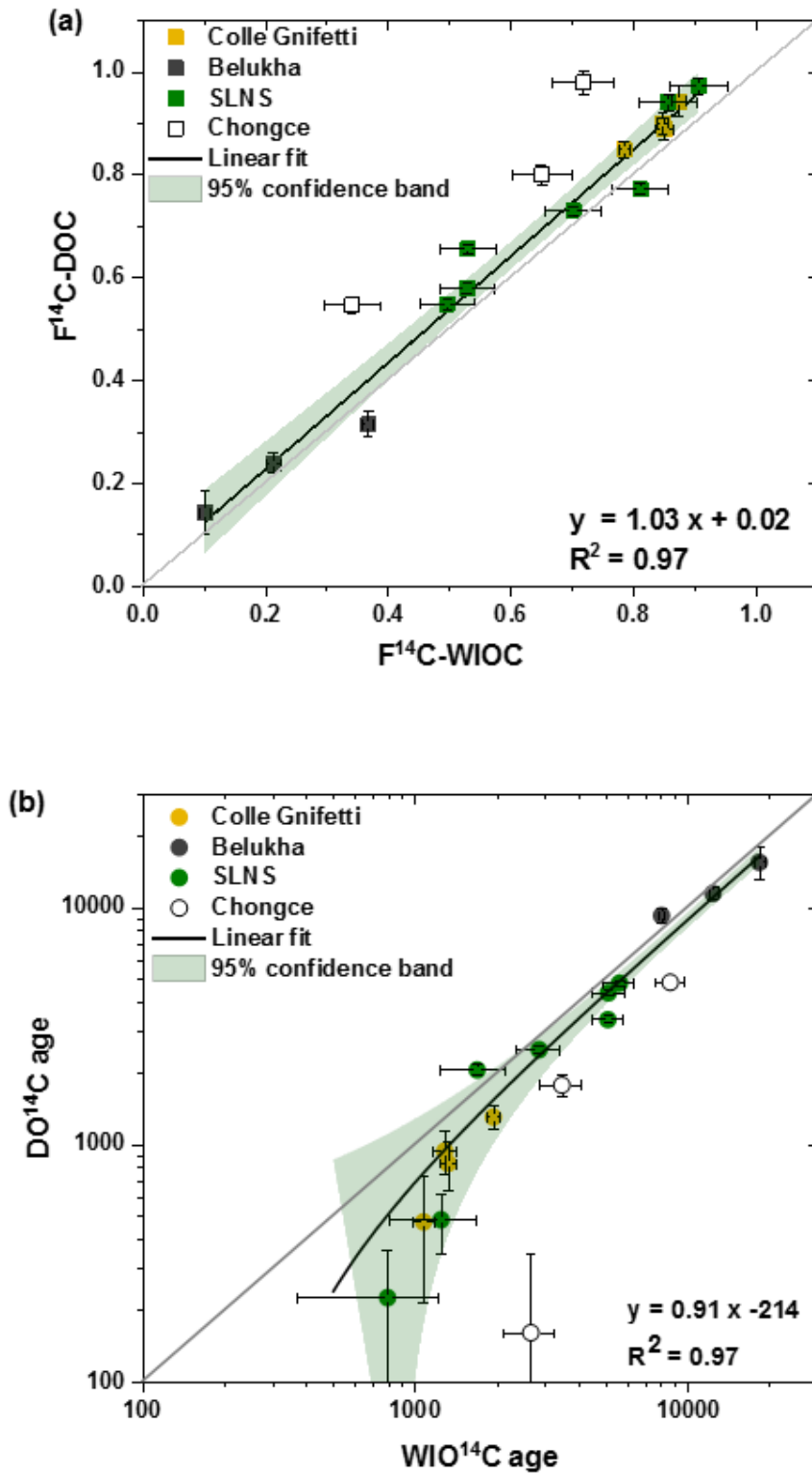


Figure 4.3: Linear regression of DOC and WIOC in $F^{14}C$ (a) and ^{14}C age (b). The black line with shade area is the linear fit together with 95% confidence band. 1:1 ratio indicated with gray line. The ^{14}C ages are shown on logarithmic scales.

4.4 Discussion

4.4.1 Potential contribution of carbonates to WIOC dating

We observed an average age offset of around 700 years between the DOC and WIOC fraction for samples from Colle Gnifetti, Belukha and SLNS, but this was significantly larger (around 2000 years) for samples with high dust content from Chongce. We assume that the discrepancy is caused by incomplete removal of carbonates contained in mineral dust, which are depleted in ^{14}C ($F^{14}\text{C}$ values close to 0). These carbonates on the filters should have been converted to CO_2 by the acidification. However, when the dust loading is high, this removal might not be fully efficient. The low $F^{14}\text{C}$ values of carbonates would result in the largest bias for the young sample based on the ^{14}C mass balance:

$$C_{\text{meas}} \times F^{14}\text{C}_{\text{meas}} = \text{WIOC} \times F^{14}\text{C}_{\text{sample}} + \text{Carbonates residual} \times F^{14}\text{C}_{\text{carbonates}}$$

C_{meas} and $F^{14}\text{C}_{\text{meas}}$ are the measured carbon amount and $F^{14}\text{C}$ values. WIOC and $F^{14}\text{C}_{\text{WIOC}}$ is the WIOC carbon amount and the corresponding $F^{14}\text{C}$ value. Carbonates residual is the carbon from carbonates remaining on the filter after acidification, $F^{14}\text{C}_{\text{carbonates}}$ was set to 0.005. For example, if the sample contained 20 μgC WIOC with $F^{14}\text{C}$ values of 0.92, 1 μgC of carbonates residual would introduce a bias of 0.05 to resulting $F^{14}\text{C}$. Nevertheless, for an old sample with $F^{14}\text{C}$ of 0.22 and the same WIOC amount of 20 μgC , 1 μgC of carbonates would only result in 0.01 difference of the $F^{14}\text{C}$ value.

Based on the ^{14}C mass balance equation described before and applying the least squares to find the best estimation of remaining carbonates for the four glaciers, CG, Belukha, SLNS and Chongce contained about 2.2, 5.0, 4.0 and 6.9 μgC of carbonates remaining on the filters, respectively. As proxy for mineral dust we used Ca^{2+} , which showed much higher concentrations in the Chongce (2170 $\mu\text{g}/\text{kg}$ over the time period of 1903-1992, ChongYi et al., 2016) and dated Belukha core (5165 $\mu\text{g}/\text{kg}$) compared to dated Colle Gnifetti samples (83 $\mu\text{g}/\text{kg}$). Ca^{2+} concentrations of SLNS data are not available yet, instead we used the Ca^{2+} concentrations, 1700 $\mu\text{g}/\text{kg}$, from nearby Puruogangri ice cap [Thompson et al., 2006]. The estimated carbonates residuals show a relationship with the Ca^{2+} concentrations, i.e. sample with higher Ca^{2+} concentrations from Chongce and Belukha contain larger fraction of remaining

carbonates. Most of the carbonates (>95%) were removed by the acidification, but for the samples with high dust load a bias of the $F^{14}C$ nevertheless resulted (Table 4.4).

The $F^{14}C$ values corrected for residual carbonates and the corresponding ^{14}C ages are shown in Figure 4.4. Based on the linear regression of ^{14}C age, our assumption that the offset is mainly due to carbonates seems to slightly overestimate the impact. This assumed offset from carbonates residual is in the same range with 1σ uncertainties (Figure 4.5). In addition, similar to the analytical 1σ uncertainty, youngest samples are influenced most and with increased age the bias decreases significantly. The age bias from carbonates residual is largest for the group younger than 1000 years with 49% offset, but the analytical uncertainty is also $\pm 23\%$ of the mean age (Table 4.4). For the age group between 1000-2000 years, this bias is not obvious anymore, $\pm 23\%$ comparable with the analytical uncertainty of $\pm 16\%$. For samples > 2000 years, the carbonates residual bias ($\pm 7\%$) is masked by the dating uncertainty ($\pm 10\%$). In the review paper about WIO ^{14}C dating (Uglietti et al. 2016), all ice samples discussed were older than around 1000 years. Thus, the bias did not play a role.

Most of the WIO ^{14}C data previously reported by our group have been calibrated with deposition sequence model, which normally causes a shift of the mean ^{14}C age of the upper samples to younger ages in the potential age distribution area. This could have partly compensated for the bias from carbonates for samples <1000 years. In addition, for all these published ice core chronologies, the age-depth relationships were modeled (2p model or Copra for Ortles). Thereby, the models were constrained by independent dating methods (ALC, Horizons) in the younger part of the core. Therefore, a potential age bias of ^{14}C results younger than 1000 years was significantly reduced resulting in the final age scales to be not biased significantly within the published uncertainties.

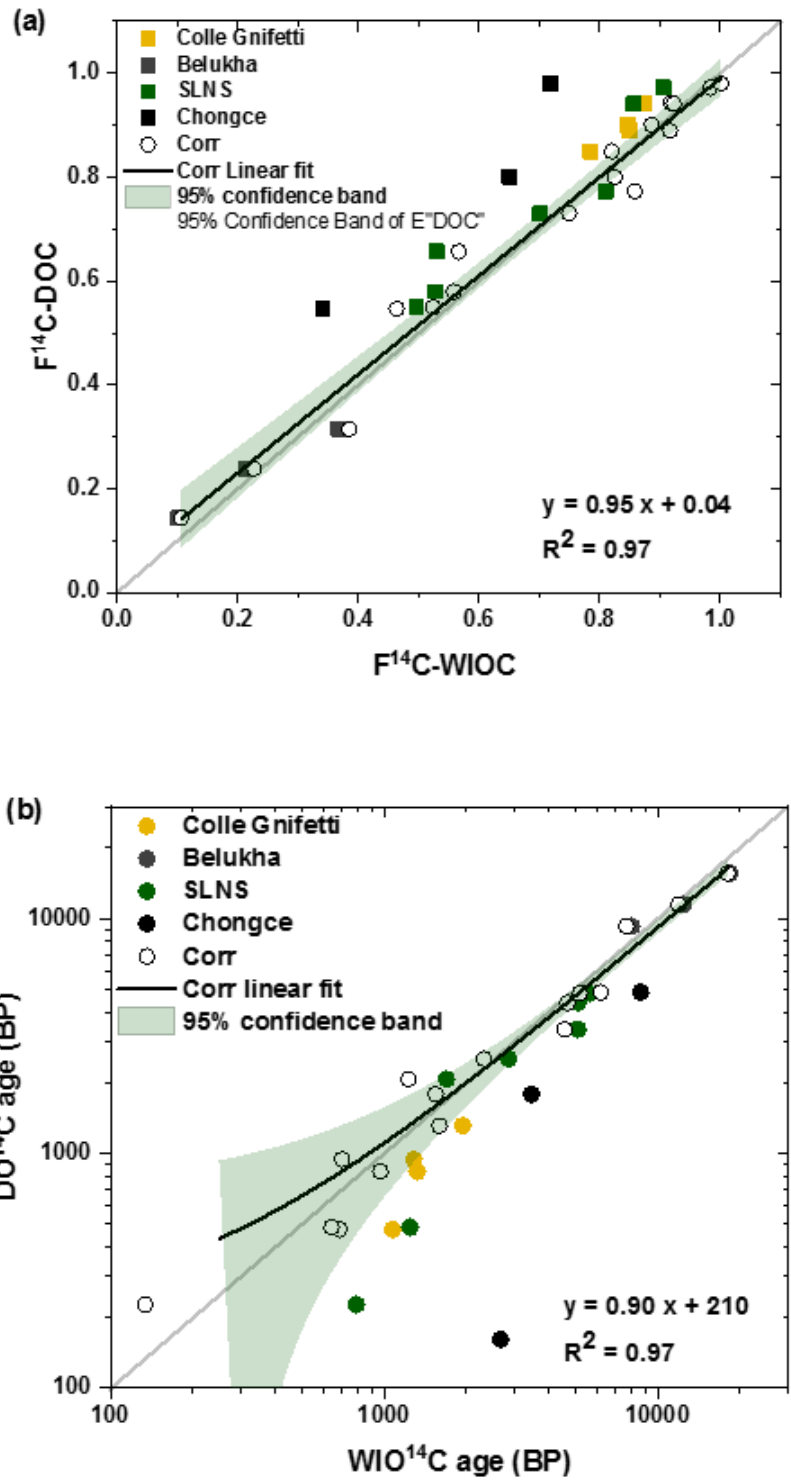


Figure 4.4 Carbonates corrected F¹⁴C (a) and ¹⁴C age (b) of the WIOC fraction compared with the DOC fraction. Corrected WIOC values are indicated as gray circles.

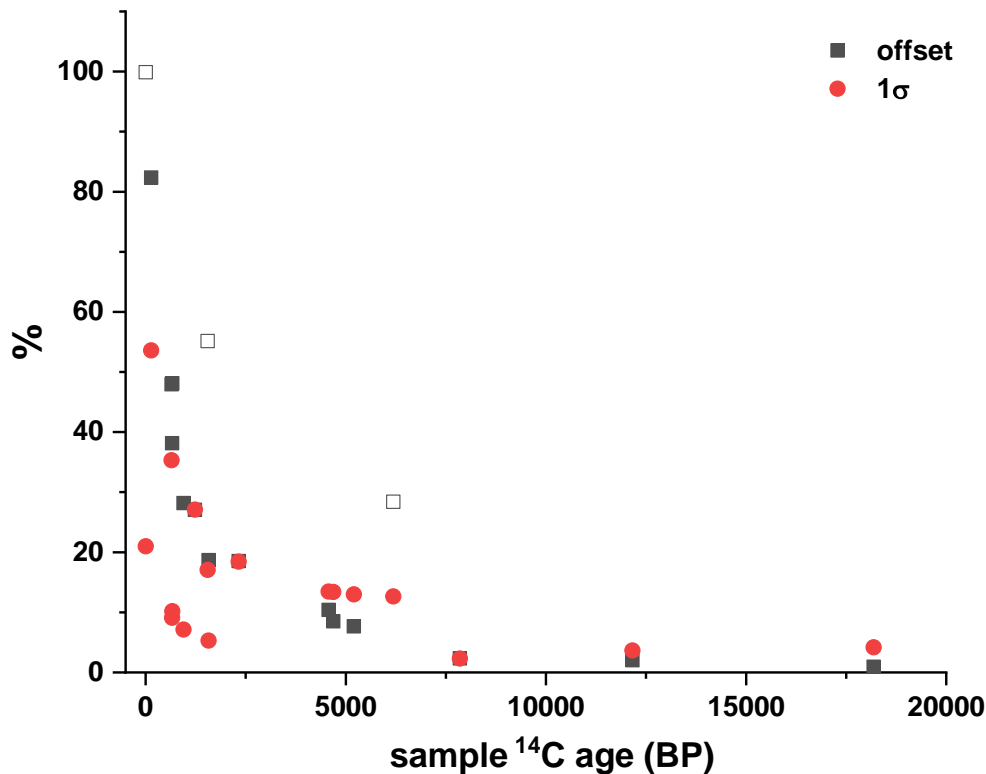


Figure 4.5 Assumed WIO¹⁴C age offset due to carbonates and the corresponding 1 σ analytical uncertainty of each sample versus sample ¹⁴C age.

4.4.2 Age scales

Calibrated ¹⁴C age distributions (cal BP) of DOC and carbonates corrected WIOC using OxCal V4.3.2 with IntalCal13 are shown in the Table 4.3 [Reimer et al., 2013; Ramsey, 2017]. We also applied the deposition sequence model to constrain our data, the results are given as calibrated ¹⁴C ages (cal BP) with deposition sequence model [Ramsey, 2008].

The bottom ages of the four glaciers clearly show a decrease with latitude. The Belukha core is much older than other glaciers (Figure 4.6). A mean age > 20,000 year cal BP for the deepest sample of Belukha core was obtained from both DO¹⁴C and WIO¹⁴C dating, indicating that the Belukha glacier is of Pleistocene origin. This is older than the previously reported age of ~11,000 year BP at 0.67 m weq above the bedrock of the Belukha 2003 core, which was

retrieved from Belukha West Plateau and not from the saddle [Aizen et al., 2016; Uglietti et al., 2016]. The two glaciers from the Tibetan Plateau (SLNS and Chongce) show similar bottom ages of around 5500-6000 year BP, which agree with the previously reported age ranges of TP glaciers [Hou et al., 2018]. The bottom age of Chongce core 1 (5580 ± 295 cal BP) is in the same range as the bottom sample for the Chongce core 2 (6220 ± 223 cal BP). Previous WIOC dating from a core obtained in 2003 at Colle Gnifetti showed an age older than 15000 years just above bedrock (Jenk et al., 2009). The bottom most sample of the Colle Gnifetti 2015 was not dated because of the small amount of ice. Nevertheless, the younger ages of the 2015 core imply that bedrock was probably not reached.

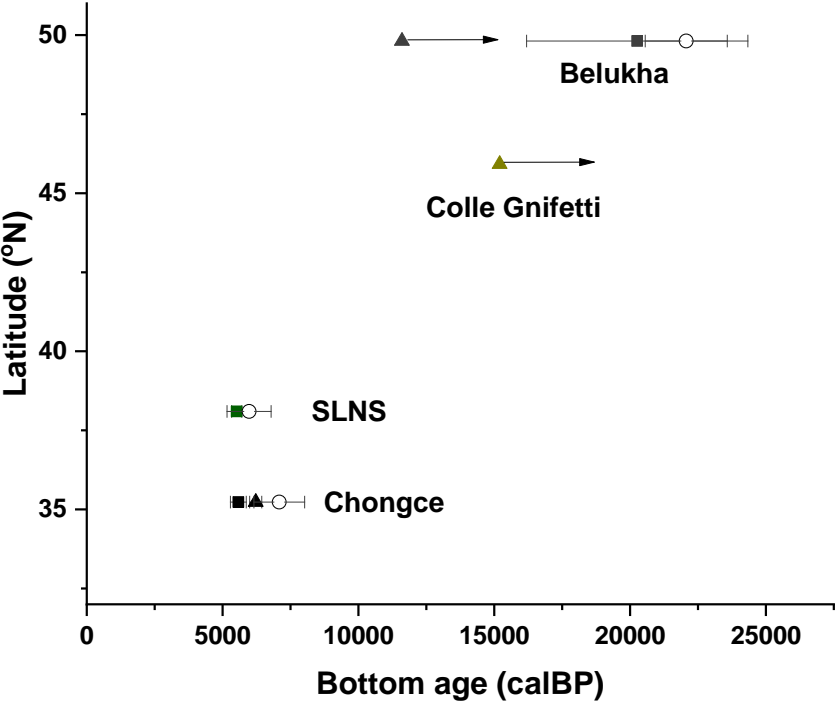


Figure 4.6 The bottom ages of the four glaciers shown with latitude, DO¹⁴C dates shown in filled squares and carbonates corrected WIO¹⁴C ages indicated as open circles. Previously reported Belukha bottom age indicated as triangle, the arrow indicate the age is larger than 11600 calBP [Uglietti et al., 2016]. The Colle Gnifetti bottom age is from Jenk et al. (2009) and based on WIOC. For the bottom age of Chongce, results from core 2 are also shown as triangle [Hou et al., 2018].

Table 4.3 Calibrated ¹⁴C micro age 1 σ range using OxCal V4.3.2 with Intcal13 and sequence deposition model constrained age.

Core section	WIOC Cal age (cal BP)	WIOC Cal age with sequence (cal BP)	DOC Cal age (cal BP)	DOC Cal age with sequence (cal BP)
CG110	1024±110	1003±99	464±235	403±196
CG111	1238±96	1198±81	810±169	749±123
CG112	1209±130	1310±98	901±176	947±139
CG113	1898±130	1890±123	1222±153	1248±144
Belukha412	8954±247	8953±247	10695±867	10701±861
Belukha414	14740±690	14741±691	13646±893	15063±737
Belukha415	22343±950	22343±949	20264±4073	20605±3936
SLNS101	850±395	707±317	250±145	226±137
SLNS113	1299±452	1264±333	480±131	505±111
SLNS122	1764±513	1902±427	2057±129	2056±129
SLNS127	3177±677	3223±625	2585±125	2585±125
SLNS136	6014±820	5424±617	3635±138	3636±137
SLNS139	6014±818	6171±567	5014±191	5007±187
SLNS141-142	6617±828	7069±676	5519±188	5531±176
CC237	3039±694	2956±564	237±151	233±153
CC244	4050±764	4214±699	1737±211	1738±212
CC252	10950±1661	10948±1656	5580±294	5580±295

Table 4.4 Calculated residual carbonates of the analyzed samples together with the Ca²⁺ concentrations. Given values are the mean over analyzed core sections for each individual site.

Sample	Residual carbonates (µg C)	Fraction of WIOC (%)	Residual carbonate (µg/kg)	Ca ²⁺ (µg/kg)	Residual carbonates / Ca ²⁺ ratio (%)
Colle Gnifetti	2.2	6	4	83	4.8
Belukha	5.0	21	15.5	5165	0.3
SLNS	4.0	8	10.4	~1400 *	0.7
Chongce	6.9	28	29	2170 #	1.3

*Ca²⁺ concentration over the period of 7000 years in the Puruogangri ice cap on the central Tibetan Plateau (Thompson et al., 2006).

Ca²⁺ concentration over the period of 1903-1992 from another core drilled from Chongce ice cap (ChongYi et al., 2016).

4.5 Conclusion

We investigated the potential to use the DOC fraction in ice cores for radiocarbon dating. Our data confirmed that DOC concentrations are consistently higher than WIOC concentrations in high alpine ice cores. Obtained DO^{14}C ages are comparable with WIO^{14}C ages and with previously published results from the same glaciers, underlining the great potential for applying DO^{14}C analysis for ice core dating. Effects of in-situ ^{14}C production on DO^{14}C ages, as suspected in previous studies, were not observed. Our study demonstrates the benefits of DO^{14}C dating: reduced required ice amount, higher precision with same sample mass, less reservoir effect and no carbonates bias from mineral dust. This opens up new fields for radiocarbon dating of ice for example in remote or Polar Regions. In addition, with the DO^{14}C dating results we were able to shed light on the longstanding unresolved question about the potential WIO^{14}C dating bias due to the presence of carbonates in the ice, particularly for samples with high loadings of dust.

Supplementary

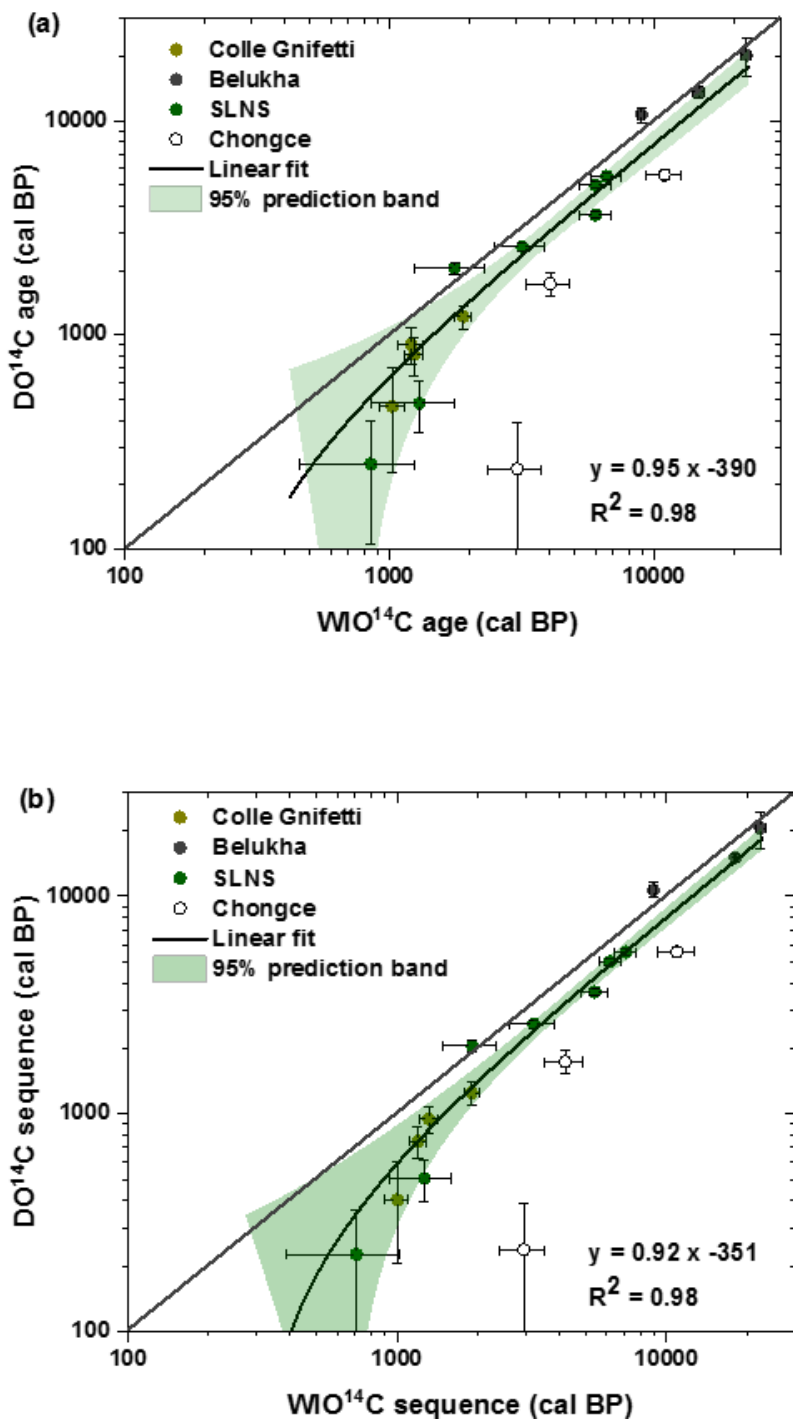


Figure S4.1 Linear fit of DOC and WIOC calibrated ¹⁴C age (a) and sequence model calibrated ¹⁴C age (b).

Bibliography

Aizen, E. M., V. B. Aizen, N. Takeuchi, P. A. Mayewski, B. Grigholm, D. R. Joswiak, S. A. Nikitin, K. Fujita, M. Nakawo and A. Zapf. Abrupt and moderate climate changes in the mid-latitudes of Asia during the Holocene. *Journal of Glaciology* **62**, 411-439, (2016).

Beaupré, S. R., E. R. Druffel, S. J. L. Griffin and O. Methods. A low-blank photochemical extraction system for concentration and isotopic analyses of marine dissolved organic carbon. **5**, 174-184, (2007).

Bolzan, J. F. Ice flow at the Dome C ice divide based on a deep temperature profile. *Journal of Geophysical Research: Atmospheres* **90**, 8111-8124, (1985).

ChongYi, E., Y. Sun, Y. Li and X. Ma (2016). The atmospheric composition changes above the West Kunlun Mountain, Qinghai-Tibetan Plateau. 2016 International Conference on Civil, Transportation and Environment, Atlantis Press.

Fang, L., J. Schindler, T. Jenk, C. Uglietti, S. Szidat and M. J. R. Schwikowski. Extraction of Dissolved Organic Carbon from Glacier Ice for Radiocarbon Analysis. **61**, 681-694, (2019).

Feng, Z., P. Bohleber, S. Ebser, L. Ringena, M. Schmidt, A. Kersting, P. Hopkins, H. Hoffmann, A. Fischer and W. Aeschbach. Dating glacier ice of the last millennium by quantum technology. *Proceedings of the National Academy of Sciences* **116**, 8781-8786, (2019).

Godwin, H. Half-life of radiocarbon. *Nature* **195**, 984-984, (1962).

Hou, S., T. M. Jenk, W. Zhang, C. Wang, S. Wu, Y. Wang, H. Pang and M. J. T. C. Schwikowski. Age ranges of the Tibetan ice cores with emphasis on the Chongce ice cores, western Kunlun Mountains. **12**, 2341-2348, (2018).

Jenk, T., S. Szidat, M. Schwikowski, H. Gaggeler, L. Wacker, H. Synal and M. Saurer. Microgram level radiocarbon (¹⁴C) determination on carbonaceous particles in ice. *Nuclear Instruments and Methods in Physics Research Section B: Beam Interactions with Materials and Atoms* **259**, 518-525, (2007). 10.1016/j.nimb.2007.01.196

Jenk, T. M., S. Szidat, D. Boliuss, M. Sigl, H. W. Gaeggeler, L. Wacker, M. Ruff, C. Barbante, C. F. Boutron and M. Schwikowski. A novel radiocarbon dating technique applied to an ice core from the Alps indicating late Pleistocene ages. *Journal of Geophysical Research: Atmospheres* **114**, (2009).

Jenk, T. M., S. Szidat, D. Bolius, M. Sigl, H. W. Gaeggeler, L. Wacker, M. Ruff, C. Barbante, C. F. Boutron and M. J. J. o. G. R. A. Schwikowski. A novel radiocarbon dating technique applied to an ice core from the Alps indicating late Pleistocene ages. **114**, (2009).

Jenk, T. M., S. Szidat, M. Schwikowski, H. Gäggeler, L. Wacker, H.-A. Synal and M. Saurer. Microgram level radiocarbon (^{14}C) determination on carbonaceous particles in ice. *Nuclear Instruments and Methods in Physics Research Section B: Beam Interactions with Materials and Atoms* **259**, 518-525, (2007).

Jenk, T. M., S. Szidat, M. Schwikowski, H. W. Gaggeler, S. Brutsch, L. Wacker, H. A. Synal and M. Saurer. Radiocarbon analysis in an Alpine ice core: record of anthropogenic and biogenic contributions to carbonaceous aerosols in the past (1650-1940). *Atmospheric Chemistry and Physics* **6**, 5381-5390, (2006).

Lal, D., A. T. Jull, G. Burr and D. Donahue. Measurements of in situ ^{14}C concentrations in Greenland Ice Sheet Project 2 ice covering a 17-kyr time span: Implications to ice flow dynamics. *Journal of Geophysical Research: Oceans* **102**, 26505-26510, (1997).

Legrand, M., S. Preunkert, B. Jourdain, J. Guilhermet, X. Fain, I. Alekhina and J. R. Petit. Water-soluble organic carbon in snow and ice deposited at Alpine, Greenland, and Antarctic sites: a critical review of available data and their atmospheric relevance. *Climate of the Past* **9**, 2195-2211, (2013). DOI 10.5194/cp-9-2195-2013

Legrand, M., S. Preunkert, B. May, J. Guilhermet, H. Hoffman and D. Wagenbach. Major 20th century changes of the content and chemical speciation of organic carbon archived in Alpine ice cores: Implications for the long-term change of organic aerosol over Europe. *Journal of Geophysical Research: Atmospheres* **118**, 3879-3890, (2013).

Legrand, M., S. Preunkert, M. Schock, M. Cerqueira, A. Kasper-Giebl, J. Afonso, C. Pio, A. Gelencsér and I. Dombrowski-Etchevers. Major 20th century changes of carbonaceous aerosol components (EC, WinOC, DOC, HULIS, carboxylic acids, and cellulose) derived from Alpine ice cores. *Journal of Geophysical Research* **112**, (2007). 10.1029/2006jd008080

Licciulli, C., P. Bohleber, J. Lier, O. Gagliardini, M. Hoelzle and O. Eisen. A full Stokes ice-flow model to assist the interpretation of millennial-scale ice cores at the high-Alpine drilling site Colle Gnifetti, Swiss/Italian Alps. *Journal of Glaciology* **66**, 35-48, (2020).

May, B. L. Radiocarbon microanalysis on ice impurities for dating of Alpine glaciers, PhD thesis, University of Heidelberg, (2009).

May, B., D. Wagenbach, H. Hoffmann, M. Legrand, S. Preunkert and P. Steier. Constraints on the major sources of dissolved organic carbon in Alpine ice cores from radiocarbon analysis

over the bomb-peak period. *Journal of Geophysical Research: Atmospheres* **118**, 3319-3327, (2013).

Morgenstern, U., L. K. Fifield, S. G. Tims and R. G. Ditchburn. Progress in AMS measurement of natural ^{32}Si for glacier ice dating. *Nuclear Instruments and Methods in Physics Research Section B: Beam Interactions with Materials and Atoms* **268**, 739-743, (2010).

Nye, J. On the theory of the advance and retreat of glaciers. *Geophysical Journal International* **7**, 431-456, (1963).

Ramsey, C. B. J. Q. S. R. Deposition models for chronological records. **27**, 42-60, (2008).

Ramsey, C. B. J. R. Methods for summarizing radiocarbon datasets. **59**, 1809-1833, (2017).

Reimer, P. J., E. Bard, A. Bayliss, J. W. Beck, P. G. Blackwell, C. B. Ramsey, C. E. Buck, H. Cheng, R. L. Edwards, M. Friedrich, P. Grootes, T. Guilderson, H. Haflidason, I. Hajdas, C. Hatté, T. Heaton, D. L. Hoffmann, A. G. Hogg, K. A. Hughen, K. Felix Kaiser, B. Kromer, S. W. Manning, M. Niu, R. W. Reimer, D. A. Richards, E. M. Scott, J. R. Southon, R. A. Staff, C. S. Turney and J. van der Plicht. IntCal13 and Marine13 radiocarbon age calibration curves 0–50,000 years cal BP. *Radiocarbon* **55**, 1869-1887, (2013).

Sigl, M., T. M. Jenk, T. Kellerhals, S. Szidat, H. W. Gäggeler, L. Wacker, H.-A. Synal, C. Boutron, C. Barbante and J. Gabrieli. Towards radiocarbon dating of ice cores. *Journal of Glaciology* **55**, 985-996, (2009).

Smith, A., V. Levchenko, D. Etheridge, D. Lowe, Q. Hua, C. Trudinger, U. Zoppi and A. Elcheikh. In search of in-situ radiocarbon in Law Dome ice and firn. *Nuclear Instruments and Methods in Physics Research Section B: Beam Interactions with Materials and Atoms* **172**, 610-622, (2000).

Steier, P., C. Fasching, K. Mair, J. Liebl, T. Battin, A. Priller and R. Golser. A new UV oxidation setup for small radiocarbon samples in solution. *Radiocarbon* **55**, 373-382, (2013).

Stuiver, M. and H. A. Polach. Discussion reporting of ^{14}C data. *Radiocarbon* **19**, 355-363, (1977).

Thompson, L. G., Y. Tandong, M. E. Davis, E. Mosley-Thompson, T. A. Mashiotta, P.-N. Lin, V. N. Mikhailenko and V. S. J. A. o. G. Zagorodnov. Holocene climate variability archived in the Puruogangri ice cap on the central Tibetan Plateau. **43**, 61-69, (2006).

Uglietti, C., A. Zapf, T. M. Jenk, M. Sigl, S. Szidat, G. A. Salazar Quintero and M. Schwikowski. Radiocarbon dating of glacier ice: overview, optimisation, validation and potential. *The Cryosphere* **10**, 3091-3105, (2016).

Van de Wal, R., J. Van Roijen, D. Raynaud, K. Van der Borg, A. De Jong, J. Oerlemans, V. Lipenkov and P. Huybrechts. From $^{14}\text{C}/^{12}\text{C}$ measurements towards radiocarbon dating of ice. *Tellus B: Chemical and Physical Meteorology* **46**, 91-102, (1994).

Wacker, L., S. M. Fahrni, I. Hajdas, M. Molnar, H. A. Synal, S. Szidat and Y. L. Zhang. A versatile gas interface for routine radiocarbon analysis with a gas ion source. *Nuclear Instruments & Methods in Physics Research Section B-Beam Interactions with Materials and Atoms* **294**, 315-319, (2013). DOI 10.1016/j.nimb.2012.02.009

Woon, D. E. Modeling gas-grain chemistry with quantum chemical cluster calculations. I. Heterogeneous hydrogenation of CO and H₂CO on icy grain mantles. *The Astrophysical Journal* **569**, 541, (2002).

5 ^{14}C age constraints in the Mt. Hunter, Alaska ice core: implications for Central Alaska Holocene ice extent and climate

Ling Fang^{1,2,3}, Dominic Winski⁴, Karl Kreutz⁴, Erich Osterberg⁵, Seth Campbell⁴,
Cameron Wake⁶, Theo M. Jenk^{1,3}, M. Schwikowski^{1,2,3}

¹Laboratory for Environmental Chemistry, Paul Scherrer Institute, CH-5232 Villigen PSI, Switzerland

²Department of Chemistry and Biochemistry, University of Bern, CH-3012 Bern, Switzerland

³Oeschger Centre for Climate Change Research, University of Bern, CH-3012 Bern, Switzerland

⁴Climate Change Institute and School of Earth and Climate Science, University of Maine, Orono, Maine, 04469, USA.

⁵Department of Earth Sciences, Dartmouth College, Hanover, NH 03755

⁶Institute for the Study of Earth, Oceans, and Space, University of New Hampshire, Durham, NH 03824

Manuscript to be submitted to

The Cryosphere

Abstract

Investigating North Pacific climate variability during warm intervals prior to the Common Era is essential to understand the behavior of ocean-atmosphere teleconnections between low latitudes and the Arctic under future warming scenarios. However, most of the existing ice core records in the Alaska/Yukon region only allow access to climate information covering the last few centuries. Here we present a complete depth-age scale for a 208 meter surface-to-bedrock ice core recovered in 2013 from the summit plateau of Mt. Hunter (Denali National Park, central Alaska). The annual layer signal is unambiguous to a depth of 190 meters (152.8 m w.eq.), where the age of the ice is 1203 ± 41 years old (i.e. representing the year 800 CE). Below that depth, annual layering could not be identified due to glacier flow-induced thinning. By applying radiocarbon dating on the ice contained carbonaceous aerosols and a two-parameter glacier flow model, a continuous depth-age relationship has been established. This is the first time micro radiocarbon dating has been applied to a high latitude Northern Hemisphere ice core, where concentrations of ice impurities (including carbon) are particularly low. To achieve this, the amount of ice sampled to obtain the required carbon mass was increased (>1 kg) and ^{14}C analysis of 16 samples was done using established (water insoluble organic carbon [WIOC]) and new (dissolved organic carbon [DOC]) techniques. Calibrated ^{14}C ages from the two deepest samples (207.9 m, 7,946-10,226 years cal BP; 208.2 m, 7,018-7,975 years cal BP) indicate that basal ice on Mt. Hunter has an early Holocene (>8 kyr) origin. Samples from depths of 198.7 to 205.6 meters have nearly uniform ^{14}C ages (3,200 to 3,500 years cal BP), which may reflect a significant increase in snow accumulation at Mt. Hunter in the mid-Holocene coeval with regional Neoglaciation. When paired with the $\sim 20,000$ year long Mt. Logan Prospector Russel Col (PRCol) record, the Mt. Hunter ice core will allow investigation of spatial and temporal changes in the regional high-elevation Holocene hydroclimate.

5.1 Introduction

Arctic surface temperatures have increased more than twice as fast as global temperature during the early 20th century and since the 1970s [Bengtsson, 2004; Tokinaga et al., 2017; Svendsen et al., 2018]. Recent modeling results suggest that during the early 20th century, as the Pacific Decadal Oscillation (PDO) transitioned to a positive phase, there was a concomitant deepening of the Aleutian Low that warmed the Arctic through poleward low-level advection of extratropical air [Svendsen et al., 2018]. The impact of Pacific multidecadal variability on Arctic warming has considerable implications for sea ice extent [Screen and Francis, 2016], and hence the possible linkage between Arctic amplification, sea ice loss, and enhanced mid-latitude winter variability [Cohen et al., 2014; Francis et al., 2017; Cohen et al., 2018; Screen et al., 2018; Blackport et al., 2019]. Whether the present positive PDO conditions will persist and contribute to Arctic warming at an even higher rate in the future is a fundamental question [Svendsen et al., 2018]. A longer-term perspective on Pacific decadal variability and the teleconnection between the tropical Pacific, North Pacific, and the Arctic, particularly during warm intervals in the Holocene outside those captured in the instrumental record, would be an important contribution to this problem. Alpine ice cores in the North Pacific region have the advantage of sampling atmospheric moisture (e.g., snow), aerosol deposition, and preserve physical characteristics (e.g., melt), all of which can be related to Pacific climate processes [Zdanowicz et al., 2014], if Holocene (or greater) length records can be recovered.

The general timing of deglaciation in the Alaska (Brooks Range, Central Alaska Range, and southern Alaska) based on terrestrial cosmogenic radionuclide, lichenometric, and radiocarbon dating is mostly between 10 and 20 kyr BP [Dortch, 2007]. Following the Last Glacial Maximum (LGM), glaciers in the Brooks Range retreated up valley to, or even within, their modern limits by ca. 15 ka [Pendleton et al., 2015]. Given the small extent of Brooks Range glaciers prior to the Holocene thermal maximum, during which some glaciers in southern Alaska disappeared entirely [Barclay et al., 2009], it is possible that Brooks Range glaciers may have disappeared as well. It therefore is unclear where early Holocene (or older) ice is preserved in basal layers of glaciers in central Alaska. Most of the ice cores recovered from the Alaska/Yukon region (Figure 5.1) are limited in time length to the last few centuries because core recovery did not reach bedrock. The Prospector Russel Col (PRCol) ice core from Mt.

Logan is an exception, which has a bottom age of ~20,000 years based on the assumption that the large decrease in stable isotope ratio at the bottom of the core is related to last Glacial Maximum cooling [Fisher et al., 2008]. The PRCol chronology is constrained by a large isotope minima and associated chemical changes at 4.2 kaBP, and tephra from the large Alaskan eruption of Aniakchak [Walker et al., 2019]. The PRCol record serves as a Global auxiliary stratotype for the Middle/Late Holocene subdivision boundary [Walker et al., 2019]. However, there are no chronologic tie points in the PRCol record prior to the 4.2 kaBP event, and unfortunately the archive of the PRCol ice core was lost in 2017 due to a freezer malfunction [Walker et al., 2019].

New surface-to-bedrock ice cores were recovered from the Mt. Hunter plateau (Denali National Park, Alaska; Figure 5.1) in 2013 at 3900 masl [Winski et al., 2017]. Analysis of the upper 190 meters of the core (2013 - 800 CE) reveals that snow accumulation at the drilling site has doubled since ~1840 CE, coeval with warming of western tropical Pacific sea surface temperatures [Winski et al., 2017] and intensification of the Aleutian Low system [Osterberg et al., 2014; Osterberg et al., 2017]. The same core also shows a sixty-fold increase in water equivalent total annual melt between 1850 CE and present, which represents a summer warming rate of $1.92 \pm 0.31^\circ\text{C}$ per century during the last 100 years [Winski et al., 2018]. The Mt. Hunter melt layer record is significantly correlated with surface temperatures in the central tropical Pacific through a Rossby-wave like pattern that enhances temperatures over Alaska. Taken together, these hydroclimate changes are consistent with linkages between Pacific decadal variability and Arctic hydroclimate changes seen in the observational record [Svendsen et al., 2018], and demonstrate that the North Pacific hydroclimate response since 1850 CE is unprecedented in the past millennium.

An annual layer chronology in the Mt. Hunter core shows the age of ice is 1203 ± 41 years old at a depth of 190 m (152.8 m w.eq; Winski et al., 2017). Below that depth, annual layering could not be identified due to glacier flow-induced thinning. However, based on previously reported depth-age scales from alpine glacier ice cores, the bottom 20 meters of ice may reach through the Holocene and into the last glacial [Uglietti et al., 2016; Licciulli et al., 2020]. The Mt. Hunter ice core therefore provides the possibility of establishing a new Holocene North Pacific hydroclimate record prior to the Common Era, if a precise and absolutely-dated chronology could be established in the bottom 20 meters of the core. The

water-insoluble organic carbon (WIOC) ^{14}C -dating method has been validated for multiple mid-latitude ice cores [Uglietti et al., 2016; Hou et al., 2018]. The technique makes use of the transport and deposition of carbonaceous aerosols onto the glacier. Before the industrial period, carbonaceous aerosols were mainly emitted from the living biosphere and biomass burning as well as being produced by secondary organic aerosol formation from gaseous precursors. Consequently, this carbon reflects the contemporary atmospheric ^{14}C content. After deposition, the WIOC is incorporated into glacier snow, firn and ice and undergoes radioactive decay with a half-life of 5730 years [Godwin, 1962]. Here we report results from ^{14}C analysis of the Mt. Hunter ice core and use the data in conjunction with the existing late Holocene Mt. Hunter chronology [Winski et al., 2017] to produce the first radiometrically dated Holocene-length Arctic ice core chronology. We further use these data to evaluate the extent of ice in the North Pacific region during early Holocene warmth and possible mid-Holocene changes in hydroclimate.

5.2 Methods

5.2.1 Annual layer counting (ALC) in the Mt. Hunter ice core

Two surface-to-bedrock ice cores were drilled in 2013 at 3,900 meters elevation (masl) from the saddle between the north and middle peaks of Mt. Hunter, Alaska [Winski et al., 2017; Osterberg et al., 2017; Winski et al., 2018]. The ice cores were sampled continuously with an ice core melting system at Dartmouth College, which excludes potential contamination from the outside of the core. The melt water from the interior of the ice core was pumped through a laser particle counter (Abakus, Klotz) and a liquid conductivity meter (LCM). Samples were fraction-collected into pre-cleaned vials for chemical and isotopic analysis. Particle concentration and size distribution, and liquid conductivity were measured at resolution of 1 cm. Major ion concentrations were determined with ion chromatography (Dionex 5000) at a resolution of about 5 cm. Stable isotope ratios of hydrogen (δD) and oxygen ($\delta^{18}\text{O}$) in water were measured with a Cavity Ring Down Infrared Spectrometer (Picarro L2130i) also at 5 cm resolution, except for the period of 1750-1250CE where resolution was increased to 1cm.

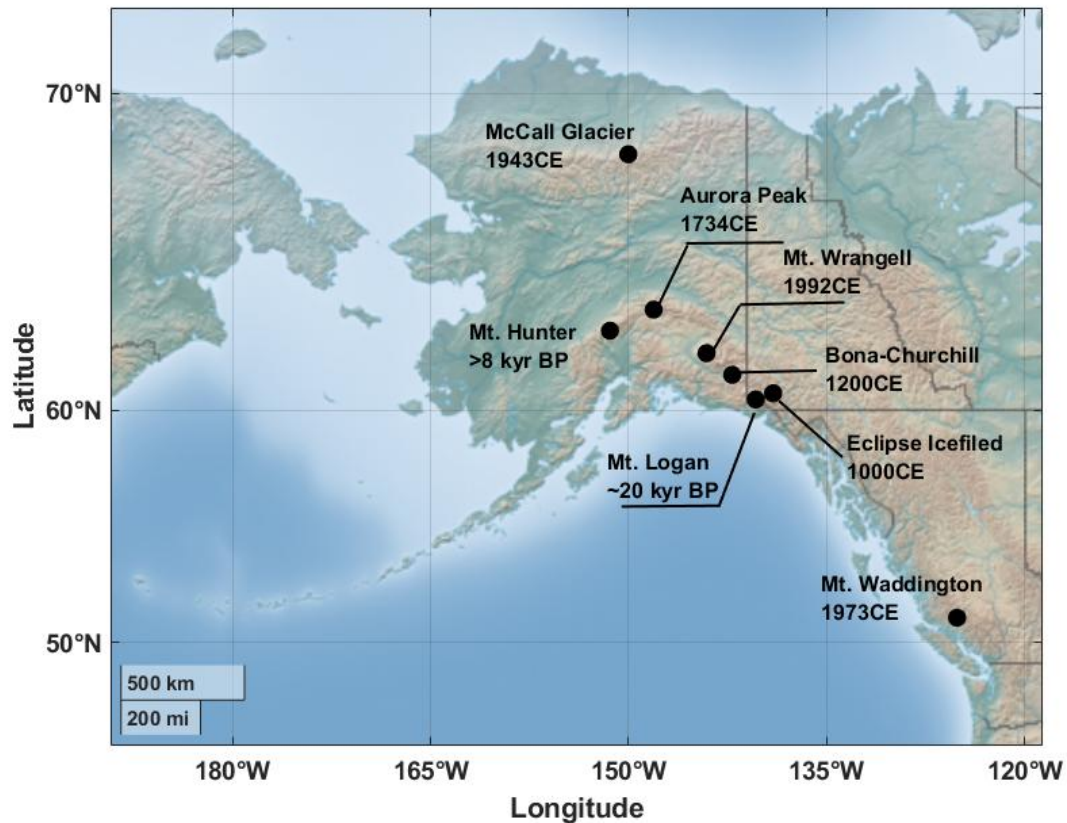


Figure 5.1 Location map of North Pacific ice core sites with ages or time span: Mt. Hunter (this study), McCall Glacier [Klein et al., 2016], Aurora Peak [Tsushima et al., 2015], Mt. Wrangell [Yasunari et al., 2007], Bona-Churchill [Porter et al., 2019], Mt. Logan [Fisher et al., 2008], Mt. Waddington [Neff et al., 2012].

To develop the Mt. Hunter ice core timescale, three experienced researchers independently counted annual layers in the Mt. Hunter ice core chemical data. The timescale to 1777 CE was determined by counting annual oscillations in $\delta^{18}\text{O}$ (summer peak), melt layers (summer peak), magnesium (spring peak), dust (spring peak), liquid conductivity (summer peak), ammonium (summer peak) and methanesulfonic acid (MSA; late summer-fall peak), consistent with previous North Pacific ice cores. Using the relative peak positions of MSA in the late summer-fall and magnesium in the spring we distinguish cold-season (September-April) and warm-season (May-August) snow accumulation on Mt. Hunter back to 1867 CE. The timescale from 1777 to 1500 CE is based on annual oscillations of $\delta^{18}\text{O}$, δD , deuterium excess, dust and liquid conductivity measurements that were made at higher resolution than the other

analytes, while conductivity and dust concentration measurements were exclusively used to date the ice core from 1500–800 CE.

The Mt. Hunter chronology is validated from 1750–2013 CE by comparing the timing of peaks in sulfate, chloride and conductivity to the known dates of explosive volcanic eruptions [Winski et al., 2017]. The volcanic events were used only as validation of the layer counting efforts and the timescale was not forced to match any particular event. There is no offset between the timescale and known volcanic eruptions as indicated by peaks in sulfate, chloride and conductivity during the 19th and 20th centuries, indicating a precision within ± 1 year throughout the last 200 years. The volcanoes in the 18th century used for chronology validation (Laki, 1784 and Pavlof, 1763) were offset by one year from the chronology. Additionally, ^{137}Cs concentrations in the Mt. Hunter core strongly peak in 1963 during the largest atmospheric nuclear weapons testing period, which closely matches other published data.

5.2.2 Mt. Hunter ice core ^{14}C analysis

Sixteen samples were selected from the lower portion of the Mt. Hunter core (Table 5.1). Because WIOC concentrations at this Arctic site were assumed to be low, ice samples were cut with at least 1 kg mass, aiming for carbon contents to be dated with reasonable uncertainty of 10-20% ($> 10 \mu\text{gC}$, Uglietti et al., 2016). Samples for WIOC ^{14}C -dating were prepared following the protocol described in Uglietti et al. (2016); a brief summary is provided here. In order to remove potential contamination in the outer layer of the ice core, pre-cut samples from the inner part of the core were rinsed with ultra-pure water. After melting, the contained carbonaceous particles were filtered onto prebaked quartz fibre filters (Pallflex Tissueqz-2500QAT-UP). These initial steps were performed in a laminar flow box to ensure clean conditions. At the University of Bern (Laboratory for the Analysis of Radiocarbon with AMS - LARA laboratory) the obtained WIOC samples were then combusted in a thermo-optical OC/EC analyzer (Model4L, Sunset Laboratory Inc, USA) equipped with a non-dispersive infrared (NDIR) cell to quantify the CO_2 produced, using the well-established Swiss 4S protocol for OC/EC separation (Zhang et al., 2012). Being coupled to a 200 kV compact accelerator mass spectrometer (AMS, mini radiocarbon dating system MICADAS) equipped with a gas ion source and a Gas Interface System (GIS, Ruff et al., 2007; Synal et al., 2007, Szidat et al., 2014),

the coupled LARA Sunset-GIS-AMS system [Agrios et al., 2015; Agrios et al., 2017] then allowed for final, direct online ^{14}C measurements of the CO_2 produced from the WIOC fraction.

Dating of the deepest sample (Denali 235, mid-depth 169.9 m w.eq, above bedrock) was most challenging due to the small ice amount available (~200 gram). To ensure a carbon mass above the critical limit of 10 μgC for final ^{14}C analysis, the dissolved organic carbon (DOC) fraction - found to be higher in concentration than WIOC in ice cores from the Alps [Legrand et al., 2013] - was used for ^{14}C dating of this sample. DOC was extracted from the ice using a dedicated system and the procedure is described in detail in Fang et al. (2019). Initial results show that the DOC fraction yields similar ^{14}C ages as those derived for the WIOC fraction [Fang et al., in prep.].

All ^{14}C results are expressed as fraction modern ($F^{14}\text{C}$), which is the $^{14}\text{C}/^{12}\text{C}$ ratio of the sample divided by the same ratio of the modern standard (NIST standard oxalic acid II, SRM 4990C). Final values presented in Table 5.1 are the AMS $F^{14}\text{C}$ raw data after corrections accounting for constant contamination and cross contamination in the Sunset-GIS-AMS system and the procedural blank contribution introduced by the preparation of ice samples. For details please refer to Uglietti et al. (2016) and Fang et al. (2019) regarding WIO^{14}C and DO^{14}C , respectively. To obtain final dates, corrected $F^{14}\text{C}$ were calibrated using OxCal v4.3.2 [Ramsey, 2017] with the IntCal13 calibration curve [Reimer et al., 2013]. The calibrated ^{14}C ages are presented as the 1σ range in years before present (cal BP, with BP referring to the year 1950).

5.3 Results

5.3.1 Mt. Hunter ice core ^{14}C data

The WIOC concentrations range from 6 to 31 $\mu\text{g}/\text{kg}$ with an average of $13 \pm 7 \mu\text{g}/\text{kg}$ (Table 5.1). This is slightly higher than Greenland snow at summit (4.6 $\mu\text{g}/\text{kg}$, Hagler et al., 2007), but only about half of the pre-industrial WIOC concentrations found in European Alpine ice cores, with $24 \pm 9 \mu\text{g}/\text{kg}$ [Legrand et al., 2007] and 32 ± 18 [Jenk et al., 2009] from Colle Gnifetti, Monte Rosa, Switzerland and $24 \pm 7 \mu\text{g}/\text{kg}$ from Fiescherhorn glacier [Jenk et al., 2006]. In agreement

Table 5.1 ^{14}C results of Mt. Hunter ice core samples, given as $F^{14}\text{C}$, calibrated ^{14}C age and modelled ^{14}C . All samples were dated using the WIOC fraction, except D235 for which the DOC fraction was analyzed.

Sample	Mid Depth (m weq)	Carbon amount ($\mu\text{g C}$)	WIOC ($\mu\text{g/kg}$)	Be nr.	$F^{14}\text{C}$ (1σ)	Calibrated ^{14}C age (cal BP, 1σ range)	Calibrated ^{14}C age with deposition sequence model (cal BP, 1σ range)
Denali164*	115.9	7.0	6.2	10013.1.1	0.910 ± 0.058	305-1255	--
Denali183	131.4	10.8	10.1	10015.1.1	0.921 ± 0.042	301-975	695-modern
Denali209*	151.2	9.2	9.8	10016.1.1	0.826 ± 0.044	989-1927	--
Denali210-211	152.3	10.8	20.0	8997.1.1	0.922 ± 0.033	327-925	630-931
Denali214	155.0	13.7	11.8	10017.1.1	0.831 ± 0.036	983-1735	965-1419
Denali215-216*	156.2	8.8	12.0	8998.1.1	0.925 ± 0.039	306-926	--
Denali217*	157.3	6.7	6.1	10018.1.1	0.731 ± 0.054	1902-3350	--
Denali219-220	158.9	12.0	16.8	8615.1.1	0.841 ± 0.026	1010-1555	1245-1714
Denali223	161.0	21.4	17.3	10019.1.1	0.608 ± 0.029	3926-4967	3160-3483
Denali224-225	163.1	33.9	17.5	11923.1.1	0.653 ± 0.010	3511-3843	3267-3535
Denali228*	165.1	8.7	10.0	10020.1.1	0.627 ± 0.043	3415-4863	--
Denali229-230	166.1	38.6	20.0	11924.1.1	0.691 ± 0.009	2991-3325	3328-3572

Denali231	167.2	11.3	11.5	10021.1.1	0.523 ± 0.037	5320-6655	3840-4250
Denali232-233	168.2	54.8	30.8	11925.1.1	0.629 ± 0.008	3926-4236	4067-4410
Denali234*	169.2	9.8	11.7	10022.1.1	0.378 ± 0.043	7745-9890	--
Denali235 [#]	169.7	20.7	80.3 (DOC)	12465.1.1	0.437 ± 0.025	7018-7975	7019-7982

*Sample with carbon mass less than 10 µg C. These data are not used in the final depth age scale following the recommendation in Uglietti et al., 2016.

[#]DOC fraction was analyzed for ¹⁴C dating

with expectations based on previous studies [Legrand et al., 2007], the concentration of DOC (80 $\mu\text{g}/\text{kg}$) measured in the deepest sample was significantly higher than all WIOC concentrations measured in this core.

The calibrated WIO¹⁴C ages range from 301-975 years cal BP at 131.4 m w.eq. to 7,745-9,890 years cal BP at 169.2 m w.eq. (Table 5.1). For each sample, the probability distribution over the calibrated age range (1σ and 2σ) is shown in Figure 5.2a. Samples containing less than 10 μg carbon are generally characterized by a wide age range which is expected due to the small carbon amount and the resulting larger analytical uncertainty [Uglietti et al., 2016]. Although we used a considerable amount of ice for each sample (~ 1 kg), the total carbon amount in 6 samples was still below the 10 μg limit for this ¹⁴C dating method (recommended to obtain an acceptable dating uncertainty of less than 20%; Uglietti et al., 2016). Therefore, these 6 samples were not included in the Mt. Hunter ice core chronology. Around the Mt. Hunter drill site, no folding was observed in ground penetrating radar data and the bedrock geometry appears to be uncomplicated [Campbell et al., 2013]. Based on this information, final ¹⁴C calibration was performed using the OxCal deposition sequence model (Figure 5.2b, samples $> 10 \mu\text{gC}$) which is valid for archives where increasing age with increasing depth can be assumed [Ramsey, 2008; Ramsey, 2017]. The sequence model has poor agreement with samples between 161 – 167 m w.eq. depth ($A < 60$, see Figure 5.2b), which may challenge the validity of this assumption or the reliability of analyses for these samples unless this observation can be explained by some other glaciological or climatological reason. Considering the radar images (and the rather unlikely case of ice undulations more than 10 meters above bedrock), we believe the underlying assumption justifying application of the sequence model to be reasonable, and will discuss a possible explanation for almost indistinguishable ages over the aforementioned depth interval further below (see section 5.4.2). Aiming to derive a first continuous age-depth relationship for the entire length of the Mt. Hunter ice core, calibrated ¹⁴C ages as derived from the deposition sequence model will be used.

The following three main results can be summarized: (i) the derived radiocarbon dated ages are in reasonable agreement with independently derived ages from the annual layer counting reported in Winski et al. (2017). For sample Denali184 from a depth of 131.4 m w.e., the 1σ age range from 695 years cal BP to modern (mean age about 410 years before 2013) is in very close agreement with the respective annual layer counting age of 422 years before 2013 at this

depth. The 1σ ^{14}C age range for Denali210-211 (152.3 m w.eq.) is 630-931 years cal BP (850 \pm 150 before 2013) and slightly younger compared to the annual layer counting age of 1170 \pm 40 years before 2013 but still within the 2σ dating uncertainty. (ii) Samples of indistinguishable ages with regard to the achieved dating uncertainty were observed in the depth interval from 161 – 167 m w.e., resulting in a bad agreement for the applied ^{14}C calibration sequence model (Denali223, Denali224-225, Denali229-230, Denali231). In terms of age, this interval corresponds to the time period from around 4000 to 3000 years BP. (iii) The ^{14}C dating of the lowest two samples in the Mt. Hunter ice core, Denali234 (169.2 m w.eq. depth, less than 10 μg of carbon) and Denali235 (169.9 m w.eq, last sample before bedrock), revealed ages from the early Holocene with 7745-9890 years cal BP and 7018-7975 years cal BP, respectively.

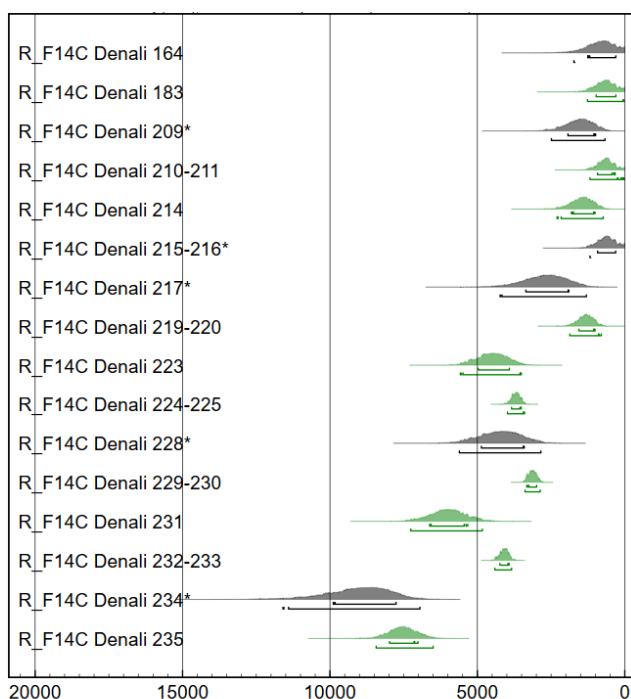
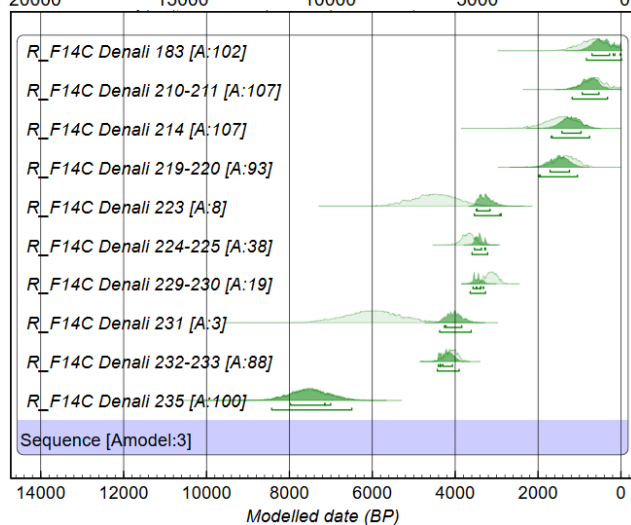


Figure 5.2 Calibrated ^{14}C age probability distributions using OxCal v4.3.2 (Bronk Ramsey 2017, Reimer et al., 2013).

(a) The Samples with carbon content for AMS analysis being $> 10 \mu\text{g}$ are shaded in green (gray for $< 10 \mu\text{g}$). The 1σ and 2σ range is indicated by the lines below the probability distribution areas.



(b) Calibrated ^{14}C age probability distributions with deposition sequence model (samples $> 10 \mu\text{gC}$). The dark shade areas show the newly resulting calibrated age probabilities and light green areas same as in (a). The agreement between two age distributions given on the plot after the sample name as A.

5.3.2 Age scale modeling

Modeling the age scale in alpine ice cores can be attempted either by applying a rather simple glaciological 2D flow model (e.g. Nye, 1963; Dansgaard and Johnsen, 1969) or by more complex 3D glaciological models which require observational data from glaciological surveys (e.g. Campbell et al., 2013; Licciulli et al., 2020). In the context of age scale modeling, even complex 3D models are strongly limited in predicting accurate ice ages in the deepest part of ice cores from alpine glaciers [Licciulli et al., 2020]. This is most directly related to unknown past accumulation (deposition) rates and their variation in time. Without this information, a constant accumulation rate based on recent observational data has to be assumed for the entire record. For this reason, the availability of absolutely dated horizons is crucial, especially for the oldest, near-bedrock ice sections where ice flow becomes potentially complex. Such dated horizons indirectly contain information of past accumulation rates by the depth they are located at. They thus do not only allow testing of a model (e.g. Dansgaard and Johnsen, 1969) but can also provide a crucial improvement of the model dating accuracy when fitted to match these time markers (e.g. Jenk et al., 2009, Uglietti et al., 2016).

In the case of the Mt. Hunter ice core, accurate dating by annual layer counting supported with independent time horizons for the upper two thirds of the core and absolute dated horizons for the bottom section of the core (^{14}C dates) are available. Further, an existing 3D model developed for this site [Campbell et al., 2013] was used in combination with the annual layer counting to reconstruct a significant increase in accumulation rates since ~1850 CE [Winski et al., 2017]. The use of a simple 2D model, the so-called two parameter model (2p-model; Thompson et al., 1989) which has previously been applied in combination with ^{14}C ages to establish the chronologies of a variety of high-alpine ice cores [Jenk et al., 2009; Uglietti et al., 2016], will not result in a good age fit for the entire Mt. Hunter record given the constant accumulation assumption. Regardless, applying the same procedure, a fixed glacier thickness of 170.1 m w.eq. and in this case constraining the 2p-model with the calibrated ^{14}C ages only, shows that even under these circumstances this approach is capable of providing reasonable results, similar to the layer counted ages considering the uncertainty. However, model uncertainties at the respective depths exceed the uncertainty of the calibrated ^{14}C ages by about a factor of two (see Figure S5.1 in the Supplement Material). The fit to the ^{14}C dates only, with

an adjusted R^2 of 0.95, results with a reasonable annual average accumulation of 1.00 ± 0.34 m w.e. close to the average value derived by Winski et al. (2017) for the period 800 to 2013 CE (ranging from 0.3 to 1.5 m w.eq). The model produces a bad match with ALC in the upper/younger part where accumulation is known to have changed, i.e. increased significantly. In summary, this first attempt indicates that while the approach using a single 2p model to derive a continuous age scale for this specific core is clearly limited it still produces reasonable results, although coming along with rather high uncertainties.

With the ^{14}C dating independently supporting the accuracy of the annual layer counting performed down to a depth of 152 m w. eq. we used this dating as an anchor to derive a final, best possible continuous age scale over the entire ice core in the next step. Therefore, while keeping the input to the 2p-model as before, the annual average accumulation rate was tuned to derive a smooth transition from the ALC to the modeled age allowing combination of these two (Figure 5.3). This was achieved for an average annual accumulation rate of 0.58 m w.e. while only slightly reducing the goodness of the fit to the ^{14}C dates (adjusted $R^2 = 0.94$) and not affecting the derived age for the ice close to bedrock and older than around 3000 years (see Supplemental Material, Figure S5.1). The value of 0.58 m w.eq. is reasonable, being right in the middle of the range (0.2-0.7 m w.eq) previously derived for the period before 1400 CE, the period prior to significant accumulation change [Winski et al., 2017]. The dating uncertainty of the so derived continuous age-depth scale is as reported in Winski et al. (2017) for the upper section based on the ALC (0-152 m w.eq.) and estimated based on the 95% confidence band for the section dated by the 2p model. Below the transition from ALC to 2p-model, the size of the uncertainty is a 100-year linear increase from the ALC uncertainty to match the 2p model uncertainty. We note that this final age-depth relationship yields a bad fit through the calibrated ^{14}C points between around 4000 -3000 years BP previously discussed in section 3.1 (161 to 167 m w.eq). As will be discussed in section 4.1, we believe the ages being indistinguishable with the achieved analytical precision over this section to be a real signal. Therefore, the age scale presented here is likely to undergo revision with substantial adjustments to younger ages between around 3000 to 2000 years BP on the order of a few hundred years. To improve the dating accuracy of this section, we suggest future efforts to obtain independent evidence from volcanic tephra and additional ^{14}C dating of the two core segments covering this depth interval (Denali221 and Denali222).

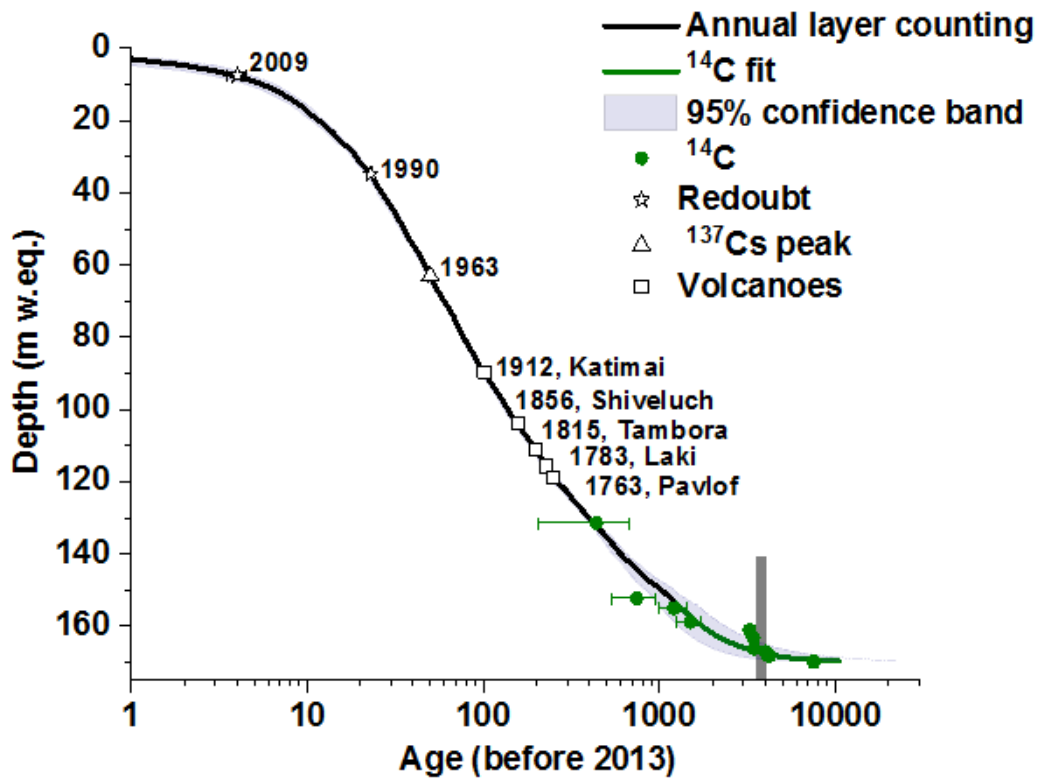


Figure 5.3 The depth-age relationship of the Mt. Hunter core. The black line is the annual layer counting with uncertainty and the green dots for the modelled calibrated mean ^{14}C ages with 1σ range. The green line represents the 2p-model fit with the upper and lower 95% of confidence interval. The grey shaded bar between the 3500 to 3900 years indicates the strong increase in precipitation reconstructed from pollen data in Heusser et al., 1985.

5.4 Discussion

5.4.1 Implications for North Pacific/Arctic ice core chronologies

The ^{14}C dating of two samples from the very bottom part of the Mt. Hunter ice core, Denali234 (169.2 m w.e. depth, less than $10\ \mu\text{g}$ of carbon) and Denali235 (last sample reaching down to bedrock), reveal ages from the early Holocene with 7745-9890 cal BP and 7018-7975 cal BP, respectively. These results clearly indicate the bottom age of Mt. Hunter is > 8 Kyr BP and Mt. Hunter glacier is to be of early Holocene origin considering the deepest sample age is the

integrated mean age over the bottom. This is the first application of ^{14}C analysis on an Arctic ice core. While advances in the WIOC ^{14}C technique have allowed radiocarbon dating of various high-alpine ice cores from low- and mid-latitudes, the technique has not to be applied in Arctic settings before because of the generally lower carbon content in Arctic ice. The WIOC concentration from Mt. Hunter core is lower than in ice cores from the Alps. Nevertheless, most of the samples could be dated with ^{14}C using a reasonable ice amount. In addition, with the help of the new technique of DOC extraction, we could decrease the required ice amount to reach the 10 μg carbon criteria. This study shows the great potential for ^{14}C dating on low carbon content samples from North Pacific/ Arctic ice cores.

The existing cores from North Pacific region were dated only within the last millennium except for the Mt. Hunter and Mt. Logan PRCol cores (Figure 5.1). A 186 m long core was drilled to the bedrock at the summit plateau of Mt. Logan (60.59 °N, 140.50 °W; 5340 m asl.) in 2001 and 2002. Although there is no tie point constraining in the deep part of PRCol core from Mt. Logan, the ice flow model simulation suggested the bottom age of PRCol core is about 20 Kyr BP [Fisher et al., 2008]. Most of the cores extracted from Eastern Beringia region have short time spans of a few centuries. A 152 m ice core was drilled from the McCall Glacier (69.29 °N, 143.78 °W; ~2310 m asl.) in 2008. The core was dated by using a combination of annual layer counting and specific horizons. The upper 37 m of ice date back to 65 years and the full 152 m core dates approximately back over 200 years [Klein et al., 2016]. The Aurora Peak ice core (63.52 °N, 146.54 °W; 2825 m asl.) is located at southeast of Mt. Hayes and was drilled in 2008. The total ice thickness at the drilling site is 252 ± 10 m, but this core (180.17 m) did not reach the bed rock. By annual layer counting, the estimated bottom age of Aurora Peak core is about 274 years [Tsushima et al., 2015]. Two cores were collected at Eclipse Icefield (60.51 °N, 139.47 °W; 3107 m asl.) in 2002. The chronology of the Eclipse ice core is based on multi-parameter annual layer counting of seasonal oscillations in the stable isotope ($\delta^{18}\text{O}$) and major ion records (Na^+) and volcanic eruptions. The longest core (core 2, 345 m) covers the period 1000 to 2002 [Yalcin et al., 2007]. In 2004, a 216 m ice core were drilled from Mt. Wrangell (62.00 °N, 144.00 °W; 4100 m asl.). The ice depth in the summit caldera is probably over 900 m, but the definite bottom has not yet been detected [Benson et al., 2007]. No time scale is available from literature for this core. The record from Mt. Waddington (51.38 °N, 125.26 °W; 3000 m asl.) only covers a period of 1973-2010 [Neff et al., 2012]. The total

length of Mt. Waddington core is 141 m, but the total ice thickness at the drilling site is about 250 m.

In summary, all of the above described cores from the Eastern Beringia region were either not drilled to bedrock or the ice close to the bed was not dated using an absolute dating method. The large difference between the age of the oldest ice found in these cores is thus likely not an indication of a difference in the time of oldest ice at these sites. With the first application of ^{14}C analysis on a high-latitude Northern Hemisphere ice core presented here, a complete dating of the bedrock reaching Mt. Hunter ice core was achieved. The successful first absolute dating of bottom ice from this region clearly indicates that the glaciers from the North Pacific region can be of early Holocene or potentially even late glacial origin, highlighting the great potential of ^{14}C dating on low carbon content samples from North Pacific/Arctic ice cores.

5.4.2 Holocene ice extent and hydroclimate in Central Alaska

The ^{14}C dating of two samples from the very bottom part of the Mt. Hunter ice core, Denali234 (169.2 m w.eq. depth, less than 10 μg of carbon) and Denali235 (last sample reaching down to bedrock), reveal ages from the early Holocene with 7745-9890 years cal BP and 7018-7975 years cal BP, respectively. These results clearly indicate the bottom age of Mt. Hunter to be older than 8 kyr BP and the Mt. Hunter glacier to be of at least early Holocene origin. These results also allow the first continuous depth age scale over the entire Mt. Hunter ice core by combining the independent dating based on annual layer counting and a glaciological 2D flow model fit through the absolutely dated horizons by ^{14}C analysis from ice-incorporated carbonaceous aerosols, and an estimate of ice age near bedrock likely >8000 years (Fig. 3). This preserved old ice in the bottom of Mt. Hunter core confirms that at least some ice from central Alaska Range glaciers survived during the Holocene thermal maximum. We also observe a small increase in ^{14}C ages between the depth 161.0 m w.eq. to 167.2 m w.eq. dated to the period 4 kyr to 3 kyr BP. This very slow increase in age with depth could be explained by a significant increase in annual accumulation rates over this period reflecting a real, natural signal preserved in the Mt. Hunter ice core record. Supporting evidence for such a mid-Holocene hydroclimate change in the North Pacific may come from previous research in the region. For example, the time period corresponds to the onset of the regional Neoglaciation

lasting from around 3.5 to 2.5 kyr BP in the Yukon Territory Denton and Karlén, 1977; Anderson et al., 2005. Past tree lines provide evidence for significant glacier extension in the St. Elias Mountains over the period 3.6-3.0 kyr BP Denton and Karlén, 1977. While a mid-Holocene temperature decrease may have played a role, an increase in regional precipitation could also be responsible for glacier expansion. Based on pollen reconstructions, Heusser et al. (1985) found that Southern Alaskan mean annual precipitation may have almost doubled from around 3.9 to 3.5 kyr BP. The Mt. Hunter results presented here may provide corroborating evidence for a mid-Holocene hydroclimate shift, however applying other independent dating methods in the parallel remaining ice sections from this depth interval will help to better constrain and improve the time scale presented in Section 3.2. Therefore, to improve the dating accuracy of this section, future efforts will target independent evidence from volcanic tephra and additional ^{14}C dating of the two core segments covering the according depth interval (Denali221 and Denali222).

5.5 Conclusion

Although the WIOC ^{14}C technique has allowed radiocarbon dating of various high-alpine ice cores from low- and mid-latitudes, this technique has not been applied before in high latitude ice cores because of the generally lower carbon content. The ^{14}C results from Mt. Hunter ice core are the first from a subarctic ice core and were achieved by increasing the amount of ice (>1 kg) to obtain the required carbon mass and by using a new technique based on the dissolved organic carbon fraction in ice for ^{14}C analysis. Combining dating by annual layer counting, previously established to a depth of 190 m (150 m w.eq., 1170 ± 40 years) where the signal becomes ambiguous, and the new ^{14}C dated horizons, a complete continuous chronology over the entire core was established. For the overlapping sections, ages based on annual layer counting are confirmed by the agreement with the independent results from ^{14}C dating. ^{14}C dating of two samples just above bedrock at 208 m depth yielded the first results of absolutely dated ages of near bedrock ice in the region (Denali234, 207.6-208.3 m, 168.9-169.6 m w.eq.; Denali235, 208.3-208.7 m, 169.6-170.1 m w.eq.). Dated to ~8 kyrs BP, they indicate the very bottom ice to be of early Holocene or even late glacial origin. The Mt. Hunter ice core has previously been reported to be affected by significant changes in annual accumulation rates

over the last few centuries. Samples of nearly indistinguishable ages with regard to the achieved dating precision were observed in the depth interval from 198.7 – 205.6 m (161 – 167 m w.eq.), dated to the time period from around 4000 to 3000 years BP. We believe this to be explained by similarly significant changes in accumulation rates during the period of regional Neoglaciation matching in its timing with the ages derived. Such significant changes in accumulation, highlight the limitation of age-depth modeling with glaciological flow models. In the absence of absolute dated horizons, the accumulation rate needs to be assumed and kept constant. With regard to the analytical ^{14}C dating uncertainty and in the absence of further proof for an accumulation change in this earlier period, the modeling approach to derive the presented first continuous Mt. Hunter ice core chronology did also not consider changing accumulation in the older part of the record. Investigation of tephra particles from well-known volcanic eruption events archived in the Mt. Hunter ice core, with their most likely location now being reasonably constrained by the current dating, will help to further constrain and improve the here presented time scale in the future. Our results show the applicability and great potential of ^{14}C dating on low carbon content samples from North Pacific/Arctic ice cores. While they indicate the Mt. Hunter ice core to currently be one of the few existing archives in the North Pacific region providing an opportunity to reconstruct Holocene hydroclimate variability, we do expect that similar or even longer paleo ice core records can be recovered from central Alaska glaciers where bedrock is reached.

Author contributions. LF, TMJ and MS measured the ^{14}C , DW, KK, EO, SC, and CW drilled the core, conducted the chemical and physical properties analysis, and constructed the original depth-age scale. All authors contributed to the discussion of the results.

Competing interests. The authors declare there is no conflict of interest.

Acknowledgements. Thanks to the Laboratory of the Analysis of Radiocarbon with AMS (LARA) group at the University of Bern, especially to Martin Raubber for helping with the MICADAS measuring. We thank Denali National Park, Polar Field Services and Talkeetna Air Taxi for providing air support and field assistance, Mike Waszkiewicz for ice core drilling, Brad Markle, Dave Silverstone, Tim Godaire and Elizabeth Burakowski for field assistance,

and to more than 25 students for their support in the field and the lab. The work in this manuscript was funded by the U.S. National Science Foundation (AGS-1806422).

Supplementary

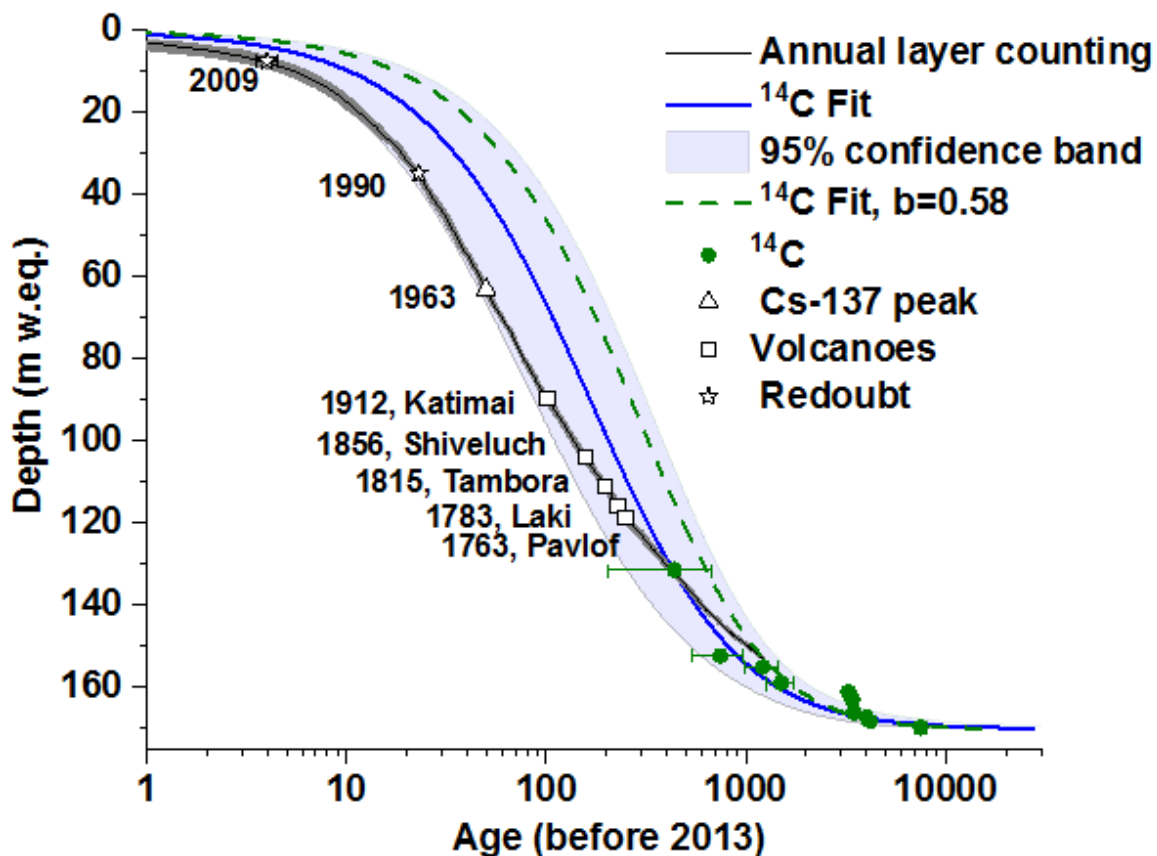


Figure S5.1. 2p-model fit constrained with ¹⁴C dates only and 95% confidence band (blue line and shading). The black line indicates the annual layer counting together with previously reported time horizons. The green dashed line shows the 2p-model fit to the ¹⁴C dates with a fixed accumulation of 0.58 m w.eq.

Bibliography

- Agrios, K., G. Salazar and S. Szidat. A Continuous-Flow Gas Interface of a Thermal/Optical Analyzer With ^{14}C AMS for Source Apportionment of Atmospheric Aerosols. *Radiocarbon* **59**, 921-932, (2017).
- Agrios, K., G. Salazar, Y.-L. Zhang, C. Uglietti, M. Battaglia, M. Luginbühl, V. G. Ciobanu, M. Vonwiller and S. Szidat. Online coupling of pure O_2 thermo-optical methods— ^{14}C AMS for source apportionment of carbonaceous aerosols. *Nuclear Instruments and Methods in Physics Research Section B: Beam Interactions with Materials and Atoms* **361**, 288-293, (2015).
- Anderson, L., M. B. Abbott, B. P. Finney and S. J. Burns. Regional atmospheric circulation change in the North Pacific during the Holocene inferred from lacustrine carbonate oxygen isotopes, Yukon Territory, Canada. *Quaternary Research* **64**, 21-35, (2005).
- Barclay, D. J., G. C. Wiles and P. E. Calkin. Holocene glacier fluctuations in Alaska. *Quaternary Science Reviews* **28**, 2034-2048, (2009).
- Bengtsson, L. S., V. A.; Johannessen, O. M. The Early Twentieth-Century Warming in the Arctic—A Possible Mechanism. *Journal of Climate* **17**, 4045-4057, (2004). [10.1175/1520-0442\(2004\)017<4045:tetwit>2.0.co;2](https://doi.org/10.1175/1520-0442(2004)017<4045:tetwit>2.0.co;2)
- Benson, C., R. Motyka, S. McNUTT, M. Luethi and M. Truffer. Glacier–volcano interactions in the North Crater of Mt Wrangell, Alaska. *Annals of Glaciology* **45**, 48-57, (2007).
- Blackport, R., J. A. Screen, K. van der Wiel and R. J. N. C. C. Bintanja. Minimal influence of reduced Arctic sea ice on coincident cold winters in mid-latitudes. **9**, 697-704, (2019).
- Campbell, S., S. Roy, K. Kreutz, S. A. Arcone, E. C. Osterberg and P. Koons. Strain-rate estimates for crevasse formation at an alpine ice divide: Mount Hunter, Alaska. *Annals of Glaciology* **54**, 200-208, (2013).
- Cohen, J., K. Pfeiffer and J. A. J. N. c. Francis. Warm Arctic episodes linked with increased frequency of extreme winter weather in the United States. **9**, 869, (2018).
- Cohen, J., J. A. Screen, J. C. Furtado, M. Barlow, D. Whittleston, D. Coumou, J. Francis, K. Dethloff, D. Entekhabi and J. J. N. g. Overland. Recent Arctic amplification and extreme mid-latitude weather. **7**, 627-637, (2014).
- Dansgaard, W. and S. Johnsen. A flow model and a time scale for the ice core from Camp Century, Greenland. *Journal of Glaciology* **8**, 215-223, (1969).
- Denton, G. H. and W. Karlén. Holocene glacial and tree-line variations in the White River Valley and Skolai Pass, Alaska and Yukon Territory. *Quaternary Research* **7**, 63-111, (1977).
- Dortch, J. M. Defining the Timing of Glaciation in the Central Alaska Range, University of Cincinnati, (2007).

Fisher, D., E. Osterberg, A. Dyke, D. Dahl-Jensen, M. Demuth, C. Zdanowicz, J. Bourgeois, R. M. Koerner, P. Mayewski, C. Wake, K. Kreutz, E. Steig, J. Zheng, K. Yalcin, K. Goto-Azuma, B. Luckman and S. Rupper. The Mt Logan Holocene—late Wisconsinan isotope record: tropical Pacific—Yukon connections. *The Holocene* **18**, 667-677, (2008). 10.1177/0959683608092236

Fisher, D., E. Osterberg, A. Dyke, D. Dahl-Jensen, M. Demuth, C. Zdanowicz, J. Bourgeois, R. M. Koerner, P. Mayewski and C. J. T. H. Wake. The Mt Logan Holocene—late Wisconsinan isotope record: tropical Pacific—Yukon connections. **18**, 667-677, (2008).

Francis, J. A., S. J. Vavrus and J. J. W. I. R. C. C. Cohen. Amplified Arctic warming and mid-latitude weather: new perspectives on emerging connections. **8**, e474, (2017).

Godwin, H. J. N. Half-life of radiocarbon. **195**, 984, (1962).

Hagler, G. S., M. H. Bergin, E. A. Smith, J. E. Dibb, C. Anderson and E. J. Steig. Particulate and water-soluble carbon measured in recent snow at Summit, Greenland. *Geophysical Research Letters* **34**, (2007).

Heusser, C. J., L. Heusser and D. Peteet. Late-Quaternary climatic change on the American North Pacific coast. *Nature* **315**, 485-487, (1985).

Hou, S., T. M. Jenk, W. Zhang, C. Wang, S. Wu, Y. Wang, H. Pang and M. J. T. C. Schwikowski. Age ranges of the Tibetan ice cores with emphasis on the Chongce ice cores, western Kunlun Mountains. **12**, 2341-2348, (2018).

Jenk, T. M., S. Szidat, D. Bolius, M. Sigl, H. W. Gaeggeler, L. Wacker, M. Ruff, C. Barbante, C. F. Boutron and M. J. J. o. G. R. A. Schwikowski. A novel radiocarbon dating technique applied to an ice core from the Alps indicating late Pleistocene ages. **114**, (2009).

Klein, E., M. Nolan, J. McConnell, M. Sigl, J. Cherry, J. Young and J. J. Q. S. R. Welker. McCall Glacier record of Arctic climate change: Interpreting a northern Alaska ice core with regional water isotopes. **131**, 274-284, (2016).

Legrand, M., S. Preunkert, M. Schock, M. Cerqueira, A. Kasper-Giebl, J. Afonso, C. Pio, A. Gelencsér and I. Dombrowski-Etchevers. Major 20th century changes of carbonaceous aerosol components (EC, WinOC, DOC, HULIS, carboxylic acids, and cellulose) derived from Alpine ice cores. *Journal of Geophysical Research* **112**, (2007). 10.1029/2006jd008080

Licciulli, C., P. Bohleber, J. Lier, O. Gagliardini, M. Hoelzle and O. Eisen. A full Stokes ice-flow model to assist the interpretation of millennial-scale ice cores at the high-Alpine drilling site Colle Gnifetti, Swiss/Italian Alps. *Journal of Glaciology* **66**, 35-48, (2020).

Neff, P. D., E. J. Steig, D. H. Clark, J. R. McConnell, E. C. Pettit and B. Menounos. Ice-core net snow accumulation and seasonal snow chemistry at a temperate-glacier site: Mount Waddington, southwest British Columbia, Canada. *Journal of Glaciology* **58**, 1165-1175, (2012). 10.3189/2012JoG12J078

Nye, J. On the theory of the advance and retreat of glaciers. *Geophysical Journal International* **7**, 431-456, (1963).

Osterberg, E. C., P. A. Mayewski, D. A. Fisher, K. J. Kreutz, K. A. Maasch, S. B. Sneed and E. Kelsey. Mount Logan ice core record of tropical and solar influences on Aleutian Low variability: 500–1998 A.D. *Journal of Geophysical Research: Atmospheres* **119**, 2014JD021847, (2014). 10.1002/2014JD021847

Osterberg, E. C., D. A. Winski, K. J. Kreutz, C. P. Wake, D. G. Ferris, S. Campbell, D. Introne, M. Handley and S. Birkel. The 1200 year composite ice core record of Aleutian Low intensification. *Geophysical Research Letters* **44**, 7447-7454, (2017). 10.1002/2017GL073697

Pendleton, S. L., E. G. Ceperley, J. P. Briner, D. S. Kaufman and S. Zimmerman. Rapid and early deglaciation in the central Brooks Range, Arctic Alaska. *Geology* **43**, 419-422, (2015).

Porter, S. E., E. Mosley-Thompson and L. G. Thompson. Ice core $\delta^{18}O$ record linked to Western Arctic sea ice variability. *Journal of Geophysical Research: Atmospheres* **124**, 10784-10801, (2019).

Ramsey, C. B. J. Q. S. R. Deposition models for chronological records. **27**, 42-60, (2008).

Ramsey, C. B. J. R. Methods for summarizing radiocarbon datasets. **59**, 1809-1833, (2017).

Reimer, P. J., E. Bard, A. Bayliss, J. W. Beck, P. G. Blackwell, C. B. Ramsey, H. C. Caitlin E Buck, R. L. Edwards, M. Friedrich, P. M. Grootes, T. P. Guilderson, H. Haflidason, I. Hajdas, C. Hatté, T. J. Heaton, D. L. Hoffmann, A. G. Hogg, K. A. Hughen, K. F. Kaiser, B. Kromer, S. W. Manning, M. Niu, R. W. Reimer, D. A. Richards, E. M. Scott, J. R. Southon, R. A. Staff, C. S. M. Turney and J. v. d. Plicht. Intcal13 and Marine13 radiocarbon age calibration curves 0-50,000 years cal BP. *Radiocarbon* **55**, 1869-1887, (2013).

Screen, J. A., C. Deser, D. M. Smith, X. Zhang, R. Blackport, P. J. Kushner, T. Oudar, K. E. McCusker and L. J. N. G. Sun. Consistency and discrepancy in the atmospheric response to Arctic sea-ice loss across climate models. **11**, 155-163, (2018).

Screen, J. A. and J. A. J. N. C. C. Francis. Contribution of sea-ice loss to Arctic amplification is regulated by Pacific Ocean decadal variability. **6**, 856, (2016).

Svendsen, L., N. Keenlyside, I. Bethke, Y. Gao and N.-E. J. N. C. C. Omrani. Pacific contribution to the early twentieth-century warming in the Arctic. **8**, 793, (2018).

Thompson, L. G., E. Mosley-Thompson, M. Davis, J. Bolzan, J. Dai, L. Klein, T. Yao, X. Wu, Z. Xie and N. J. S. Gundestrup. Holocene—late Pleistocene climatic ice core records from Qinghai-Tibetan Plateau. **246**, 474-477, (1989).

Tokenaga, H., S.-P. Xie and H. J. P. o. t. N. A. o. S. Mukougawa. Early 20th-century Arctic warming intensified by Pacific and Atlantic multidecadal variability. **114**, 6227-6232, (2017).

- Tsushima, A., S. Matoba, T. Shiraiwa, S. Okamoto, H. Sasaki, D. J. Solie and K. Yoshikawa. Reconstruction of recent climate change in Alaska from the Aurora Peak ice core, central Alaska. *Clim. Past* **11**, 217-226, (2015). 10.5194/cp-11-217-2015
- Uglietti, C., A. Zapf, T. M. Jenk, M. Sigl, S. Szidat, G. Salazar and M. Schwikowski. Radiocarbon dating of glacier ice: overview, optimisation, validation and potential. *The Cryosphere* **10**, 3091-3105, (2016). 10.5194/tc-10-3091-2016
- Uglietti, C., A. Zapf, T. M. Jenk, M. Sigl, S. Szidat, G. A. Salazar Quintero and M. Schwikowski. Radiocarbon dating of glacier ice: overview, optimisation, validation and potential. *The Cryosphere* **10**, 3091-3105, (2016).
- Walker, M., M. J. Head, J. Lowe, M. Berkelhammer, S. Björck, H. Cheng, L. C. Cwynar, D. Fisher, V. Gkinis and A. Long. Subdividing the Holocene Series/Epoch: formalization of stages/ages and subseries/subepochs, and designation of GSSPs and auxiliary stratotypes. *Journal of Quaternary Science* **34**, 173-186, (2019).
- Winski, D., E. Osterberg, D. Ferris, K. Kreutz, C. Wake, S. Campbell, R. Hawley, S. Roy, S. Birkel and D. Introne. Industrial-age doubling of snow accumulation in the Alaska Range linked to tropical ocean warming. *Scientific reports* **7**, 1-12, (2017).
- Winski, D., E. Osterberg, D. Ferris, K. Kreutz, C. Wake, S. Campbell, R. Hawley, S. Roy, S. Birkel, D. Introne and M. Handley. Industrial-age doubling of snow accumulation in the Alaska Range linked to tropical ocean warming. *Scientific Reports* **7**, 17869, (2017). 10.1038/s41598-017-18022-5
- Winski, D., E. Osterberg, K. Kreutz, C. Wake, D. Ferris, S. Campbell, M. Baum, A. Bailey, S. Birkel and D. J. J. o. G. R. A. Introne. A 400-Year Ice Core Melt Layer Record of Summertime Warming in the Alaska Range. **123**, 3594-3611, (2018).
- Yalcin, K., C. P. Wake, K. J. Kreutz, M. S. Germani and S. I. Whitlow. Ice core paleovolcanic records from the St. Elias Mountains, Yukon, Canada. *Journal of Geophysical Research: Atmospheres* **112**, (2007).
- Yasunari, T. J., T. Shiraiwa, S. Kanamori, Y. Fujii, M. Igarashi, K. Yamazaki, C. S. Benson and T. Hondoh. Intra-annual variations in atmospheric dust and tritium in the North Pacific region detected from an ice core from Mount Wrangell, Alaska. *Journal of Geophysical Research: Atmospheres* **112**, (2007).
- Zdanowicz, C., D. Fisher, J. Bourgeois, M. Demuth, J. Zheng, P. Mayewski, K. Kreutz, E. Osterberg, K. Yalcin and C. Wake. Ice cores from the St. Elias Mountains, Yukon, Canada: their significance for climate, atmospheric composition and volcanism in the North Pacific region. *Arctic* **35-57**, (2014).

6 Enhancement of biogenic secondary organic aerosol formation during the 20th century: insights from radiocarbon in organic carbon from a high Alpine glacier

Ling Fang^{1,2,3†}, Fang Cao^{1,4†}, Yan-Lin Zhang^{1,2,4}, Lukas Wacker⁵, Alexander. L. Vogel⁶, Stephan Henne⁷, Gary Salazar², Sönke Szidat², Margit Schwikowski^{1,2,3} and Theo M. Jenk^{1,3,*}

¹Paul Scherrer Institute, 5232 Villigen PSI, Switzerland

²Department of Chemistry and Biochemistry, University of Bern, CH-3012 Bern, Switzerland

³Oeschger Centre for Climate Change Research, University of Bern, CH-3012 Bern, Switzerland

⁴Yale-NUIST Center on Atmospheric Environmental, Nanjing University of information Science and Technology, 210044 Nanjing, China

⁵Laboratory of Ion Beam Physics, ETH Zurich, 8093 Zurich, Switzerland

⁶ now at Institute for Atmospheric and Environmental Sciences, Goethe University Frankfurt, 60438 Frankfurt, Germany

⁷Department of Mobility, Energy and Environment, Swiss Federal Laboratories for Materials Science and Technology Empa, Switzerland

†Co-first author

* Correspondence to Dr. Theo M. Jenk (theo.jenk@psi.ch); Phone: +41 56 310 2530

Manuscript to be submitted to

Nature Geoscience

Abstract

The impact of aerosol particles on the Earth's radiation balance remains poorly constrained, leading to considerable uncertainties in predicting the climate sensitivity to greenhouse gases. A large part of these uncertainties is related to the deficient knowledge of the magnitude of pre-industrial emissions, particularly for carbonaceous compounds forming a major fraction of the atmospheric aerosol. Here we present a 340-year concentration record of water insoluble organic carbon (WIOC), water soluble organic carbon (WSOC), and elemental carbon (EC) separated into fossil and non-fossil contribution using the ^{14}C content from Fiescherhorn ice core (Swiss Alps). Total carbonaceous aerosol concentration (sum of WIOC, WSOC and EC) were a factor of three higher at the end of 20th century compared to pre-industrial background. Radiocarbon based source apportionment shows that fossil fuel combustion contributed up to ~32% of enrichment. EC has highest values in the first half of the 20th century, to a large extent caused by fossil fuel emissions. In contrast, OC (WIOC and WSOC) shows a strong increasing trend between 1940 and 1980, mostly of non-fossil origin, which is not reflected in the potential source region emission estimates of OC with a mismatch of up to one magnitude in the second half of the 20th century. We attribute this trend primarily to enhancement of SOA formation caused by the presence of anthropogenic precursor gases or by the increase of the atmospheric oxidative capacity. Thus, bottom-up emission inventories seem to heavily underestimate the atmospheric OC loading by not accounting adequately for SOA formation, limiting the capacity of current models in estimating anthropogenic aerosol forcing.

6.1 Introduction

Carbonaceous particles which comprise organic carbon (OC) and elemental carbon (EC; depending on the analytical technique applied also referred to as black carbon, BC) are of increasing interest globally because they are a major contributor to the overall aerosol mass and thus have an impact on the radiative balance of the Earth via direct and indirect effects [Pöschl, 2005]. However, the magnitude of the atmospheric aerosol effect on climate is still uncertain, largely due to the lack of knowledge about the pre-industrial aerosol loading. The global mean cloud albedo of the pristine pre-industrial atmosphere may have been very sensitive to changes in natural emissions, with strong implications for the estimation of anthropogenic aerosol forcing [Carslaw et al., 2013]. An accurate estimation of climate forcing from carbonaceous aerosols requires good knowledge of historical, fraction resolved emissions. One of the most promising approaches to constrain the pre-industrial aerosol burden is to obtain records from ice cores. They do exist for major aerosol fractions such as sulphate, nitrate, ammonium, sea salt, mineral dust and black carbon, but pre-industrial records of organic aerosols are very rare [Legrand et al., 2007; Thevenon et al., 2009; May et al., 2013; Ruppel et al., 2014]. Organic aerosols attracted attention recently, since it was shown that new particle formation can alone be driven by the oxidation of biogenic volatile organic compounds (BVOCs), while it was previously thought that gas-phase sulfuric acid needs to be involved [Kirkby et al., 2016]. EC exclusively originates from fossil-fuel combustion and biomass burning, while OC sources are complex. OC can be emitted directly as primary organic aerosol (POA) from biogenic sources, biomass burning and fossil-fuel combustion or can be formed in the atmosphere as secondary organic aerosol (SOA) [Pöschl, 2005]. Recent studies suggest that SOA formation rates are not adequately constrained in current models limiting accurate simulation of their climate effect [Hodzic et al., 2016; Shilling et al., 2013].

Radiocarbon analysis (^{14}C) is a powerful tool for unambiguous distinction between biogenic (non-fossil) and fossil sources of carbonaceous particles since biogenic carbon is of contemporary origin and therefore contains ^{14}C of a known level, whereas fossil carbon is extinct in ^{14}C due to its half-life of 5730 years [Currie, 2000; Zhang et al., 2015]. ^{14}C -based source apportionment has been applied for ambient aerosols in many locations including Switzerland, Sweden, China and USA [Szidat et al., 2006; Shilling et al., 2013; Zhang et al.,

2015]. It was found that fossil-fuel combustion is the dominant EC source, while non-fossil sources (e.g. biomass burning and biogenic SOA) are important contributors to OC even in polluted areas such as the Los Angeles Basin [Zotter et al., 2014], Beijing [Zhang et al., 2015] and Mexico City [Hodzic et al., 2010]. Long-term records of fossil and non-fossil contributions to OC and EC are largely lacking since ambient samples are at most available for the last several decades and ^{14}C measurements in OC and EC extracted from environmental archives such as ice cores are very challenging due to low concentration levels. Nevertheless, they would be fundamental to constrain source contributions, emission estimates, and the effect of atmospheric aerosols on global and/or regional climate; a prerequisite for a reasonable implementation of air pollution and climate mitigation measures.

High-altitude glaciers offer the possibility to derive information on past changes in emission sources, atmospheric loading and composition of aerosols due to their proximity to major source areas, and are therefore well-suited to overcome the lack of long-term data. Here we present the first complete ice core concentration record of the different bulk carbonaceous particle fractions WIOC, WSOC, and EC, along with their fossil and non-fossil contributions covering the preindustrial time to the present, which was obtained from the Fiescherhorn glacier in the Swiss Alps.

6.2 Results and Discussion

6.2.1 Temporal trends in concentration of carbonaceous aerosols

Combining our previously published WIOC and EC concentrations from the older part of the core (1660-1939) with our new data including WSOC concentrations, a complete record for the period 1660 to 2002 is obtained (1660-1990 for WSOC, Figure 6.1). For the period 1940-2002 mean WSOC, WIOC and EC concentrations of 132 ± 58 $\mu\text{g}/\text{kg}$, 90 ± 40 $\mu\text{g}/\text{kg}$ and 20 ± 10 $\mu\text{g}/\text{kg}$ were observed, respectively. They are overall consistent with values from other European ice cores such as from Col du Dôme, Mt Blanc, France (WSOC 147 $\mu\text{g}/\text{kg}$ for 1971-1988; WIOC: 25-50 $\mu\text{g}/\text{kg}$, EC: 7-16 $\mu\text{g}/\text{kg}$ for 1940-1990, Legrand et al., 2007) and Colle Gnifetti, Switzerland (EC: ~ 20 $\mu\text{g}/\text{kg}$ for 1950-1980, Thevenon et al., 2009). Further, the temporal variation in the EC record is in very good agreement with a more recent BC record from Colle Gnifetti ($R=0.71$, $p<0.005$, Sigl et al., 2018). Over the entire period, WSOC is the dominant

fraction accounting for 45-67% of TC, comparable with atmospheric observations at alpine high elevation [Pio et al., 2007]. The total carbonaceous particle concentration (TC: the sum of EC, WIOC, and WSOC) increased by factor of 3 at the end of 20th century compared to the pre-industrial level (1680-1850). Our results point to a relatively strong steady increase in WSOC and WIOC from 1940 to 2000. This confirms the OC increase trend in the Alps by 20th century [Legrand et al., 2007; May et al., 2013]. Historical trend of biogenic SOA tracers in ice core from Kamchatka Peninsula showed a high level of SOA tracers in the pre-industrial period (1700-1800) probably due to change in atmospheric circulation, emission and oxidative capacity [Fu et al., 2016]. However, the carbonaceous aerosol record from Alpine ice cores could not confirm the high pre-industrial OC loading.

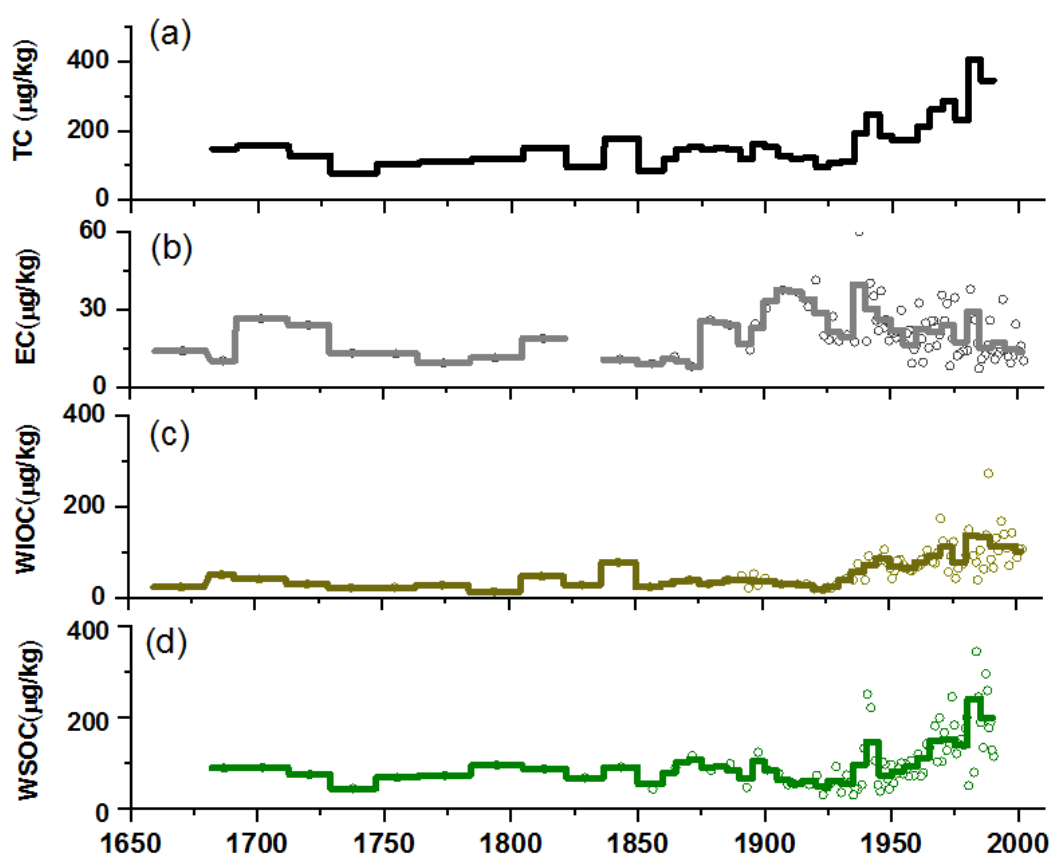


Figure 6.1 Fiescherhorn ice core concentration record of a) Total carbonaceous particles (TC) b) elemental carbon (EC), c) water insoluble organic carbon (WIOC) and d) water soluble organic carbon (WSOC) covering the period 1660–2002. Results from individual measurement are plotted as circles. Back to 1860, the record is shown in 5-year resolution and before 1860

in 10 to 20-year resolution. TC is the sum of WSOC, EC and WIOC (where missing, EC values were interpolated) over the period of 1680-1990.

¹⁴C-based source apportionment suggests fossil fuel combustion accounts for about 35% of the TC enhancement compared to the pre-industrial background (average before 1850s, Figure 6.2). The non-fossil TC trend is mainly driven by non-fossil WSOC (WSOC_b), but non-fossil WIOC (WIOC_b) became more significant after 1940s. The WSOC concentration has increased strongly since 1940s due to both, fossil and biogenic input (Figure S6.5). This trend since 1940s is consistent with the DOC record from Col du Dôme [May et al., 2013]. However, different to their conclusion that the fossil fuel contribution remained constant, our data indicate fossil fuel derived fraction of WSOC (WSOC_f) steadily increased up to 33% at the end of 20th century. Thus, emissions from fossil fuel use have significantly changed the WSOC composition (Figure 6.2 and Figure S6.5). In contrast, the strong increasing trend of WIOC between 1940 and 1980 is mostly of non-fossil origin (Figure S6.4). In the year 2002, 93± 6% of WIOC was non-fossil, which is comparable to the mean value of 84±5% for WIOC extracted from precipitation samples at a suburban site in Switzerland in the period April 2012 to March 2013 [Zhang et al., 2015] and to the 5-year mean of 78±8% non-fossil contribution to total OC of PM10 (particulate matter with a diameter smaller than 10 μm) samples collected at various locations north of the Alps during winter-smog episodes from 2008 to 2012 [Zotter et al., 2014]. The EC peak in the first half of the 20th century is largely due to fossil sources, presumably hard coal burning (Figure 6.1 and Figure S6.3). From 1950s on the EC fossil contribution decreased steadily, reflecting the effect of emission reductions due to the replacement of coal with liquid fuel in the 1960s, improved combustion technology and other air pollution control measures since the 1970s. Although petroleum consumption simultaneously increased significantly [Kander et al., 2008], the related emission factors are much lower compared to coal combustion [Bond et al., 2004; Pio et al., 2011]. Non-fossil EC contributes on average around 40% and does not show a long-term trend, suggesting that emissions from biomass-burning sources including both, natural forest fires and anthropogenic emissions from the combustion of biogenic materials, have not significantly changed over the investigated period.

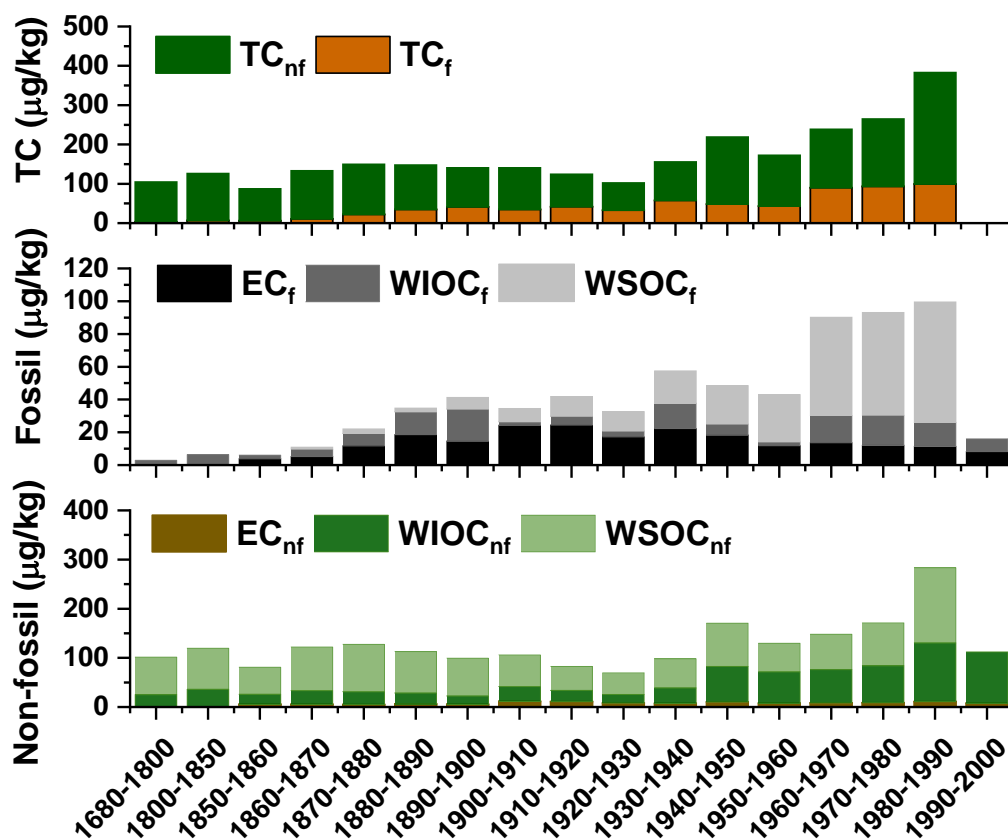


Figure 6.2 ^{14}C -based source apportionment of carbonaceous aerosol records. Pre-industrial averaged over two period, 1680-1800 and 1800-1850. After 1850, 10 years averaged.

6.2.2 Constraints on BC emissions

To investigate the potential emission source of carbonaceous particles in the Fiescherhorn ice core, we used the atmospheric transport and deposition model FLEXPART (detail see the Methods). The resulting footprint indicates that central Europe including Switzerland, eastern France, northern Italy and southern Germany is the main potential source region (Figure S6.2). Atmospheric loading of BC, organic carbon (OC) and non-methane volatile organic compound (NMVOC) at the ice core site were estimated based on the footprint and regional emission inventories for the period 1850-2000 [Bond et al., 2007; Lamarque et al., 2010]. Ice core derived 10-years average EC concentrations and atmospheric BC concentrations from the major sources (domestic, traffic, industrial and grass fires etc.) show a significant correlation (Pearson

Correlation = 0.83, $p < 0.01$, $n = 15$, Figure S6.6) and the resulting mean volume based scavenging ratio ω_v of 0.06×10^6 is in the range of reported values, $0.02-0.18 \times 10^6$ [Cerqueira et al., 2010]. Whereas the timing of the concentration increase after 1850 is similar for ice core EC and estimated atmospheric BC concentrations, (Figure 6.3), the downward trend in our ice core record started already after 1920 compared to 1940 in atmospheric BC. An analogous disagreement of the onset BC decline trend also was reported from another eastern European ice core BC record from Mt. Elbrus [Lim et al., 2017]. This mismatch between ice core observations and emission estimates is in contrast to the finding that sulphate concentration trends in Alpine ice cores agree well with the corresponding deposition trends simulated with atmospheric chemical transport models using emission estimates as input parameters [Fagerli et al., 2007; Engardt et al., 2017]. Therefore, we are confident that Alpine ice cores reliably preserve the EC emission history and that the above discussed discrepancy is related to uncertainties in BC emission estimates. Thus, we propose to use ice-core based EC records to better constrain European BC emissions.

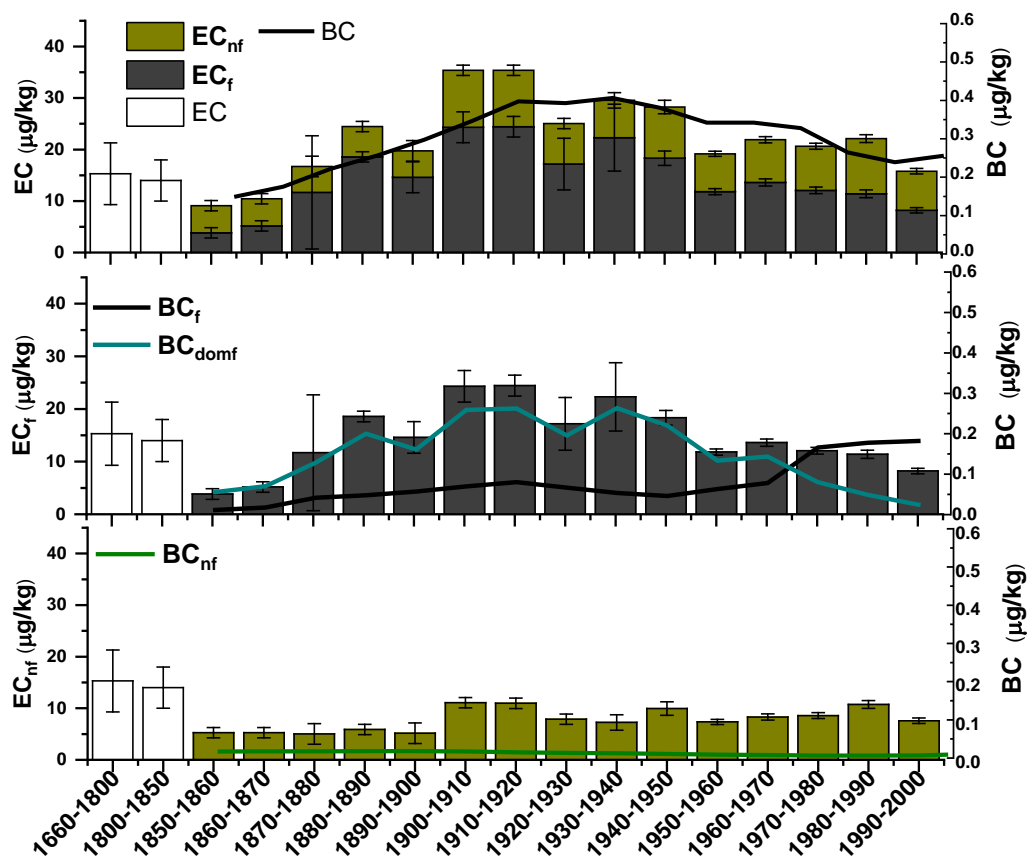


Figure 6.3 Comparison between the EC concentration in ice core and atmospheric BC load in 10-year resolution. The definition of BC_f , BC_{nf} and BC_{domf} see in the text.

For the major contributor to BC, i.e. domestic emissions (Figure S6.2), the amount originating from fossil and non-fossil sources is not known. Based on the good agreement between values of atmospheric BC concentrations from domestic emissions (BC_{dom}) and ice core EC_f (Figure 6.3 and Figure S6.2) we deduce that fossil fuel was the main the household energy source in Central Europe for the period of 1870-1950. After 1950, BC_{dom} shows a strong downward trend, which is compensated for by other anthropogenic fossil BC emissions (Figure 6.3, BC_f : air, ene, ind, shp, tra and slv). In contrast, the non-fossil contributions to BC from agriculture, grassfire and forest fire (BC_{nf}) were stable over time (Figure 6.3 and Figure S6.2). This is consistent with the ice core EC_{nf} concentration, except that EC_{nf} concentrations were constantly higher than the estimated BC_{nf} , since they also include non-fossil domestic emissions. Accordingly, we define the difference between EC_{nf} and BC_{nf} as non-fossil fraction of BC_{dom} . The fossil contribution of BC_{dom} was low before 1850 (~ 35%), increased to more than 90% during 1890-1920 (Figure S6.7), after which it declined steadily. Finally, at the end of 20th century domestic emissions were dominated by non-fossil sources.

Non-fossil EC contributed on average around 37% of total EC and the EC_{nf} concentration does not show a long-term trend as mentioned above, suggesting that emissions from biomass-burning sources including both, natural forest fires and anthropogenic emissions from the combustion of biogenic materials, have not changed over the investigated period. Our data also suggests that domestic heating was the major source of EC_{nf} , whereas natural fires played a negligible role.

6.2.3 Sources of enhanced non-fossil OC in late 20th century

Whereas our results of EC are overall in reasonable agreement with simulated BC concentrations, we find a striking mismatch between the ice core OC concentrations (sum of WSOC and WIOC) and the modelled concentrations of primary OC (Figure 6.4). Ice core OC concentrations steadily increased from 1940 to 2000, but modelled primary OC does not show a trend until around 1960 and a decline thereafter (Figure S6.2). While the ice core records anthropogenic and biogenic POA and SOA, biogenic POA emissions and secondary aerosol formation from both anthropogenic and biogenic precursors are not considered in the FLEXPART model. The dominant fraction of the ice core OC increase after 1940s is of non-

fossil (i.e. biogenic) origin. The fossil OC fraction increased as well, which can be explained by anthropogenic POA emissions and SOA formed from fossil NMVOC emissions as indicated by the similar trends (Figure 6.4). Discussed point-by-point in the following, possible sources for elevated non-fossil OC concentrations can be summarized by 1) changes in biogenic POA and BVOCs emissions, 2) the enhancement of biogenic SOA formation due to increased anthropogenic emissions of NO_x and SO_2 involved in relevant formation reaction mechanisms, 3) an increase in biogenic SOA formation related to anthropogenically induced changes of the oxidative capacity of the atmospheres.

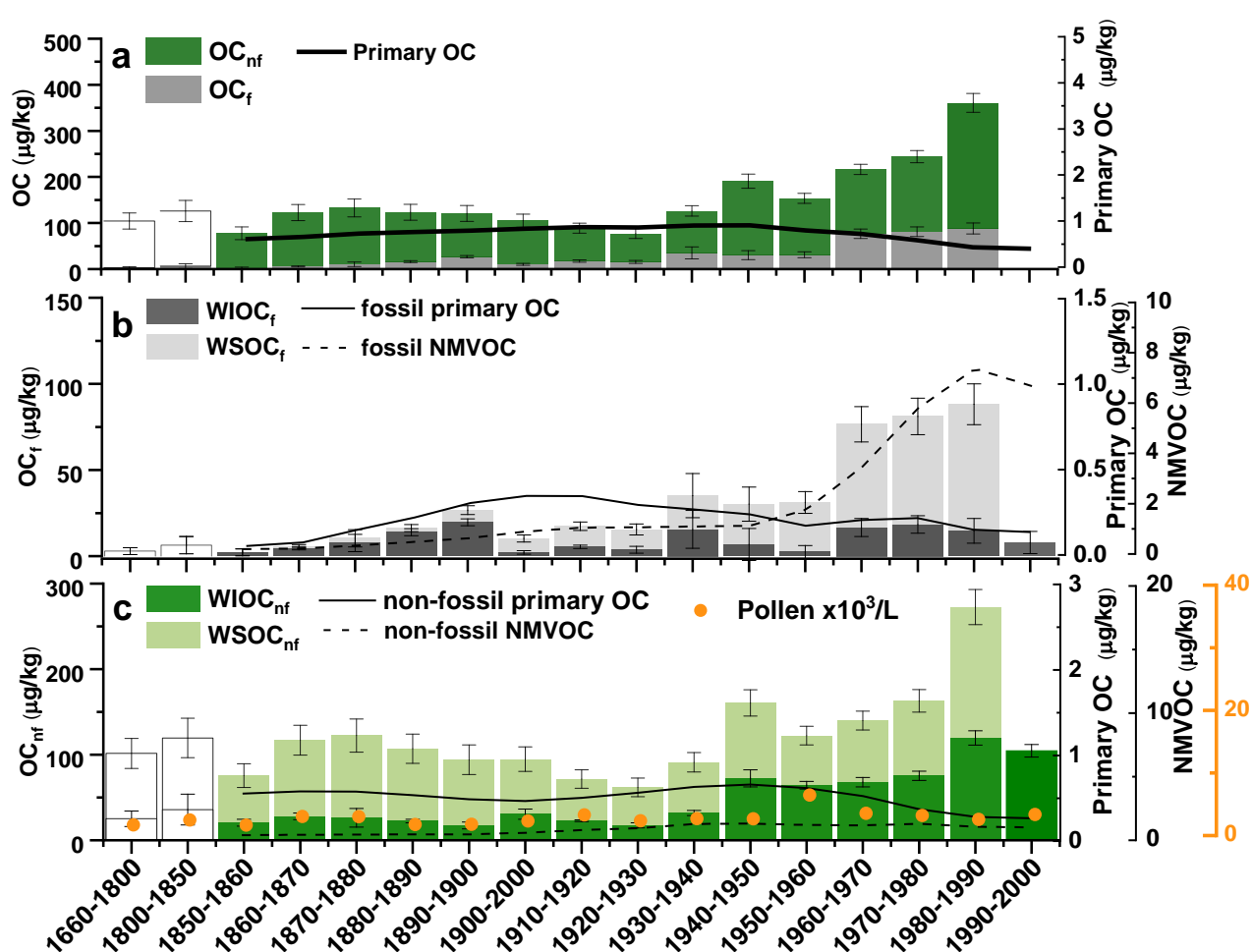


Figure 6.4 Comparison between the OC (sum of WIOC and WSOC) concentration in ice core and primary OC and NMVOC load in 10-year resolution. We redistribute the domestic consumption emission into fossil and non-fossil fraction based on BC record.

1) Wildfires can emit both biogenic POA and BVOCs as SOA precursors. Since EC_{nf} concentrations did not show a trend over the considered time period, wildfires can be excluded as source for the recent increase in ice core OC concentrations. The recent increase in temperature might have influenced biological activity and pollen production. Ice core pollen concentrations are available from Colle Gnifetti glacier, about 70 km south of Fiescherhorn glacier [S. Brugger et al., in preparation]. The estimated pollen carbon mass accounts for $25 \pm 11\%$ of the non-fossil OC concentration and explains the observed $WIOC_{nf}$ concentrations before 1940 (Figure 6.4). Pollen concentrations peaked in the 1960s and slightly declined afterwards to a level at the end of the century 1990-2000 about 45.7% higher than the pre-industrial value. This is comparable with Switzerland total forest area change, which increased 50% in 2000 compared to 1850 [Loran et al., 2016]. This indicates that primary biogenic OC emission from vegetation and biomass burning was the main source of $WIOC_{nf}$ before 1940, but after that other sources became more important. Overall BPOA accounted for about 4 % of OC increase after 1960.

Modelling studies showed that on a global scale SOA precursors are dominated by BVOCs [Hallquist et al., 2009] and their emissions are expected to increase in response to warming [Paasonen et al., 2013]. Land-use has changed significantly in Europe over the last century with an enormous intensification of agriculture, often associated with deforestation and urbanization. Globally, modelling studies suggest that land-use changes have decreased isoprene (i.e., one of most important precursors of biogenic derived SOA) emissions by about 20% [Lathière et al., 2010; Unger, 2013]. In contrast to the global trend, emissions of BVOCs in Europe have increased significantly in summer between 1920–1950 and 1970–1990 [Acosta Navarro et al., 2014]. For example in the Alpine region, isoprene, monoterpene, and sesquiterpene emissions grew 10–40%, 10–20%, and 10–30%, respectively, during this period [Acosta Navarro et al., 2014]. If we assume the SOA formation rate constant over time, the increase in BVOCs could induce about 10-40% increase of pre-industrial OC_{nf} . This can explain 3-12 % of the increase in the non-fossil OC concentration.

2) Many studies provide evidence that anthropogenic emissions of precursor gases such as of NO_x , SO_2 , and VOCs can lead to an enhancement in biogenic-derived SOA formation [Hoyle et al., 2011; Fuzzi et al., 2015]. Hoyle et al. (2011) attribute the enhancement of biogenic SOA by anthropogenic pollutants to a shift of the partitioning of biogenic organics from the gas to

the aerosol phase due to the presence of anthropogenic aerosol mass. SOA yields might also be affected by the presence of NO_x [Shilling et al., 2013]. Rollins et al. (2012) found evidence for NO_x control over nighttime SOA in ambient atmospheric organic aerosol due to the nitrate radical product of anthropogenic NO_x emissions. Also, organics were shown to contribute together with sulfuric acid to new particle formation and growth [Hoyle et al., 2011; Ehn et al., 2014; Riccobono et al., 2014]. Shilling et al. (2013) found evidence that anthropogenic and biogenic emissions interact to enhance organic aerosol production from biogenic species, with an enhancement factor of 2–4 when biogenic and anthropogenic emissions mix during summertime in the Sacramento region (USA). A best estimate is that 50–70% of the total organic aerosol budget may be composed of SOA produced from BVOCs, but at the same time is controlled by anthropogenic emissions [Carlton et al., 2010; Spracklen et al., 2011]. Using a global model, Lin et al. suggested that anthropogenic emissions in present days have substantially increased the SOA formation rate by 29 Tg/yr (93%) since pre-industrial times [Lin et al., 2014]. In Europe anthropogenic emissions of SO₂ and NO_x increased strongly after 1950 as shown in Figure 6.5, which has also been demonstrated by direct atmospheric measurements, atmospheric chemical transport models, and other ice core observations, (e.g. Legrand et al., 2013). SO₂ emissions were reduced by air pollution control measures introduced in the 1970s, whereas NO_x emissions remained high far into the 1990s. The good correlation ($p < 0.01$, $r(90) = 0.83$) between the temporal concentration trends of nitrate and non-fossil OC in the FH ice core suggests that these processes indeed have played an important role. Thus, the enhancement of SOA formation may well explain the observed increase in OC starting around 1940 (Figure 6.5).

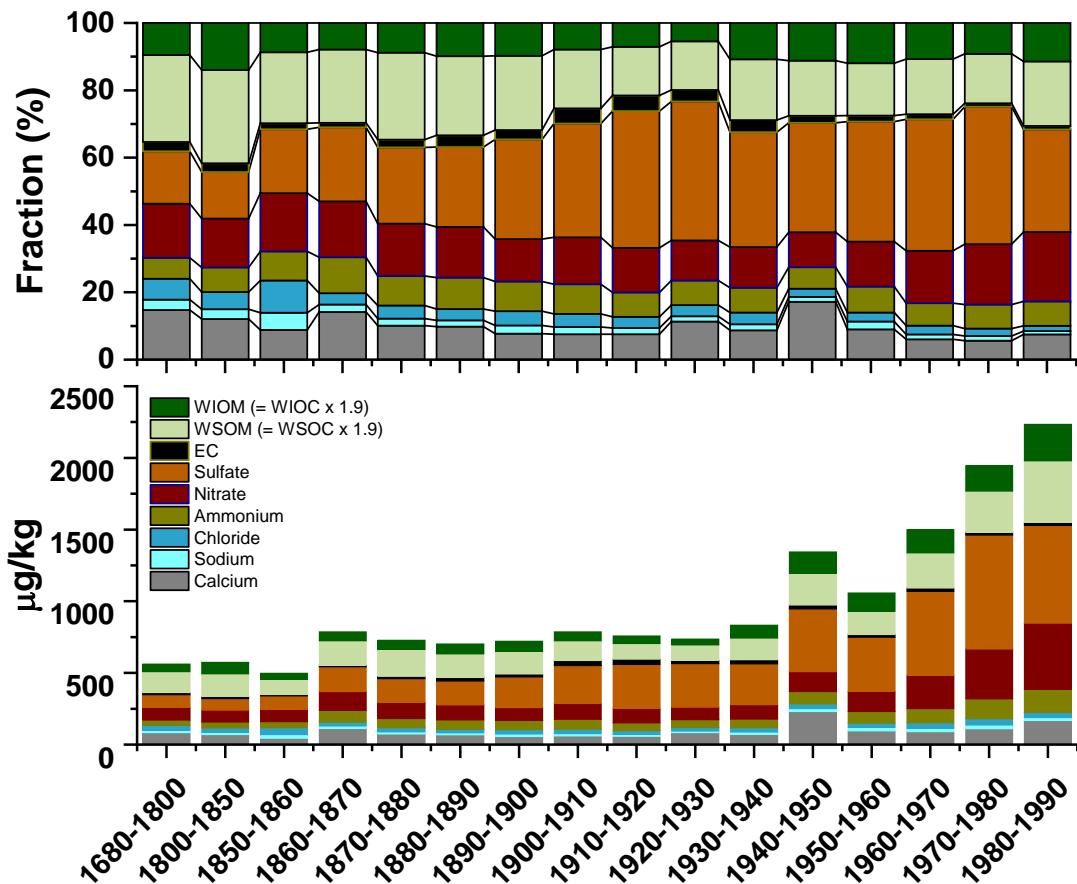


Figure 6.5 Concentration records of different aerosol constituents from Fiescherhorn ice core averaged for the indicated pre-industrial (1680-1800 and 1800-1850) and 10 year average for industrial time periods in $\mu\text{g}/\text{kg}$.

3) Measurements in the Northern Hemisphere indicate that surface ozone concentrations approximately doubled over the last century [Isaksen et al., 2009; Cooper et al., 2014], whereas a global modelling study predicted concentrations in Europe reaching 70 ppbv in July under present-day conditions, which is a factor of three higher than in pre-industrial times [Liao and Seinfeld, 2005]. The increase in oxidative capacity may have enhanced the formation of biogenic SOA through the oxidation of BVOCs. Also this mechanism may have contributed to the observed increase in OC.

In summary, this first pre-industrial to industrial ice record of carbonaceous aerosol concentrations indicated that fossil and non-fossil concentrations of different carbonaceous aerosol fractions show characteristic differences in their temporal variation. This demonstrates that the separation into the fossil and non-fossil component is crucial for a quantitative reconstruction of OC and EC emissions. The EC record shows a maximum in concentrations at the beginning of the 20th century, largely related to fossil fuel emissions, whereas biomass burning sources contributed generally less than 37% without significant temporal variation. The EC concentration level remained virtually constant between 1950 and 2002, challenging the strong decline of estimated BC emissions after 1970. The most prominent feature of the OC record is a significant increasing trend starting around 1940. The dominant fraction of OC is of non-fossil (i.e. biogenic) origin, in agreement with recent modelling studies showing that globally, SOA is mostly biogenic [Hoyle et al., 2011; Hodzic et al., 2016]. We attribute the observed trend primarily to enhancement of SOA formation caused by the presence of anthropogenic precursor gases such as NO_x, SO₂, and VOCs or by the increase of the atmospheric oxidative capacity. Higher emissions of biogenic POA and VOCs due increased biological activity, land-use changes and intensification of agriculture contributed likely less than 50%. The strong OC trend is not reflected in the respective emission estimates of OC. Thus, bottom-up emission inventories seem to heavily underestimate the atmospheric OC loading by not accounting adequately for SOA formation, limiting the capacity of current models in estimating anthropogenic aerosol forcing. For better constraining emission estimates, further source resolved OC records with a good spatial coverage would be highly desirable.

6.3 Methods

6.3.1 Sample selection

Samples analyzed in this study originate from a 150.5 m ice core drilled at the Fiescherhorn glacier (FH, 46°33'3.2''N, 08°04'0.4''E; 3900 m asl.) in December 2002 [Jenk et al., 2006]. During ice core drilling, the obtained core sections (0.7 m long, 8 cm in diameter) were handled wearing gloves at all times. They were packed right after extraction into polyethylene tubes to prevent contamination, and then transported frozen to the cold room at the Paul Scherrer

Institute for storage at -20°C . The core covers the time period from 1660-2002. Subsampling and analysis of the ice core was already conducted in a previous study and the dating of the core is described in detail therein [Jenk et al., 2006]. Briefly, it was performed by a multiproxy approach including: (1) annual layer counting using the seasonal variations of the stable hydrogen isotope ratio (δD) and the concentration of NH_4^+ as well as (2) the detection of time markers such as the Chernobyl accident in 1986 (from the ^{137}Cs peak), the thermonuclear bomb tests in 1963 (from the ^3H maximum) and well-documented Saharan dust events. Since publication of the record to 1940 [Jenk et al., 2006], analyses of major ion concentrations and water stable isotopes were completed, allowing a more accurate and slightly revised dating by annual layer counting [Mariani et al., 2014]. Based on this revised dating, a record of water stable isotopes and accumulation for FH was published for the more recent part [Mariani et al., 2014]. The changes applied to the initial dating are in the order of ± 1 -2 years back to 1900, gradually increasing to around -10 to -15 years for the oldest part of the record. As a result, the age of the oldest sample changed from around 1650 to around 1660. Here, the new and more accurate dating was used and the previously published data [Jenk et al., 2006] were revised accordingly to result in a consistent and most reliable combined record. The dating uncertainty is estimated to ± 30 years for the oldest part of the record (1660) gradually decreasing to ± 3 years for the period 1940-1962 and ± 1 years for the period 1962-2002. In this work, 62 samples from the uppermost part of the Fiescherhorn ice core covering the period 1940-2002 and largely consisting of firn were analyzed.

6.3.2 Sample Preparation

The density profile shows that samples from above ~ 40 m depth (~ 1990 -2002) consist of firn ($\rho < 800 \text{ kg m}^{-3}$), samples from ~ 40 -80 m depth (~ 1960 -1990) contain the firn-ice transition ($800 \text{ kg m}^{-3} < \rho < 917 \text{ kg m}^{-3}$) whereas samples from layers below (older than ~ 1960) are solid ice samples. For the firn and firn-ice transition part of the ice core analyzed in this study, the sections were cut into pieces, the potentially contaminated outer layers (~ 0.5 cm of the surface) were removed using a pre-cleaned stainless-steel band saw, and the derived samples were further decontaminated by chiseling off possible contamination from the previous step with a specifically made smoothing plane. All cutting, and decontamination steps were carried out in

a cold room (-20°C). Sections were then combined aiming for annually resolved samples resulting in 200-700 g of ice, then melted at room temperature and filtered using quartz fiber filters (Pallflex TissuquartzTM, 2500QAO-UP, ~ 11 mm diameter, pre-heated for >4 h at 650°C). Filters were subsequently acidified three times with ~ 50 μL of 0.2 M HCl to remove carbonates and placed for ~ 2 -3 h in a laminar flow-box until complete dryness.

6.3.3 WIOC and EC separation and quantification

WIOC and EC were separated with a recently developed thermal-optical method (Swiss_4S), quantified with a non-dispersive infrared (NDIR) detector using an OC/EC analyzer (Sunset Laboratory Inc., USA) and evolving CO_2 being individually trapped cryogenically and finally sealed in glass ampoules for ^{14}C analysis [Zhang et al., 2012; Cao et al., 2013]. Because we only consider the filtered, insoluble part in this study, this fraction is denoted as water-insoluble OC (WIOC). In contrast to the previously used purely thermal method [Szidat et al., 2004; Jenk et al., 2007], losses or artificial formation (charring) of EC during the thermal treatment was evaluated by monitoring the optical transmittance of the filter samples. This allowed to significantly suppress charring, which on average accounted for less than 10% EC only.

6.3.4 WSOC estimation

Dissolved organic carbon (DOC) were photochemical oxidized with UV (the detail of DOC analyses could found in Fang et al., 2019). Ice samples were rinsed using ultra-pure water and melted in the reactor. After the ice melted, sample is filtrated by a pre-baked quartz filter. Filtration is performed at inert gas conditions, always preserving a little overpressure to prevent ambient air from leaking into the setup. The sample volume is determined by measuring the reactor fill level. The filtrate is acidified by mixing with base water. After the degassing of IC, 1ml of 40mM H_2O_2 injected into reactor right before the irradiation start. During UV oxidation, water vapor is removed by cryogenic trap at -60°C and CO_2 is trap in liquid nitrogen. The sample CO_2 is further cleaned from residual water vapor, quantified manometrically. In the end, CO_2 is sealed in a glass vial for ^{14}C analyses. DOC concentrations are calculated from measured CO_2 pressure and sample volume. In 2007, Legrand et al. proposed using DOC subtract

monoacids and formaldehyde as proxy of WSOC preserved in ice core. We estimated WSOC by subtracting most abundant monoacids, formate and acetate. Although lacking data of other organic gases could leading to overestimated WSOC concentration, regarding low concentration of these organic gases in ice (< 5% of DOC in 1990s), the offset should as low as few ppbC level [Legrand et al., 2007; Legrand et al., 2013]. WSOC record only obtain for the period before 1990 because the contamination of dissolved organic carbon for low-density firn samle[Fang et al., 2019].

6.3.5 ^{14}C analysis

^{14}C measurements were carried out at the Laboratory of Ion Beam Physics (ETH Zürich, Switzerland) and the new Laboratory for the Analysis of Radiocarbon at the Bern University (LARA) using the MIni CARbon DAting System (MICADAS) equipped with a gas ion source Wacker et al., 2013; Szidat et al., 2014. All ^{14}C results were expressed as fraction modern ($F^{14}\text{C}$) defined as the fraction of the measured $^{14}\text{C}/^{12}\text{C}$ ratio related to the $^{14}\text{C}/^{12}\text{C}$ ratio of the reference year 1950 Reimer et al., 2004. $F^{14}\text{C}(\text{OC})$ was corrected for the procedural blanks with a carbon mass of $2.8 \pm 0.8 \mu\text{g}$ ($n=11$) and an $F^{14}\text{C}$ value of 0.81 ± 0.13 ($n=4$) The blank contribution for $F^{14}\text{C}(\text{EC})$ is negligible because the carbon mass of the EC blank ($0.32 \pm 0.14 \mu\text{g}$, $n=4$) with an estimated $F^{14}\text{C}$ value of ~ 0.3 Jenk et al., 2006 is around 10 times lower than the ^{14}C -AMS limit of detection ($\sim 3\text{-}5 \mu\text{g}$) and thus no correction was applied.

6.3.6 Radiocarbon based source apportionment

Fossil carbon is characterized by $F^{14}\text{C}=0$ due the decay of ^{14}C with a half-life of 5730 years. Note that since 1955, the $F^{14}\text{C}$ value of contemporary carbon from biogenic sources and biomass burning (i.e., $F^{14}\text{C}_{\text{bio}}$ and $F^{14}\text{C}_{\text{bb}}$, respectively) is bigger than $F^{14}\text{C}=1$, the theoretical modern level of contemporary carbon, due to the excess from nuclear-bomb testing in the 1950s and 1960s Szidat et al., 2006; Levin et al., 2010. For source apportionment, the obtained $F^{14}\text{C}$ is converted to the fraction of non-fossil (f_{NF}) using the following equation Zhang et al., 2012:

$$f_{\text{NF}} = \frac{F^{14}\text{C}}{f_{\text{NF}}(\text{ref})} \quad (1)$$

$f_{\text{NF}}(\text{ref})$ is the reference value representing $F^{14}\text{C}$ of non-fossil sources at the time when the particles were deposited on the glacier (i.e. age of surrounding ice layer as defined by the dating of the core). It includes biogenic (bio) and biomass-burning (bb) sources and assumes contributions from other non-fossil sources (e.g. cooking emissions) to be negligible. Accordingly, $f_{\text{NF}}(\text{ref})$ is obtained by:

$$f_{\text{NF}}(\text{ref}) = p_{\text{bio}} \times F^{14}\text{C}_{\text{bio}}(\text{ref}) + (1 - p_{\text{bio}}) \times F^{14}\text{C}_{\text{bb}}(\text{ref}) \quad (2)$$

where p_{bio} refers to the fraction of the biogenic sources to the total non-fossil sources. The value of $F^{14}\text{C}_{\text{bb}}$ was estimated by a tree-growth model including 10-year, 20-year, 40-year, 70-year and 85-year old trees with weights of 0.2, 0.2, 0.4, 0.1, and 0.1, respectively Mohn et al., 2008. The resulting reservoir age is 19 ± 4 yrs. The value of $F^{14}\text{C}_{\text{bio}}$ was taken from the long-term series of atmospheric $^{14}\text{CO}_2$ measurements at the Schauinsland station Levin et al., 2010 after 1950 and the IntCal13 dataset Reimer et al., 2013 before 1950. For the tree growth model, we assumed uncertainties of 10% for both tree ages and age distribution (weighting). p_{bio} is assigned as 0 (i.e. 100% from biomass burning) for $f_{\text{NF}}(\text{ref})$ of EC since biomass burning is the only non-fossil source of EC, whereas p_{bio} is assigned as 0.5 ± 0.2 for WIOC by assuming that non-fossil WIOC equally originates from direct biogenic emissions and biomass burning with 50 % Minguillon et al., 2011. These values were constrained based on the knowledge that biomass burning contributes more to non-fossil emissions of OC compared to non-fossil EC and less compared to the contribution to dissolved organic carbon (DOC). For DOC, May et al. (2013) estimated a turnover-time of 3 years which corresponds to a value of ~ 0.8 for p_{bio} in our approach (see turnover-times indicated in Fig. S7). We assigned 0.70 ± 0.15 as p_{bio} value for DOC/WSOC. Despite the relative uncertainty of p_{bio} being rather large, its contribution to the overall uncertainty is small compared to the analytical uncertainty when propagated in all subsequent calculations. The temporal evolution of atmospheric $^{14}\text{CO}_2$, $f_{\text{NF}}(\text{ref})$ of WSOC, WIOC and EC is shown in Figure S6.1 with the defined 1σ confidence bands indicated. For the previously published data Jenk et al., 2006, such a reservoir effect was not considered. Therefore, the data was revised here for consistency although the resulting change on final values is insignificant (less than 1%) because those samples were not affected by the period of exceptional high ^{14}C fluctuation (nuclear bomb test peak). The uncertainty of f_{NF} is around 6%

on average (all samples). f_{NF} was used to calculate concentrations of non-fossil and fossil WSOC, WIOC and EC, respectively (e.g. $[WIOC] \times f_{NF}(WIOC) = [(WIOC)_{NF}]$ and $[WIOC] \times (1 - f_{NF}(WIOC)) = [(WIOC)_F]$). The uncertainty of these fractions is estimated to be less than 20% on average.

6.3.7 Potential emission source regions

To investigate the source of historical atmospheric carbonaceous aerosols, we used the atmospheric transport and deposition model FLEXPART. The resulting footprint indicates that central Europe including Switzerland, eastern France, northern Italy and southern Germany is the main potential source region (Fig. S6.2). Atmospheric loading of BC, organic carbon (OC) and non-methane volatile organic compound (NMVOC) at the ice core site were estimated based on the footprint and regional emission inventories for the period 1850-2000 [Bond et al., 2007; Lamarque et al., 2010]. The model run based on the assumption of that on a decadal time scale there is little change in atmospheric transport. All the simulation was applied to Jungfraujoch where meteorological observation available. We assume the transport and deposition of aerosol to Jungfraujoch were similar to Fiescherhorn since these two location are not far from each other. The final footprint is showed in the Fig. S6.2. The simulation indicated that central Europe are the sources to atmospheric aerosol loading in Jungfraujoch/Fiescherhorn atmospheric column. Switzerland, east France, north Italy and Germany are the main potential source regions. Atmospheric BC, OC and NMVOC loading transport to Jungfraujoch were estimated based on this footprint and potential region historical emission inventories in the decadal scale for the period 1850-2000. The sources considered were agriculture, air traffic, agricultural waste burning, domestic consumption, energy production (power plants), industry, shipping, solvent emission, land traffic, waste emission, forest fires, and grassfires. The result then is a time series of 10-year average mass mixing ratios (ug/kg) of the above compounds at the location of Jungfraujoch and for the period of 1850 to 2000 (Fig. S6.2). Domestic emission (residential and commercial consumption) is the dominated source of BC and OC, whereas traffic and solvent emission are the major component for NMVOC after 1960s. The traffic emission increase since 1950s for both BC, OC and NMVOC. In order to perform comparison our record to historical emission data, we re-categorized the sources into fossil, non-fossil origin. Air flight, surface traffic, industry, shipping, solvent and power plants emission are fossil emission since the main fuel consumption is fossil fuel. Agriculture, grassfire, agriculture waste and forest fire are categorized as non-fossil emission. As we mentioned above, domestic emission is dominate for atmosphere BC and OC load but with complicate energy structure. It was dominated by wood burning

in the pre-industrial and earlier industrial period. Then more fossil contribution after industrial revolution but emission decrease since 1940s because of the emission regulation in Europe. Based on the good agreement between values of atmospheric BC_{dom} and ice core EC_f (Fig. 6.2) we deduce that fossil fuel was the main source of domestic BC emission in Central Europe for the period of 1900-1950. Accordingly, we define the difference between EC_f and BC_f as fossil fraction of BC_{dom} (BC_{domf}). Individual samples shown as circles in the Fig. S6.7, and the line are the smoothed fits. The fossil contribution to BC_{dom} was low before 1850 (~ 29%), increased to more than 80% during 1890-1920 (Fig. S6.7), then it declined steadily to low level at the end of 20th century.

Data availability

The data supporting the presented findings are available from the authors upon reasonable request.

Acknowledgements

This study was partly supported by the PEGASOS project funded by the European Commission under the Framework Programme 7 (FP7-ENV-2010-265148) F.C. acknowledges funding from the China Scholarship Council Fund of the Chinese Academy of Sciences. Pavlina Pavlova helped cutting the ice samples.

Contributions

L.F., F.C., Y.Z., S.S., T.J. and M.S. conducted and designed the experiments. L.F. conducted the DOC analysis and F.C. conducted the OC/EC filtration. L.F., F.C., Y.Z., S.S., G.S., and L.W. performed ^{14}C measurement and corresponding data analysis. L.F., F.C., Y.Z., S.S. and T.J. analyzed data. T.J. prepared the figures. L.F., F.C., M.S. and T.J. wrote the manuscript with contributions from all authors.

Competing interests

The authors declare no competing interests

Supplementary

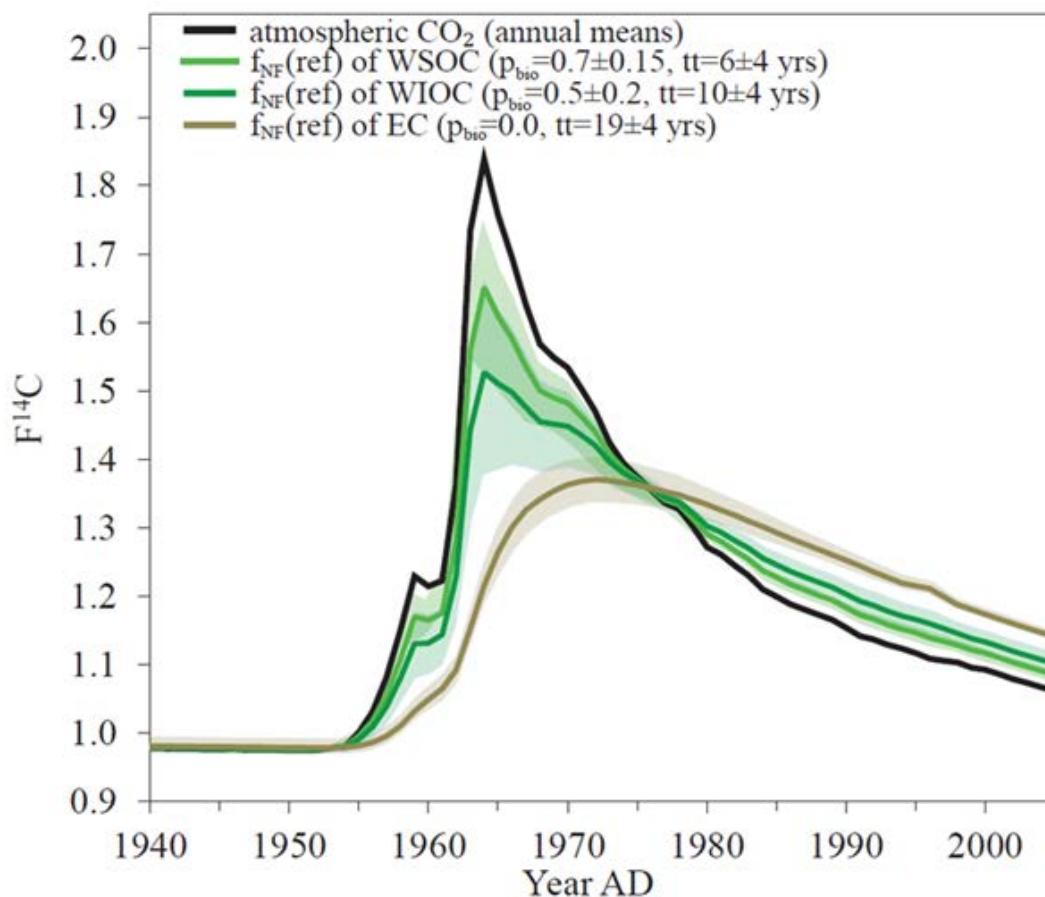


Figure S6.1 Fraction modern ($F^{14}C$) of atmospheric CO_2 as well as $F^{14}C$ reference values for non-fossil sources ($f_{NF(ref)}$) of WSOC, WIOC and EC for the period 1940-2002. The shaded areas indicate the 1σ confidence band estimated by error propagation including the uncertainty related to the reservoir age in trees (tree age and tree age distribution) and additionally for WSOC and WIOC the uncertainty regarding p_{bio} , i.e. the fraction of the biogenic sources unrelated to combustion processes (0.7 ± 0.15 , 0.5 ± 0.2 and 0.0 for WSOC, WIOC and EC, respectively). Numerical values for the estimated turnover times (tt , in years) are also indicated.

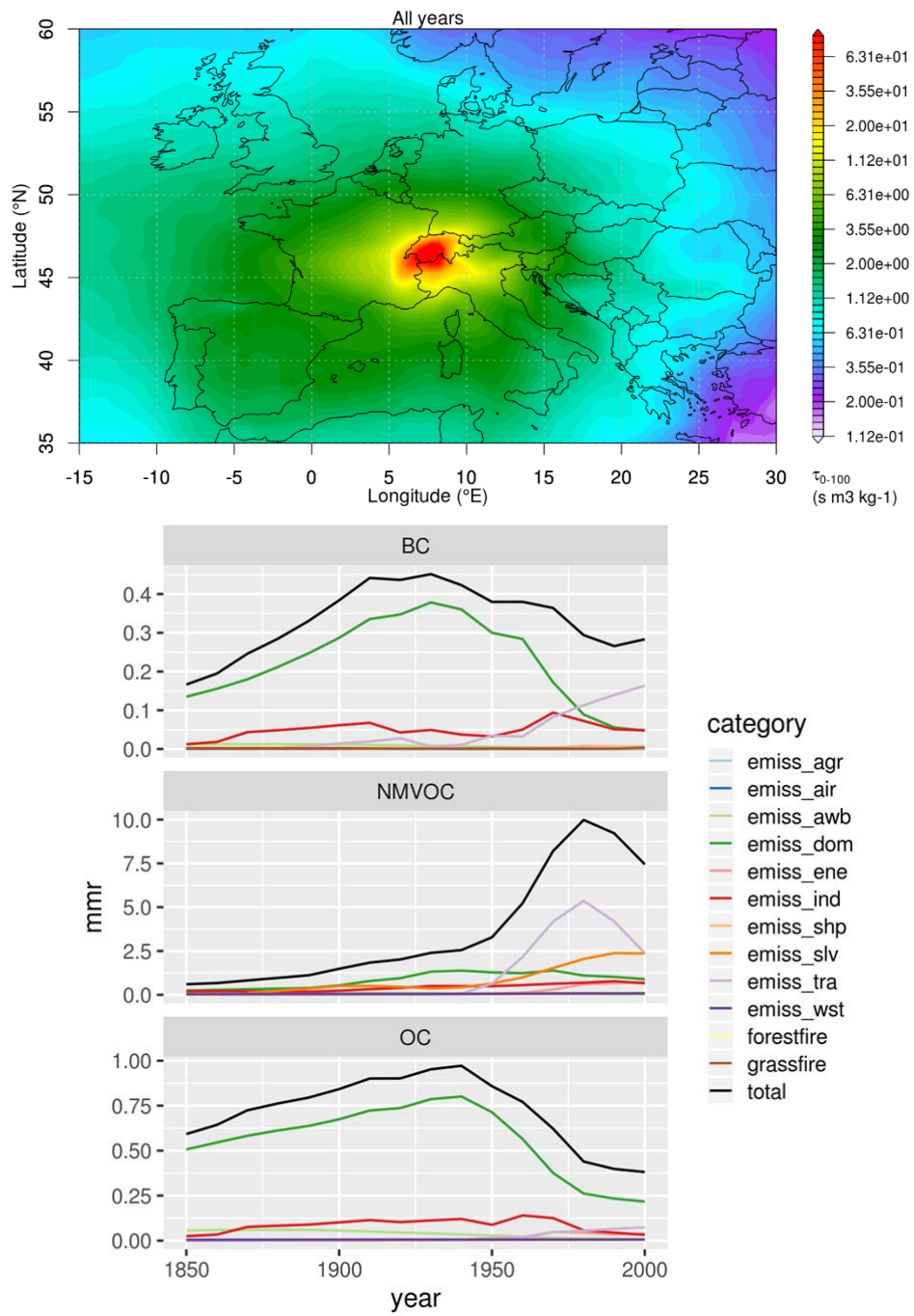


Figure S6.2 a) Footprint of potential emission sources, b) Estimated atmospheric BC, NMVOC and primary OC mass mixing ratio at Jungfraujoch from 12 emission sectors

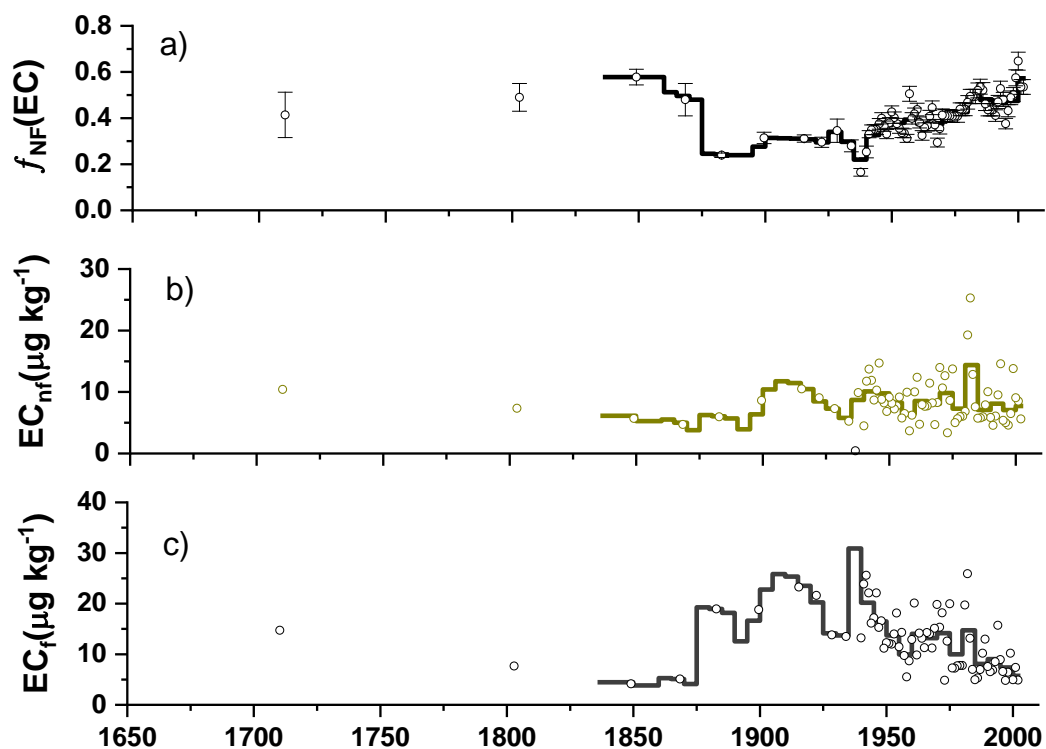


Figure S6.3 Non-fossil fraction of EC ($f_{NF}(EC)$) for the time period 1840-2002 a) and the corresponding concentrations from non-fossil b) and fossil c) sources as attributed based on ^{14}C . The data shown are the combined results from samples analysed in this study (1940–2002) and Jenk et al., 2006 (1660–1940), see main text. $f_{NF}(EC)$ values before 1840 (in light gray) are questionable due to very high dust load in the respective samples Jenk et al., 2006. 1σ uncertainty estimates include both, analytical and the modeling uncertainty shown in Fig. S1. Thick line: 5 -year averages (20 years before 1860).

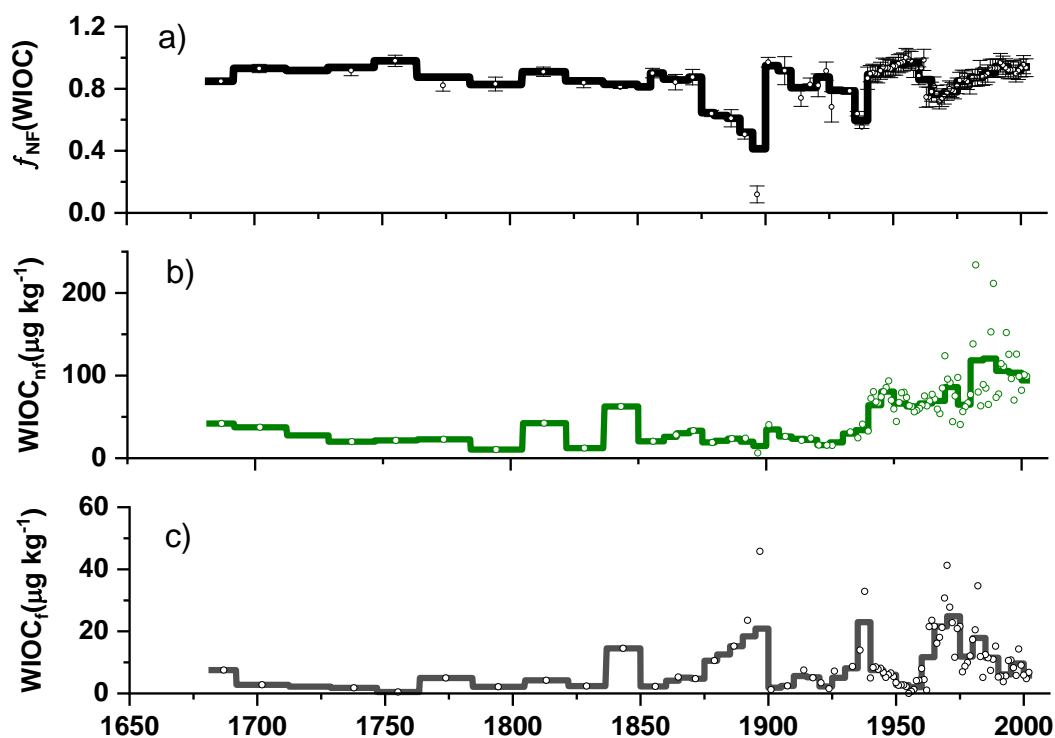


Figure S6.4 Non-fossil fraction of WIOC ($f_{NF}(WIOC)$) for the time period 1680-2002 a) and the corresponding WIOC concentrations from non-fossil b) and fossil c) sources as attributed based on ^{14}C . The data shown are the combined results from samples analysed in this study (1940–2002) and [Jenk et al., 2006] (1660–1940), see main text. 1σ uncertainty estimates include both, the analytical and the modeling uncertainty shown in Figure S6.1. Thick line: 5-year averages (10 to 20 years before 1860).

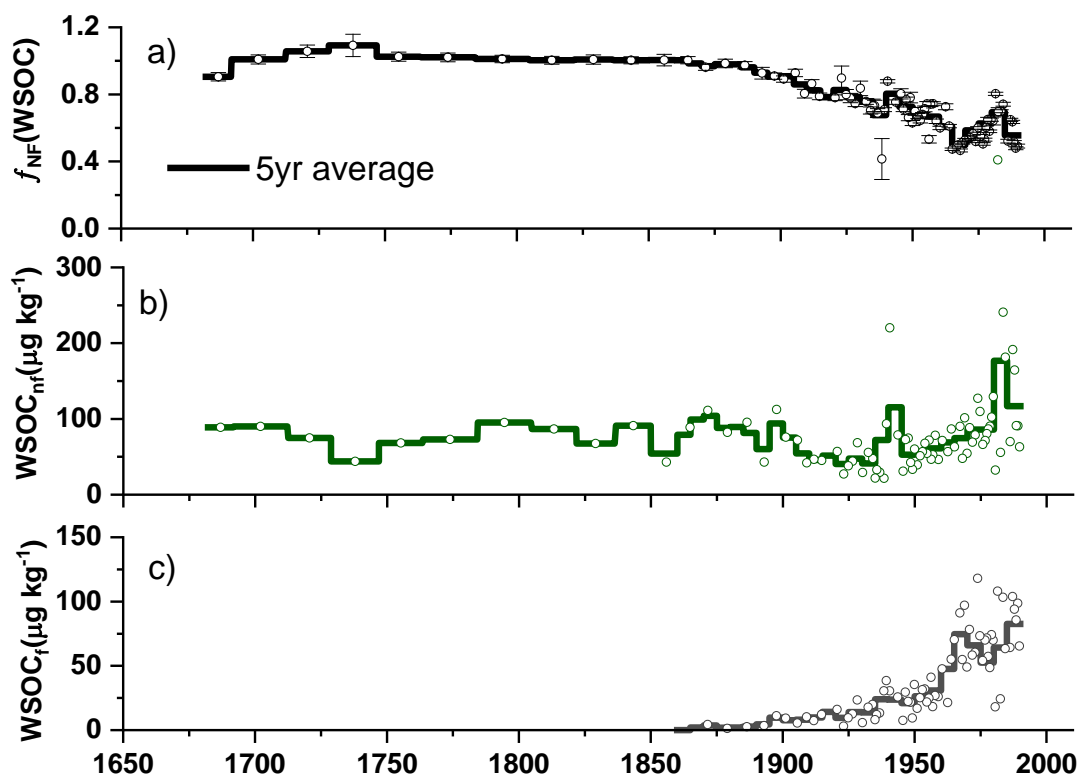


Figure S6.5 Non-fossil fraction of WSOC ($f_{NF}(WSOC)$) for the time period 1680-1990 a) and the corresponding WSOC concentrations from non-fossil b) and fossil c) sources as attributed based on ^{14}C . The WSOC data only reach up to 1990 due to the firm sample contamination Fang et al., 2019. 1σ uncertainty estimates include both, the analytical and the modeling uncertainty shown in Figure S6.1. Thick line: 5-year averages (10 to 20 years before 1860).

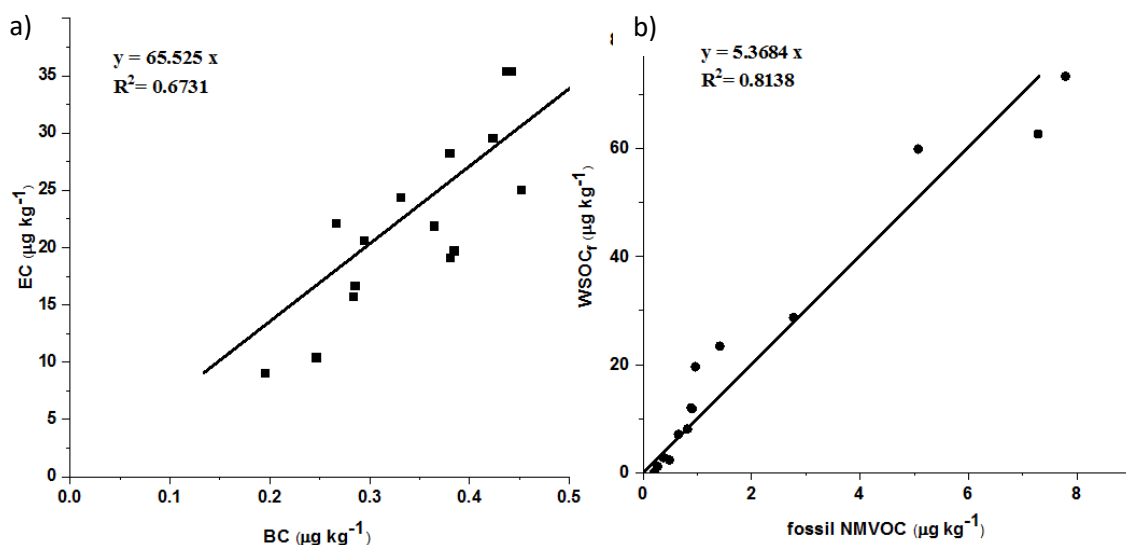


Figure S6.6 a) The linear regression between atmospheric BC load and EC concentration in ice core. b) the linear regression between fossil NMVOC and WSOC_f.

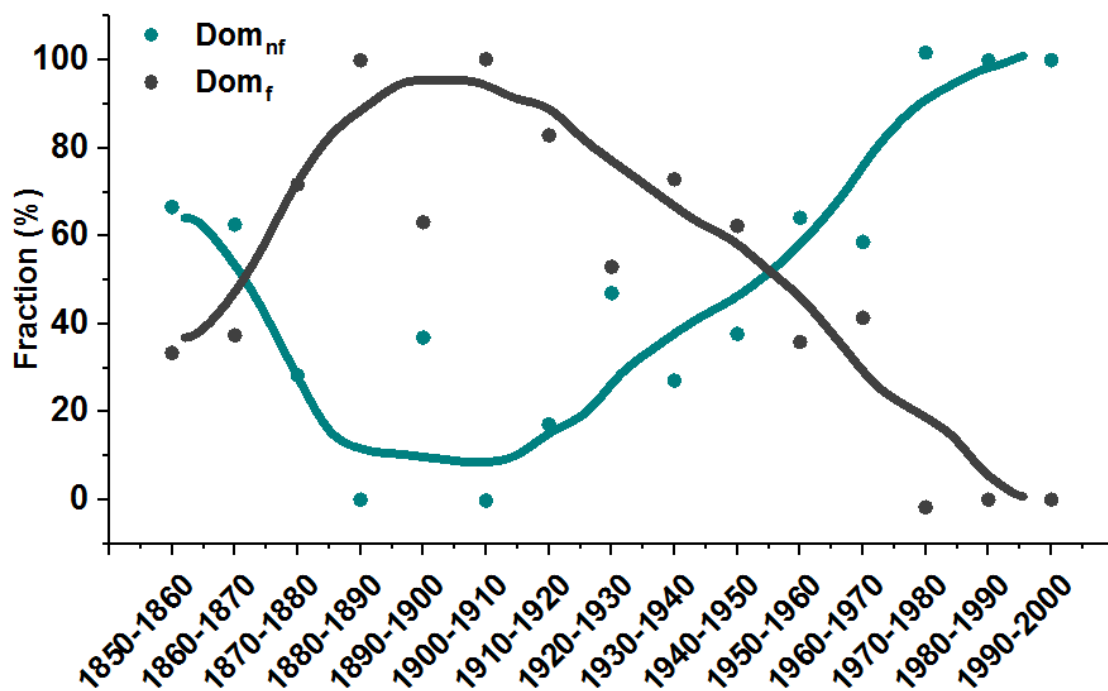


Figure S6.7 The historical fossil and non-fossil contribution to domestic consumption based on the BC record. We assume the discrepancy between EC_f and BC_f, is caused by residential fossil consumption. The calculated 10-year average values indicated as dots and the line is the smoothed estimation curve.

Bibliography

Acosta Navarro, J. C., S. Smolander, H. Struthers, E. Zorita, A. M. Ekman, J. Kaplan, A. Guenther, A. Arneth and I. Riipinen. Global emissions of terpenoid VOCs from terrestrial vegetation in the last millennium. *Journal of Geophysical Research: Atmospheres* **119**, 6867-6885, (2014).

Bond, T. C., E. Bhardwaj, R. Dong, R. Jogani, S. Jung, C. Roden, D. G. Streets and N. M. J. G. B. C. Trautmann. Historical emissions of black and organic carbon aerosol from energy-related combustion, 1850–2000. **21**, (2007).

Bond, T. C., D. G. Streets, K. F. Yarber, S. M. Nelson, J. H. Woo and Z. Klimont. A technology-based global inventory of black and organic carbon emissions from combustion. *Journal of Geophysical Research-Atmospheres* **109**, D14203, (2004). DOI:10.1029/2003jd003697

BUWAL. Vom Menschen verursachte Luftschadstoff - Emissionen in der Schweiz von 1900 bis 2010. Bern, Bundesamt für Umwelt, Wald und Landschaft: 122,(1995).

Cao, F., Y.-L. Zhang, S. Szidat, A. Zapf, L. Wacker and M. Schwikowski. Microgram level radiocarbon determination of carbonaceous particles in firn samples: pre-treatment and OC/EC separation. *Radiocarbon* **55**, 383-390 (2013). 10.2458/azu_js_rc.55.16291

Carlton, A. G., R. W. Pinder, P. V. Bhave and G. A. Pouliot. To what extent can biogenic SOA be controlled? *Environmental science & technology* **44**, 3376-3380, (2010).

Carslaw, K., L. Lee, C. Reddington, K. Pringle, A. Rap, P. Forster, G. Mann, D. Spracklen, M. Woodhouse and L. Regayre. Large contribution of natural aerosols to uncertainty in indirect forcing. *Nature* **503**, 67-71, (2013).

Cerqueira, M., C. Pio, M. Legrand, H. Puxbaum, A. Kasper-Giebl, J. Afonso, S. Preunkert, A. Gelencsér and P. J. J. o. A. S. Fialho. Particulate carbon in precipitation at European background sites. **41**, 51-61, (2010).

Cooper, O. R., D. Parrish, J. Ziemke, N. Balashov, M. Cupeiro, I. Galbally, S. Gilge, L. Horowitz, N. Jensen and J.-F. Lamarque. Global distribution and trends of tropospheric ozone: An observation-based review. *Elementa: Science of the Anthropocene* **2**, 000029, (2014).

Currie, L. A. Evolution and multidisciplinary frontiers of ¹⁴C aerosol science. *Radiocarbon* **42**, 115-126, (2000).

Ehn, M., J. A. Thornton, E. Kleist, M. Sipilä, H. Junninen, I. Pullinen, M. Springer, F. Rubach, R. Tillmann, B. Lee, F. Lopez-Hilfiker, S. Andres, I.-H. Acir, M. Rissanen, T. Jokinen, S.

Schobesberger, J. Kangasluoma, J. Kontkanen, T. Nieminen, T. Kurtén, L. B. Nielsen, S. Jørgensen, H. G. Kjaergaard, M. Canagaratna, M. D. Maso, T. Berndt, T. Petäjä, A. Wahner, V.-M. Kerminen, M. Kulmala, D. R. Worsnop, J. Wildt and T. F. Mentel. A large source of low-volatility secondary organic aerosol. *Nature* **506**, 476, (2014). 10.1038/nature13032

El-Zanan, H. S., D. H. Lowenthal, B. Zielinska, J. C. Chow and N. J. C. Kumar. Determination of the organic aerosol mass to organic carbon ratio in IMPROVE samples. **60**, 485-496, (2005).

Engardt, M., D. Simpson, M. Schwikowski and L. Granat. Deposition of sulphur and nitrogen in Europe 1900–2050. Model calculations and comparison to historical observations. *Tellus B: Chemical and Physical Meteorology* **69**, 1328945, (2017).

Fagerli, H., M. Legrand, S. Preunkert, V. Vestreng, D. Simpson and M. Cerqueira. Modeling historical long-term trends of sulfate, ammonium, and elemental carbon over Europe: A comparison with ice core records in the Alps. *Journal of Geophysical Research: Atmospheres* **112**, (2007).

Fang, L., J. Schindler, T. Jenk, C. Uglietti, S. Szidat and M. J. R. Schwikowski. Extraction of Dissolved Organic Carbon from Glacier Ice for Radiocarbon Analysis. **61**, 681-694, (2019).

Fuzzi, S., U. Baltensperger, K. Carslaw, S. Decesari, H. D. van Der Gon, M. C. Facchini, D. Fowler, I. Koren, B. Langford, U. Lohmann, E. Nemitz, S. Pandis, I. Riipinen, Y. Rudich, M. Schaap, J. G. Slowik, D. V. Spracklen, E. Vignati, M. Wild, M. Williams and S. Gilardoni. Particulate matter, air quality and climate: lessons learned and future needs. *Atmospheric Chemistry and Physics* **15**, 8217-8299, (2015). 10.5194/acp-15-8217-2015

Hallquist, M., J. C. Wenger, U. Baltensperger, Y. Rudich, D. Simpson, M. Claeys, J. Dommen, N. M. Donahue, C. George, A. H. Goldstein, J. F. Hamilton, H. Herrmann, T. Hoffmann, Y. Iinuma, M. Jang, M. E. Jenkin, J. L. Jimenez, A. Kiendler-Scharr, W. Maenhaut, G. McFiggans, T. F. Mentel, A. Monod, A. S. H. Prevot, J. H. Seinfeld, J. D. Surratt, R. Szmigielski and J. Wildt. The formation, properties and impact of secondary organic aerosol: current and emerging issues. *Atmospheric Chemistry and Physics* **9**, 5155-5236, (2009).

Heldstab, J., B. Schaepfi, F. Weber and M. Sommerhalder. Switzerland's Informative Inventory Report 2017, Tech. Rep., Federal Office for the Environment, Bern, available at: <https://www.bafu.admin.ch/bafu/de/home/themen/luft.html>,(2017).

Hodzic, A., J. L. Jimenez, A. S. H. Prévôt, S. Szidat, J. D. Fast and S. Madronich. Can 3-D models explain the observed fractions of fossil and non-fossil carbon in and near Mexico City? *Atmospheric Chemistry and Physics* **10**, 10997-11016, (2010). 10.5194/acp-10-10997-2010

Hodzic, A., P. S. Kasibhatla, D. S. Jo, C. D. Cappa, J. L. Jimenez, S. Madronich and R. J. Park. Rethinking the global secondary organic aerosol (SOA) budget: stronger production, faster removal, shorter lifetime. *Atmos. Chem. Phys.* **16**, 7917-7941, (2016). 10.5194/acp-16-7917-2016

Hoyle, C. R., M. Boy, N. M. Donahue, J. L. Fry, M. Glasius, A. Guenther, A. G. Hallar, K. H. Hartz, M. D. Petters, T. Petaja, T. Rosenoern and A. P. Sullivan. A review of the anthropogenic influence on biogenic secondary organic aerosol. *Atmospheric Chemistry and Physics* **11**, 321-343, (2011). DOI 10.5194/acp-11-321-2011

Isaksen, I. S. A., C. Granier, G. Myhre, T. K. Berntsen, S. B. Dalsøren, M. Gauss, Z. Klimont, R. Benestad, P. Bousquet, W. Collins, T. Cox, V. Eyring, D. Fowler, S. Fuzzi, P. Jöckel, P. Laj, U. Lohmann, M. Maione, P. Monks, A. S. H. Prevot, F. Raes, A. Richter, B. Rognerud, M. Schulz, D. Shindell, D. S. Stevenson, T. Storelvmo, W. C. Wang, M. van Weele, M. Wild and D. Wuebbles. Atmospheric composition change: Climate–Chemistry interactions. *Atmospheric Environment* **43**, 5138-5192, (2009). <http://dx.doi.org/10.1016/j.atmosenv.2009.08.003>

Jenk, T., S. Szidat, M. Schwikowski, H. Gaggeler, L. Wacker, H. Synal and M. Saurer. Microgram level radiocarbon (¹⁴C) determination on carbonaceous particles in ice. *Nuclear Instruments and Methods in Physics Research Section B: Beam Interactions with Materials and Atoms* **259**, 518-525, (2007). 10.1016/j.nimb.2007.01.196

Jenk, T. M., S. Szidat, M. Schwikowski, H. W. Gaggeler, S. Brutsch, L. Wacker, H. A. Synal and M. Saurer. Radiocarbon analysis in an Alpine ice core: record of anthropogenic and biogenic contributions to carbonaceous aerosols in the past (1650-1940). *Atmospheric Chemistry and Physics* **6**, 5381-5390, (2006).

Kander, A. K., P. Malanima and P. Warde. Energy transitions in Europe: 1600-2000, Lund University, CIRCLE-Center for Innovation, Research and Competences in the Learning Economy,(2008).

Kirkby, J., J. Duplissy, K. Sengupta, C. Frege, H. Gordon, C. Williamson, M. Heinritzi, M. Simon, C. Yan, J. Almeida, J. Tröstl, T. Nieminen, I. K. Ortega, R. Wagner, A. Adamov, A. Amorim, A.-K. Bernhammer, F. Bianchi, M. Breitenlechner, S. Brilke, X. Chen, J. Craven, A. Dias, S. Ehrhart, R. C. Flagan, A. Franchin, C. Fuchs, R. Guida, J. Hakala, C. R. Hoyle, T. Jokinen, H. Junninen, J. Kangasluoma, J. Kim, M. Krapf, A. Kürten, A. Laaksonen, K. Lehtipalo, V. Makhmutov, S. Mathot, U. Molteni, A. Onnela, O. Peräkylä, F. Piel, T. Petäjä, A. P. Praplan, K. Pringle, A. Rap, N. A. D. Richards, I. Riipinen, M. P. Rissanen, L. Rondo, N. Sarnela, S. Schobesberger, C. E. Scott, J. H. Seinfeld, M. Sipilä, G. Steiner, Y. Stozhkov, F. Stratmann, A. Tomé, A. Virtanen, A. L. Vogel, A. C. Wagner, P. E. Wagner, E. Weingartner, D. Wimmer, P. M. Winkler, P. Ye, X. Zhang, A. Hansel, J. Dommen, N. M. Donahue, D. R. Worsnop, U. Baltensperger, M. Kulmala, K. S. Carslaw and J. Curtius. Ion-induced nucleation of pure biogenic particles. *Nature* **533**, 521, (2016). 10.1038/nature17953

Lamarque, J.-F., T. C. Bond, V. Eyring, C. Granier, A. Heil, Z. Klimont, D. Lee, C. Liousse, A. Mieville, B. J. A. C. Owen and Physics. Historical (1850–2000) gridded anthropogenic and biomass burning emissions of reactive gases and aerosols: methodology and application. **10**, 7017-7039, (2010).

Lathièrre, J., C. N. Hewitt and D. J. Beerling. Sensitivity of isoprene emissions from the terrestrial biosphere to 20th century changes in atmospheric CO₂ concentration, climate, and land use. *Global Biogeochemical Cycles* **24**, n/a-n/a, (2010). 10.1029/2009GB003548

Legrand, M., S. Preunkert, B. Jourdain, J. Guilhermet, X. Fain, I. Alekhina and J. R. Petit. Water-soluble organic carbon in snow and ice deposited at Alpine, Greenland, and Antarctic sites: a critical review of available data and their atmospheric relevance. *Climate of the Past* **9**, 2195-2211, (2013). DOI 10.5194/cp-9-2195-2013

Legrand, M., S. Preunkert, B. May, J. Guilhermet, H. Hoffman and D. Wagenbach. Major 20th century changes of the content and chemical speciation of organic carbon archived in Alpine ice cores: Implications for the long-term change of organic aerosol over Europe. *Journal of Geophysical Research: Atmospheres* **118**, 3879-3890, (2013).

Legrand, M., S. Preunkert, M. Schock, M. Cerqueira, A. Kasper-Giebl, J. Afonso, C. Pio, A. Gelencsér and I. Dombrowski-Etchevers. Major 20th century changes of carbonaceous aerosol components (EC, WinOC, DOC, HULIS, carboxylic acids, and cellulose) derived from Alpine ice cores. *Journal of Geophysical Research* **112**, (2007). 10.1029/2006jd008080

Levin, I., T. Naegler, B. Kromer, M. Diehl, R. J. Francey, A. J. Gomez-Pelaez, L. P. Steele, D. Wagenbach, R. Weller and D. E. Worthy. Observations and modelling of the global distribution and long-term trend of atmospheric ¹⁴CO₂. *Tellus Series B* **62**, 26-46, (2010). DOI 10.1111/j.1600-0889.2009.00446.x

Liao, H. and J. H. Seinfeld. Global impacts of gas-phase chemistry-aerosol interactions on direct radiative forcing by anthropogenic aerosols and ozone. *Journal of Geophysical Research: Atmospheres* **110**, n/a-n/a, (2005). 10.1029/2005JD005907

Lim, S., X. Fain, P. Ginot, V. Mikhailenko, S. Kutuzov, J.-D. Paris, A. Kozachek, P. J. A. C. Laj and Physics. Black carbon variability since preindustrial times in the eastern part of Europe reconstructed from Mt. Elbrus, Caucasus, ice cores. **17**, 3489-3505, (2017).

Lin, G., J. E. Penner, M. G. Flanner, S. Sillman, L. Xu and C. Zhou. Radiative forcing of organic aerosol in the atmosphere and on snow: Effects of SOA and brown carbon. *Journal of Geophysical Research: Atmospheres* **119**, 7453-7476, (2014). 10.1002/2013JD021186

Loran, C., C. Ginzler and M. Bürgi. Evaluating forest transition based on a multi-scale approach: forest area dynamics in Switzerland 1850–2000. *Regional environmental change* **16**, 1807-1818, (2016).

Mariani, I., A. Eichler, T. Jenk, S. Brönnimann, R. Auchmann, M. Leuenberger and M. Schwikowski. Temperature and precipitation signal in two Alpine ice cores over the period 1961–2001. *Climate of the Past* **10**, 1093-1108, (2014).

May, B., D. Wagenbach, H. Hoffmann, M. Legrand, S. Preunkert and P. Steier. Constraints on the major sources of dissolved organic carbon in Alpine ice cores from radiocarbon analysis over the bomb-peak period. *Journal of Geophysical Research: Atmospheres* **118**, 3319-3327, (2013).

Minguillon, M. C., N. Perron, X. Querol, S. Szidat, S. M. Fahrni, A. Alastuey, J. L. Jimenez, C. Mohr, A. M. Ortega, D. A. Day, V. A. Lanz, L. Wacker, C. Reche, M. Cusack, F. Amato, G. Kiss, A. Hoffer, S. Decesari, F. Moretti, R. Hillamo, K. Teinila, R. Seco, J. Penuelas, A. Metzger, S. Schallhart, M. Muller, A. Hansel, J. F. Burkhardt, U. Baltensperger and A. S. H. Prevot. Fossil versus contemporary sources of fine elemental and organic carbonaceous particulate matter during the DAURE campaign in Northeast Spain. *Atmospheric Chemistry and Physics* **11**, 12067-12084, (2011). DOI 10.5194/acp-11-12067-2011

Mohn, J., S. Szidat, J. Fellner, H. Rechberger, R. Quartier, B. Buchmann and L. Emmenegger. Determination of biogenic and fossil CO₂ emitted by waste incineration based on ¹⁴CO₂ and mass balances. *Bioresource Technology* **99**, 6471-6479, (2008). DOI 10.1016/j.biortech.2007.11.042

Paasonen, P., A. Asmi, T. Petaja, M. K. Kajos, M. Aijala, H. Junninen, T. Holst, J. P. D. Abbatt, A. Arneth, W. Birmili, H. D. van der Gon, A. Hamed, A. Hoffer, L. Laakso, A. Laaksonen, W. Richard Leitch, C. Plass-Dulmer, S. C. Pryor, P. Raisanen, E. Swietlicki, A. Wiedensohler, D. R. Worsnop, V.-M. Kerminen and M. Kulmala. Warming-induced increase in aerosol number concentration likely to moderate climate change. *Nature Geosci* **6**, 438-442, (2013). 10.1038/ngeo1800

<http://www.nature.com/ngeo/journal/v6/n6/abs/ngeo1800.html#supplementary-information>

Pio, C., M. Cerqueira, R. M. Harrison, T. Nunes, F. Mirante, C. Alves, C. Oliveira, A. S. de la Campa, B. Artinano and M. Matos. OC/EC ratio observations in Europe: Re-thinking the approach for apportionment between primary and secondary organic carbon. *Atmospheric Environment* **45**, 6121-6132, (2011). DOI 10.1016/j.atmosenv.2011.08.045

Pio, C. A., M. Legrand, T. Oliveira, J. Afonso, C. Santos, A. Caseiro, P. Fialho, F. Barata, H. Puxbaum and A. J. J. o. G. R. A. Sanchez-Ochoa. Climatology of aerosol composition (organic versus inorganic) at nonurban sites on a west-east transect across Europe. **112**, (2007).

Pöschl, U. J. A. C. I. E. Atmospheric aerosols: composition, transformation, climate and health effects. **44**, 7520-7540, (2005).

Reimer, P., T. Brown and R. Reimer. Discussion: reporting and calibration of post-bomb ^{14}C Data. *Radiocarbon* **46**, 1299-1304, (2004). 10.1017/S0033822200033154

Reimer, P. J., E. Bard, A. Bayliss, J. W. Beck, P. G. Blackwell, C. B. Ramsey, H. C. Caitlin E Buck, R. L. Edwards, M. Friedrich, P. M. Grootes, T. P. Guilderson, H. Haflidason, I. Hajdas, C. Hatté, T. J. Heaton, D. L. Hoffmann, A. G. Hogg, K. A. Hughen, K. F. Kaiser, B. Kromer, S. W. Manning, M. Niu, R. W. Reimer, D. A. Richards, E. M. Scott, J. R. Southon, R. A. Staff, C. S. M. Turney and J. v. d. Plicht. Intcal13 and Marine13 radiocarbon age calibration curves 0-50,000 years cal BP. *Radiocarbon* **55**, 1869-1887, (2013).

Riccobono, F., S. Schobesberger, C. E. Scott, J. Dommen, I. K. Ortega, L. Rondo, J. Almeida, A. Amorim, F. Bianchi and M. Breitenlechner. Oxidation products of biogenic emissions contribute to nucleation of atmospheric particles. *Science* **344**, 717-721, (2014).

Rollins, A. W., E. C. Browne, K.-E. Min, S. E. Pusede, P. J. Wooldridge, D. R. Gentner, A. H. Goldstein, S. Liu, D. A. Day, L. M. Russell and R. C. Cohen. Evidence for NO_x Control over Nighttime SOA Formation. *Science* **337**, 1210-1212, (2012). 10.1126/science.1221520

Ruppel, M. M., I. Isaksson, J. Strom, E. Beaudon, J. Svensson, C. A. Pedersen and A. Korhola. Increase in elemental carbon values between 1970 and 2004 observed in a 300-year ice core from Høltedahlfonna (Svalbard). *Atmospheric Chemistry and Physics* **14**, 11447-11460, (2014). 10.5194/acp-14-11447-2014

Shilling, J. E., R. A. Zaveri, J. D. Fast, L. Kleinman, M. L. Alexander, M. R. Canagaratna, E. Fortner, J. M. Hubbe, J. T. Jayne, A. Sedlacek, A. Setyan, S. Springston, D. R. Worsnop and Q. Zhang. Enhanced SOA formation from mixed anthropogenic and biogenic emissions during the CARES campaign. *Atmos. Chem. Phys.* **13**, 2091-2113, (2013). 10.5194/acp-13-2091-2013

Sigl, M., N. J. Abram, J. Gabrieli, T. M. Jenk, D. Osmont and M. Schwikowski. No role for industrial black carbon in forcing 19th century glacier retreat in the Alps. *The Cryosphere Discuss.* **2018**, 1-34, (2018). 10.5194/tc-2018-22

Spracklen, D., J. Jimenez, K. Carslaw, D. Worsnop, M. Evans, G. Mann, Q. Zhang, M. Canagaratna, J. Allan and H. Coe. Aerosol mass spectrometer constraint on the global secondary organic aerosol budget. *Atmospheric Chemistry and Physics* **11**, 12109-12136, (2011).

Szidat, S., T. M. Jenk, H. W. Gäggeler, H.-A. Synal, I. Hajdas, G. Bonani and M. Saurer. THEODORE, a two-step heating system for the EC/OC determination of radiocarbon (^{14}C) in the environment. *Nuclear Instruments and Methods in Physics Research Section B: Beam Interactions with Materials and Atoms* **223-224**, 829-836, (2004). 10.1016/j.nimb.2004.04.153

Szidat, S., T. M. Jenk, H.-A. Synal, M. Kalberer, L. Wacker, I. Hajdas, A. Kasper-Giebl and U. Baltensperger. Contributions of fossil fuel, biomass-burning, and biogenic emissions to carbonaceous aerosols in Zurich as traced by ^{14}C . *Journal of Geophysical Research* **111**, D07206, (2006). 10.1029/2005jd006590

Szidat, S., G. A. Salazar, E. Vogel, M. Battaglia, L. Wacker, H. A. Synal and A. Turler. C-14 Analysis and Sample Preparation at the New Bern Laboratory for the Analysis of Radiocarbon with Ams (Lara). *Radiocarbon* **56**, 561-566, (2014). 10.2458/56.17457

Thevenon, F., F. S. Anselmetti, S. M. Bernasconi and M. Schwikowski. Mineral dust and elemental black carbon records from an Alpine ice core (Colle Gnifetti glacier) over the last millennium. *Journal of Geophysical Research-Atmospheres* **114**, (2009). Artn D17102

10.1029/2008jd011490

Unger, N. Isoprene emission variability through the twentieth century. *Journal of Geophysical Research: Atmospheres* **118**, 13,606-613,613, (2013). 10.1002/2013JD020978

Wacker, L., S. M. Fahrni, I. Hajdas, M. Molnar, H. A. Synal, S. Szidat and Y. L. Zhang. A versatile gas interface for routine radiocarbon analysis with a gas ion source. *Nuclear Instruments & Methods in Physics Research Section B-Beam Interactions with Materials and Atoms* **294**, 315-319, (2013). DOI 10.1016/j.nimb.2012.02.009

Zhang, Y.-L., M. Cerqueira, G. Salazar, P. Zotter, C. Hueglin, C. Zellweger, C. Pio, A. S. Prévôt and S. Szidat. Wet deposition of fossil and non-fossil derived particulate carbon: Insights from radiocarbon measurement. *Atmospheric Environment* **115**, 257-262, (2015).

Zhang, Y.-L., J. r. Schnelle-Kreis, G. I. Abbaszade, R. Zimmermann, P. Zotter, R.-r. Shen, K. Schäfer, L. Shao, A. S. H. Prévôt and S. n. Szidat. Source apportionment of elemental carbon in Beijing, China: Insights from radiocarbon and organic marker measurements. *Environmental science & technology* **49**, 8408-8415, (2015).

Zhang, Y. L., N. Perron, V. G. Ciobanu, P. Zotter, M. C. Minguillón, L. Wacker, A. S. H. Prévôt, U. Baltensperger and S. Szidat. On the isolation of OC and EC and the optimal strategy of radiocarbon-based source apportionment of carbonaceous aerosols. *Atmospheric Chemistry and Physics* **12**, 10841-10856, (2012).

Zotter, P., V. Ciobanu, Y. Zhang, I. El-Haddad, M. Macchia, K. R. Daellenbach, G. A. Salazar, R.-J. Huang, L. Wacker and C. Hueglin. Radiocarbon analysis of elemental and organic carbon in Switzerland during winter-smog episodes from 2008 to 2012-Part 1: Source apportionment and spatial variability. *Atmospheric Chemistry and Physics* **14**, 13551-13570, (2014).

Zotter, P., I. El-Haddad, Y. Zhang, P. L. Hayes, X. Zhang, Y. H. Lin, L. Wacker, J. Schnelle-Kreis, G. Abbaszade and R. Zimmermann. Diurnal cycle of fossil and nonfossil carbon using radiocarbon analyses during CalNex. *Journal of Geophysical Research: Atmospheres* **119**, 6818-6835, (2014).

7 Conclusion and Outlook

The large uncertainty of aerosol radiative forcing from anthropogenic emissions is partly related to the lack of pre-industrial background data. Glaciers are valuable natural archives not just for climate signals, but also for the atmospheric composition. Aerosols are deposited on glaciers through wet and dry deposition, the latter being mostly of minor importance. Carbonaceous aerosols, consisting of the fractions of Element Carbon (EC) or Black Carbon (BC) deepened on the analytical method, Water Insoluble Organic Carbon (WIOC), and Water Soluble Organic Carbon (WSOC), for a major part of fine particles have attracted scientific attention due to their optical properties. Glacier ice cores are a unique tool to get direct insight into pre-industrial carbonaceous aerosol variability. WSOC is analyzed in the ice as dissolved organic carbon (DOC) when an ice sample is melted, which also contains organic gases taken up during the snowfall. There are very few existing records of EC and WIOC, and even less for WSOC.

This thesis provided the first comprehensive evaluation of the great potential of applying radiocarbon analysis of the DOC fraction in ice cores at different time scale: before large scale human activities (biomass burning, fossil fuel burning, land use etc.), DO^{14}C analysis was used to determine the age of the ice and for reconstructing the natural aerosol variability. In addition, during and after the industrial revolution, ^{14}C analysis of DOC in ice cores allowed to quantify the fossil fuel and thereby anthropogenic impact on the aerosol composition. All these studies were built on the new high oxidation efficiency and low blank DOC extraction method for radiocarbon analysis in ice core samples, optimized in this thesis. This new setup with inert gas (helium) atmosphere minimized the blank to $1.9 \pm 1.6 \mu\text{g C}$ with a $F^{14}\text{C}$ value of 0.68 ± 0.13 . With the optimized DOC extraction method, it was possible to analyse the DO^{14}C in samples up to 350 g ice mass with a carbon content of as low as $25 \mu\text{g C kg}^{-1}$ ice. This high performance encouraged to re-evaluate the feasibility of applying DO^{14}C analysis for ice core dating. The first attempt to use DOC for ^{14}C dating of ice samples was not entirely conclusive, suggesting potential in-situ production of ^{14}C in the DOC fraction based on derived $F^{14}\text{C}$ values indicating super modern origin. Bottom ice samples from four glaciers (Colle Gnifetti, Belukha, ShuLeNanShan and Chongce) were dated in parallel with this new technique and with the well-established WIO^{14}C dating method. ^{14}C ages of the two fractions yielded a comparable probability distribution, confirming that ^{14}C dating of the ice entrapped DOC fraction is

applicable and a valuable future tool for the dating of ice samples. The benefits of using the DOC fraction are not just reducing the required ice mass, but also improving the analytical precision. This is due to the relatively higher DOC concentration compared to WIOC, resulting in a larger total amount of carbon. In addition, one unexpected advantage is that carbonate removal is more efficient during the DOC extraction, even for high mineral dust loading. In such samples, a bias to older ages was observed for young sample, when dated with WIO¹⁴C. Finally, with this new DO¹⁴C method, it may be possible to push radiocarbon dating of ice a step forward even to remote and Polar Regions. The chronology of the Mt. Hunter (62°56'N, 151°5'W, 3900 m asl., Central Alaska) core was successfully established based on both WIO¹⁴C and DO¹⁴C analysis techniques. This is the first time micro radiocarbon dating was applied to ice from an Arctic core, which was achieved by increasing the amount of ice (>1 kg) to obtain the required carbon mass and by using a new technique based on the dissolved organic carbon fraction. Calibrated ¹⁴C ages from the two bottom most sample (7946-10226 years cal BP and 7018-7975 years cal BP) indicate that Mt. Hunter glacier is early Holocene origin. Mt. Hunter core provides the possibility to investigate the hydroclimate variability during warm intervals outside of the Common Era.

In industrial times, anthropogenic emissions have significantly altered the aerosol composition. The radiocarbon content in organic aerosols cannot be used to date the ice core anymore, but instead it provides a unique tracer for anthropogenic activities. This allows to establish the historical record of carbonaceous particle concentrations and their fossil and non-fossil contributions, which is essential to understand the impact of atmospheric aerosols on global and regional climate. In this thesis, the first complete high-resolution carbonaceous aerosol record including the major fractions DOC, WIOC, and EC with the corresponding fossil and non-fossil contributions from pre-industrial to industrial times was reconstructed from the Fiescherhorn glacier ice core (3900 m asl., Swiss Alps). The total carbonaceous aerosol concentration increased by a factor of three at the end of the 20th century compared to the pre-industrial background. Fossil fuel combustion contributed up to ~32% of the increase. EC had highest values in the first half of the 20th century, to a large extent caused by fossil fuel emissions. In contrast, OC (WIOC and WSOC) showed a strong increasing trend between 1940 and 1980, mostly of non-fossil origin. Compared to atmospheric concentration estimates from aerosol modelling using the Flexpart model, the increase in non-fossil OC was not reflected in the emission estimates of OC, with a mismatch of up to one magnitude in the second half of the

20th century. We attribute this trend primarily to enhancement of SOA formation caused by the presence of anthropogenic precursor gases or by the increase of the atmospheric oxidative capacity. Thus, bottom-up emission inventories seem to heavily underestimate the atmospheric OC loading by not accounting adequately for SOA formation, limiting the capacity of current models in estimating anthropogenic aerosol forcing.

This new DOC extraction method for ^{14}C analysis has been successfully used for ice dating and quantifying the historical fossil fuel contribution to organic aerosols. From the technical aspect, upgrading the filtration system on DOC setup could help to obtain higher recovery for EC/WIOC analysis. This modification will allow rinsing of ultra-pure water through the melting vessel to increase the filtration efficiency by bringing all the particles down to the filter.

To further validate the obtained DO^{14}C ages, cross-comparison with other independent dating methods is necessary. For example, tephra dating or cut-edge ultra-high resolution laser ablation (LA) ICP-MS systems. Ultra-high resolution could possibly retrieve the annual seasonal variation signal even in the deepest part. Meanwhile, more ^{14}C analyses in both WIOC and DOC fraction is still also essential to confirm the DO^{14}C dating technique. With the upgraded filtration system the amount of ice required could be reduced by more than a factor of two for analyzing both fractions.

To further push the limit of ^{14}C analysis of low carbon content ice samples for dating, samples from remote regions, high altitude or even polar regions should be analyzed on the DOC extraction setup. For example, ice from Greenland contains WIOC as low as $5\ \mu\text{g}/\text{kg}$ which is challenging for ^{14}C analysis but may allow DO^{14}C dating. This will generate guidance criteria which ice samples can be dated by ^{14}C analysis. This new technique also sheds some light on the dating of horizontal ice cores recovered from the ablation zone where the normal dating tools are impossible.

Aerosols have very different regional scale distribution due to their short atmospheric lifetime and the uneven distribution of emissions sources. In addition, the onset of anthropogenic emissions varies from region to region. Reconstructing carbonaceous aerosol records from various locations could give more details on the regional and global picture how anthropogenic activities have affected the aerosol concentration and composition. This could

help to improve the understanding of the climate sensitivity to anthropogenic emissions at different scales and to reduce the uncertainties in aerosol forcing. In the future, the extension of carbonaceous aerosol records further back in time will enhance the knowledge about the natural aerosol variability under different climate conditions.

This new technique has great potential for applications on all kinds of aquatic samples in many different fields of study. Applying it to the melting water on the glacier surface could allow investigating the biogeochemical cycle of microorganism living on the glacier surface or in cryoconite holes. To evaluate the impact of glacier runoff with respect to carbon input into downstream ecosystems, water samples from rivers having glacier meltwater input could be collected at different distances to calculate the carbon flux based on WIOC and DOC ^{14}C analysis. In addition, this setup also could be used for studying lake, coastal, and marine carbon cycles.

Acknowledgements

This work would not have been accomplished without the support from many colleagues, friends and family. I would like to thank all of them first of all for the kind patience with me. Ice core study was a new world for me, which I started to discover little by little during my PhD. During this time, I appreciated to work and exchange with a lot of different people:

I am indebted to my supervisor, Margit Schwikowski, for her advice and support. She guided me into this marvelous ice core world. Her scientific expertise led my research direction. She always provided valuable insights and encouraged me to move forward. Her scientific achievement encourage me as female student and gave me the inspiration and motivation to work in academic.

I am particularly grateful for the advice and supervision from Theo M. Jenk. He always took time to help me solve problems. Many thanks go to him, for all his effort to keep my work on track and to help with data analysis and interpretation as well as for all the discussion about radiocarbon data processing.

I would like to express my very great appreciation to Sönke Szidat for introducing me into radiocarbon analysis with MICADAS. He also provide me great help with the manuscript writing, discussion and editing.

I would like to offer my thanks to Karl Kreutz for the collaboration work on the dating of Mt. Hunter ice core. He also invited me visiting the Climate Change Institute and School of Earth and Climate Science in University of Maine. His time for discussion, reading and review during manuscript writing.

Johannes Schindler the previous PhD who provided me with very valuable DOC extraction setup system is also acknowledged. He built the whole system, taught me how to operate it, and pointed out the possibility for the optimizing the setup.

Advice and help given by Alexander L. Vogel has been a great help in ice core cutting in the cold room and optimizing the DOC extraction for higher efficiency.

I wish to acknowledge the help provided by Anja Eichler for the basic analytical chemistry insights. While she was patient with my questions, Anja helped me solve scientific problem with enthusiasm. She also helped me settle down and adapt to the life in Switzerland.

Chiara Uglietti instructed me to the laboratory work about WIOC filtration and instructed me how to cut ice cores in the cold room. She also introduced me to the Laboratory for the Analysis of Radiocarbon with AMS (LARA) in the University of Bern.

I would like to thank, Stephan Henne from EMPA for helping with the emission data and flexpart modeling for the Jaufraujoch.

Dominic Winski for collaboration on the Mt. Hunter ice cores is acknowledged. He prepared the ice cores and transported the samples to PSI for analysis. In addition, he hosted me during my visit at University of Maine.

Assistance provided by Thomas Singer was greatly appreciated. Thomas worked together with me on the ice sample cutting and helped with DOC analysis.

I gratefully acknowledge the technical assistance from Sabine Brüttsch. She gave me an introduction to the laboratory and helped me work in the analytical laboratory.

I thank the team of LARA, Gary Salazar, Christophe Espic, Martin Rauber, Edith Vogel and Michael Battaglia for the work on radiocarbon measurements.

Martin Grosjean, as the Chair of my committee, showed great passion on my scientific output and provided many discussions regarding this work.

I also acknowledge the committee member, Peter Steier for his effort to read and review this work and the positive feedback on my work on radiocarbon studies.

I thank Andrés Laso for the technical assistance on modifying the DOC extraction setup.

In addition, I would like to acknowledge help from my officemates. Anna Dal Farra, Dimitri Osmont and Sven Avak already successfully graduated from our office. They provided me great help to start working at PSI. My great current officemates Carla Huber, Martina Barandun, Petr Nalivaika, Tatjana Münster and Thomas Singer for their endless patience with me, as well as the pleasant gym sessions, lunch breaks and our annual project of “sun fun and run with Theo”.

My flatmate, Junying Shen and Reto Gehrig provided me lot of support as friends and in domestic documentation regarding the immigration office.

Special thanks go to my parents, Guocheng Fang and Xiuying Xie, for always supporting my decisions in the end, although we argue all the time. I'm not the easiest daughter for them but they are proud of me being brave and independent.

My extended family for supporting me to pursue my dream. They provide great help to look after my parents and my grandparents. I would not have been able to get through losing two grandparents without them beside me.

I further thank my friends back home, for picking up the phone with 6 hours' time difference.

Declaration of consent

on the basis of Article 18 of the PromR Phil.-nat. 19

Name/First Name: Fang Ling

Registration Number: 16-125-734

Study program: PhD

Bachelor

Master

Dissertation

Title of the thesis: Radiocarbon analysis of dissolved organic carbon from ice cores

Supervisor: Prof. Dr. Margit Schwikowski

I declare herewith that this thesis is my own work and that I have not used any sources other than those stated. I have indicated the adoption of quotations as well as thoughts taken from other authors as such in the thesis. I am aware that the Senate pursuant to Article 36 paragraph 1 litera r of the University Act of September 5th, 1996 and Article 69 of the University Statute of June 7th, 2011 is authorized to revoke the doctoral degree awarded on the basis of this thesis.

For the purposes of evaluation and verification of compliance with the declaration of originality and the regulations governing plagiarism, I hereby grant the University of Bern the right to process my personal data and to perform the acts of use this requires, in particular, to reproduce the written thesis and to store it permanently in a database, and to use said database, or to make said database available, to enable comparison with theses submitted by others.

Villigen PSI, 2nd June, 2

Signature: 

Curriculum Vitae

Personal Information

Name: Fang Ling

M/F: Female

Date of Birth: 1991/05/15

Nationality: Chinese

Address: OFLB 102, Paul Scherrer Insitut
5232 Villigen PSI Ost
Switzerland

Phone: +41798628269

E-mail: ling.fang@psi.ch



Education

2009-2013, Bachelor Degree, Major in environmental science undergraduate student in Ocean University of China. **Bachelor thesis:**

The Numerical Model of Oil Spill in Oil Field Exploitation at The Bohai Sea (2013)

2013-2016, Master Degree, Major in biogeochemical oceanography master student in Seoul National University, South Korea. **Master thesis:**

Distribution of dissolved organic radiocarbon in the Amundsen Sea, Antarctica (2016)

2016-2020, PhD student in Laboratory of Environmental Chemistry at Paul Scherrer Institute and University of Bern, Department of Chemistry and Biochemistry and Oeschger Centre for Climate Change Research (OCCR), Switzerland. **PhD thesis:**

Radiocarbon analysis of dissolved organic carbon (DOC) in ice cores (2020)

Scientific Publications:

L. Fang, J. Schindler, T.M. Jenk, C. Uglietti, S. Szidat, M. Schwikowski: Extraction of dissolved organic carbon from glacier ice for radiocarbon analysis, Radiocarbon, 2019.

Vogel, A.L., Lauer, A., Fang, L., Arturi, K., Bachmeier, F., Daellenbach, K.R., Käser, T., Vlachou, A., Pospisilova, V., Baltensperger, U. and Haddad, I.E., A Comprehensive Nontarget Analysis for the Molecular Reconstruction of Organic Aerosol Composition from Glacier Ice Cores. *Environmental Science & Technology*, 53, 12565-12575, 2019.

Fang, L., Lee, S., Lee, S.A., Hahm, D., Kim, G., Druffel, E.R. and Hwang, J., Removal of Refractory Dissolved Organic Carbon in the Amundsen Sea, Antarctica. *Scientific reports*, 10, 1213, 2020. <https://doi.org/10.1038/s41598-020-57870-6>

L. Fang, F. Cao, T. M. Jenk, A. L. Vogel, Y.L. Zhang, L Wacker, G. Salazar, S. Szidat, M. Schwikowski: Enhancement of carbonaceous aerosol during the 20th century by anthropogenic activities: insights from an Alpine ice core, in preparation, 2020.

L. Fang, D. Winski, K. Kreutz, T.M. Jenk, M. Schwikowski, E. Osterberg, S. Campbell, C.Wake: ^{14}C age constraints in the Mt. Hunter, Alaska ice core: implications for chronology and early Holocene Arctic ice extent, in preparation, 2020.

P. Bohleber, M.S. Waldhuber, M. Schwikowski, L. Fang, A. Fischer: New glacier evidence for ice-free summits during the life of the Tyrolean Iceman, submitted to *Nature Communications*

L. Fang, T. Singer, S. Hou, S. Szidat, M. Schwikowski, T.M. Jenk: New radiocarbon dating tool for ice cores, in preparation, 2020.

Participation in Conferences and Workshops:

2017 Swiss Climate Summer School, Monte Verità, Ascona, Switzerland

Poster presentation

Ice Core Analysis Techniques (ICAT) PhD School, Copenhagen, Denmark

2018 26th European Research Course on Atmospheres (ERCA), Grenoble, France

Poster presentation

Polar 2018, Davos, Switzerland

Poster presentation

2019 12th International Conference on Carbonaceous Particles in the Atmosphere (ICCPA), European Geosciences Union (EGU) General Assembly

Vienna, Austria

Poster presentation

Internship experience:

Student Research Development Program: Sources of Water Soluble Organic Nitrogen in Atmospheric Aerosols in summer of Qingdao (05/2011-05/2012)

National University Student Innovation Program: Sources of Water Soluble Organic Nitrogen in Atmospheric Aerosols in summer of Qingdao (05/2011-05/2012)

Service to scientific community:

February 2016: Joined the scientific course for the Amundsen Sea Expedition 2015 – 2016 (ANA06B), Korean Polar Research Institute (KOPRI), South Korea

2018: Visiting the ice core drilling campaigns in Rhone glacier, Switzerland

2019: Helping the organizer of Swiss Girls on Ice project with preparing and split the flyers and communication.

2020: Member of Ice Core Young Scientists (ICYS), supporting member of the LOC of the Open Science Conference in 2020 in Switzerland of the International Partnership in Ice Core Sciences